AD-A243 237

NAVAL POSTGRADUATE SCHOOL
Monterey, California

DTIC
ELECTE
DEC 09 1991
D
D

THESIS

Exploring Plasma Sheath Solutions
for Planar and Cylindrical Anodes

by

George Scott Brown

December 1991

Thesis Advisor: Oscar Biblarz

91-17303

91 1209 010

Unclassified

Security Classification of this page

REPORT DOCUMENTATION PAGE

1a Report Security Classification Unclassified	1b Restrictive Markings
2a Security Classification Authority	3 Distribution Availability of Report
2b Declassification/Downgrading Schedule	Approved for public release; distribution is unlimited.

4 Performing Organization Report Number(s)		5 Monitoring Organization Report Number(s)
6a Name of Performing Organization Naval Postgraduate School	6b Office Symbol *(If Applicable)* 31	7a Name of Monitoring Organization Naval Postgraduate School
6c Address *(city, state, and ZIP code)* Monterey, CA 93943-5000		7b Address *(city, state, and ZIP code)* Monterey, CA 93943-5000
8a Name of Funding/Sponsoring Organization	8b Office Symbol *(If Applicable)*	9 Procurement Instrument Identification Number
8c Address *(city, state, and ZIP code)*		10 Source of Funding Numbers

Program Element Number	Project No	Task No	Work Unit Accession No

11 Title *(Include Security Classification)* EXPLORING PLASMA SHEATH SOLUTIONS FOR PLANAR AND CYLINDRICAL ANODES

12 Personal Author(s) Brown, George Scott

13a Type of Report Master's Thesis	13b Time Covered From To	14 Date of Report *(year, month,day)* December 1991	15 Page Count 100

16 Supplementary Notation The views expressed in this thesis are those of the author and do not reflect the official policy or position of the Department of Defense or the U.S. Government.

17 Cosati Codes			18 Subject Terms *(continue on reverse if necessary and identify by block number)*
Field	Group	Subgroup	Plasma, Plasma Sheaths, Anode Sheaths, Cylindrical Anodes.

19 Abstract *(continue on reverse if necessary and identify by block number)*

Anode sheaths impact the operation of many practical plasma devices. This complex region is explored in detail for collisional, isothermal (identical specie temperatures), low-temperature plasmas, where sheath dimensions are in the micron range. The selected approach involves postulation of a specific electric field distribution with two shape factors. Previous research regarding planar anodes is verified and expanded upon using greater parameter ranges. 'z', a dimensionless quantity specifying plasma composition and condition, groups diverse plasmas into 'families' exhibiting similar sheath characteristics. 'η', a nondimensional ratio of electrical energy to thermal energy in the sheath, allows temperature effects to be studied. The investigation focuses on three disparate plasma families that span a z range of 1.1729 to 2.1493, at η values defined by plasma temperatures of $6000°K$, $3000°K$, and $300°K$. Results indicate that at lower temperatures, charge production in the outer sheath is generic to the electric field distribution, and that the sheaths themselves are nearly unaffected by substantial changes in temperature (i.e., η). Conversely, sheath density and extent are shown to vary significantly for differing z values. Newly-derived equations governing cylindrical anodes generate sheaths that are virtually identical to corresponding planar cases. It is shown that only those anodes whose radii are comparable to the plasma's 'characteristic radius' (γ) must be treated with the cylindrical formulation; non-vacuous plasmas would require micron-width anodes to be thus affected. Finally, an analytical approach yields solutions that confirm the numerical results, and offers an algebraic approximation for high-η plasmas.

20 Distribution/Availability of Abstract	21 Abstract Security Classification
X unclassified/unlimited same as report DTIC user	Unclassified
22a Name of Responsible Individual Oscar Biblarz	22b Telephone *(Include Area code)* (408) 626-8175	22c Office Symbol AA/Bi

DD FORM 1473, 84 MAR   83 APR edition may be used until exhausted   security classification of this page

All other editions are obsolete   Unclassified

Exploring Plasma Sheath Solutions For Planar and Cylindrical Anodes

by

George Scott Brown
Lieutenant Commander, United States Navy
B.S., United States Naval Academy, 1980

Submitted in partial fulfillment of the
requirements for the degree of

MASTER OF SCIENCE IN
AERONAUTICAL ENGINEERING
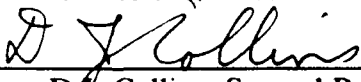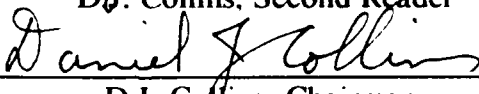
from the

NAVAL POSTGRADUATE SCHOOL

December 1991

Author: _____
George Scott Brown

Approved by: _____
O. Biblarz, Thesis Advisor

_____
D.J. Collins, Second Reader

_____
D.J. Collins, Chairman,
Department of Aeronautical Engineering

ii

ABSTRACT

Anode sheaths impact the operation of many practical plasma devices. This complex region is explored in detail for collisional, isothermal (identical specie temperatures), low-temperature plasmas, where sheath dimensions are in the micron range. The selected approach involves postulation of a specific electric field distribution with two shape factors. Previous research regarding planar anodes is verified and expanded upon using greater parameter ranges. 'z', a dimensionless quantity specifying plasma composition and condition, groups diverse plasmas into 'families' exhibiting similar sheath characteristics. 'η', a nondimensional ratio of electrical energy to thermal energy in the sheath, allows temperature effects to be studied. The investigation focuses on three disparate plasma families that span a z range of 1.1729 to 2.1493, at η values defined by plasma temperatures of 6000"K, 3000"K, and 300"K. Results indicate that at lower temperatures, charge production in the outer sheath is generic to the electric field distribution, and that the sheaths themselves are nearly unaffected by substantial changes in temperature (i.e., η). Conversely, sheath density and extent are shown to vary significantly for differing z values. Newly-derived equations governing cylindrical anodes generate sheaths that are virtually identical to corresponding planar cases. It is shown that only those anodes whose radii are comparable to the plasma's 'characteristic radius' (γ) must be treated with the cylindrical formulation; non-vacuous plasmas would require micron-width anodes to be thus affected. Finally, an analytical approach yields solutions that confirm the numerical results, and offers an algebraic approximation for high-η plasmas.

TABLE OF CONTENTS

ACKNOWLEDGMENT

My deep gratitude to Oscar Biblarz, Ph.D., who patiently taught plasma physics to a pilot.

I. INTRODUCTION

Various types of plasma devices have been in operation for over 30 years. Marshall's coaxial plasma gun [Ref. 1] was successfully accelerating volumes of hydrogen plasma as far back as the late 1950's. In the intervening years, the number of applications for plasma devices has steadily increased to include magnetohydrodynamic (MHD) power generation, laser pumping, strategic defense, and electromagnetic propulsion for interplanetary spacecraft. However, due to their somewhat complex nature, comparatively little is understood about the sometimes-destructive sheath regions surrounding the electrodes in every plasma device. This work attempts to further previous research efforts concerning description of the anode sheath.

As stated by Biblarz [Ref. 2], completely satisfactory anode sheath solutions do not exist for several plasma conditions; one such case involves steady, collisional, low-temperature, isothermal discharges. He then goes on to derive an involved, nonlinear differential equation that describes the entire plasma region affected by a planar anode, from the surface to the undisturbed plasma. A presumed (but 'shapeable') function describing the electric field in that region, selected after much deliberation [Ref. 2 and Ref. 3], ultimately allows charge production rates and electron/ion populations to be plotted as a function of distance from the anode. Nondimensional parameters make the solution profiles applicable to several families of plasmas.

In this work, numerical techniques are employed to verify the one previously solved case, and to explore planar anode solutions to several other plasma conditions. This can be readily accomplished due to the generality of the formulation and the ease with which the profiles can be produced. Sheaths and ambipolar regions are properly

1

generated for all cases. The effect of nondimensional parameter variations on the sheath is extensively investigated, and some general conclusions are hypothesized. In addition, an analytical technique is presented that supports the numerical results and allows for an accurate algebraic solution to low-temperature conditions. Finally, similar derivations produce equations that treat the cylindrical anode sheath problem: the equations and their profiles are then analyzed, and a comparison is made to planar anode findings.

II. THE CARTESIAN PROBLEM

This section discusses and validates one previous anode sheath research effort concerning steady, low-temperature collisional plasmas. In addition, several new parameter cases are examined and analyzed. The geometry of the Cartesian problem is illustrated in Figure 1.
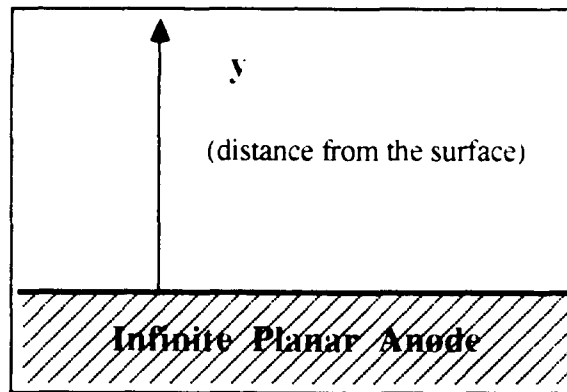
Figure 1 Cartesian Anode Geometry

A. DERIVATION REVIEW

Previous work by Biblarz [Ref. 2] treats the planar anode sheath problem in a one-dimensional Cartesian fashion, and is reviewed here as it forms the starting point for this work. Electric field intensity (E), electron and ion population densities (n_e and n_i), and all other relevant quantities are considered to vary only with linear distance (y) from the flat anode surface. The applicable relations are Gauss' equation and the two species continuity equations, as shown on the following page.

$$\frac{dE}{dy} = \left(\frac{e}{\varepsilon_0}\right)(n_i - n_e) \qquad (1a)$$

$$j_i = e\mu_i n_i E - eD_i\left(\frac{dn_i}{dy}\right) \qquad (1b)$$

$$j_e = e\mu_e n_e E + eD_e\left(\frac{dn_e}{dy}\right) \qquad (1c)$$

Note that e is the electron charge constant, ε_0 is the permittivity constant, the subscripts e and i indicate electron and ion particles, the j's are the species contributions to the total current density (i.e., $J = j_e + j_i$), the μ's are the particle mobilities, and the D's are the diffusion coefficients. Although this set does not fully constrain the problem (as an equation describing plasma reactivity, $\dot{n}_e$, is absent), any selection of a specific form for E(y) implicitly fixes that variable. It is of interest to explore the problem with 'guesstimates' of E(y) in order to facilitate solutions.

Reference 2 then introduces two new parameters, designated K^+ and K^-, which are defined by Equations (2a), (2b), and (2c). These K-terms are somewhat artificial parameters, although they are related to the total current. More meaningful is the derivative of K^+, which is directly proportional to the net production rate of charges, $\dot{n}_e$ (i.e., $(K^+)' \cong \dot{n}_e/D_i$).

$$K^+ \equiv \frac{j_i}{eD_i} + \frac{j_e}{eD_e} \qquad (2a)$$

$$K^- \equiv \frac{j_e}{eD_e} - \frac{j_i}{eD_i} \qquad (2b)$$

$$\text{and} \quad K^+ \approx -K^- + \frac{2J}{eD_e} \qquad (2c)$$

4

Manipulation of the previous six equations and the Einstein relation (which relates the mobilities to the diffusion coefficients) yields the isothermal differential equation below. Note that k is the Boltzmann constant, and that all primes denote derivatives with respect to the variable y.

$$\frac{kT_0}{e}\left(\frac{K^\cdot}{E}\right)' + K^\cdot = \frac{2J}{eD_\iota} + \left[\left(\frac{\varepsilon_0}{kT_0}\right)EE' - \left(\frac{kT_0\varepsilon_0}{e^2}\right)\left(\frac{E'''}{E} - \frac{E'E''}{E^2}\right)\right] \tag{3}$$

Advanced knowledge of E(y) considerably facilitates the solution of Equation (3). Biblarz' justification for the selected form of E(y) is detailed elsewhere [Ref. 2 and Ref. 3]. This function meets several critical conditions inherent to the stated problem, including the required distribution of E and the behavior of both K-terms at the boundaries. The function is reproduced as Equation (4) below.

$$E(y) = E_\cdot \exp\left[\frac{A}{(y+a)^2}\right] \tag{4}$$

The parameters 'a' and 'A' are shape factors, where 'a' is of the order of the sheath length, and 'A' relates to the physical parameters $\Delta\phi_\cdot$ and E. (as discussed on pages 7 and 8).

Substitution of the chosen E(y) into Equation (3), followed by an order-of-magnitude analysis, the nondimensionalization of the parameters in accordance with Figure 2, and further simplification based on field and current properties at the electrode and in the undisturbed plasma, all combine to yield the governing differential equation and boundary condition of Figure 3.

$$\tilde{y} = y/a \quad , \quad E/E_0 = \left(E_\lambda/E_0\right)\exp\left[\frac{z^2}{(\tilde{y}+1)^2}\right] \quad , \quad \tilde{K}^\cdot = \frac{K^\cdot}{J/eD_e}$$

$$\eta \equiv \left(\frac{eE_0 a}{kT_0}\right) \quad , \quad z \equiv \left(\frac{\sqrt{A}}{a}\right)$$

Figure 2   Nondimensionalized Parameters

$$\left(\frac{1}{\eta}\right)\frac{d}{d\tilde{y}}\left[\frac{\tilde{K}^+}{E/E_0}\right] + \tilde{K}^\cdot + \frac{(E/E_0)^2}{(\tilde{y}+1)^3} = 2$$

$$\tilde{K}^\cdot(0) = 1$$

**Figure 3   Simplified Nondimensional Differential Equation
and Boundary Condition Governing the 1-D Cartesian Problem**

The introduction of the dimensionless parameters η and z further generalizes the problem, in that one solution to the above equation can be applicable to a large number of specific dimensional cases. Their additional significance is discussed in a subsequent section.

As will be seen, both numerical and analytical solutions to the equations of Figure 3 are possible, yielding profiles of $\tilde{K}^\cdot$ and $\left(\tilde{K}^\cdot\right)'$ that are a function of distance from the planar anode.

Further manipulation of Equations (1) and (2) derives relations that produce electron and ion population profiles [Ref. 2]. A more precise form of these equations is given in Figure 4. Note that specific solutions for $\tilde{K}^\cdot$ are required to generate the $\tilde{n}$-profiles. Several distinct cases in the next section yield population curves that

clearly illustrate the propriety of the sheath and ambipolar regions in the plasma near the anode.

$$\bar{n} = \frac{n_i}{n} = \left(\frac{1}{2}\right)\left[\left(\frac{\dot{K}}{E/E_o}\right)\left(\frac{E_i}{E_o}\right)+\left(\frac{\varepsilon_o kT_o}{e^2 n\ a}\right)\left[\frac{6z^2}{(\bar{y}+1)^2}+\frac{4z^2}{(\bar{y}+1)^3}\right]+\left(\frac{\varepsilon_o E_o}{en\ a}\right)\left(\frac{E}{E_o}\right)\left[\frac{-2z^2}{(\bar{y}+1)^2}\right]\right]$$

$$\bar{n}_c = \frac{n_c}{n} = \left(\frac{n_i}{n}\right)+\left(\frac{\varepsilon_o E_o}{en\ a}\right)\left(\frac{E}{E_o}\right)\left[\frac{2z^2}{(\bar{y}+1)^2}\right]$$

Figure 4   Ion and Electron Population Equations

Reference 2 also presents two more useful relations from analysis involving physical observations (Equations (5) and (6)). Recent analysis has proven that the infinite series in Equation (6b) converges for all values of z. These are combined and manipulated to yield the two important equations of Figure 5, which allow determination of the parameters z and η. The procedure is as follows:

- the type of gas defines the anode potential drop $\Delta\phi$ (which is essentially equivalent to the ionization potential of the gas)

- the particular case or application specifies E, and n

- z is then found by iteration of the implicit equation at the top of Figure 5

- the choice of T_o locks in η using the bottom equation in Figure 5

$$a = \left(\frac{2\varepsilon_o E}{en}\right)z^2 \exp(2z^2)$$ (5)

$$\Delta\phi = E\sqrt{A}\ f(z)$$ (6a)

$$\text{where}\quad f(z) = z\sum_{m=0}\frac{z^{2m-1}}{(2m-1)m!}$$ (6b)

7

$$\left(\frac{en \ \Delta\phi_a}{2\varepsilon_0 E^2} \right) = z^3 f(z) \exp(2z^2)$$

$$\eta = \left(\frac{e\Delta\phi_a}{kT_0} \right) \exp(z^2) \bigg/ z \ f(z)$$

Figure 5   Equations That Yield z and η

Specific values of z and η allow computation of the electric field parameters A and a (Equations (5) and (6)), which in turn yield the tailored form of the E distribution (Equation 4), and ultimately permit the generation of $\tilde{K}^+$, $(\tilde{K}^-)'$, and $\tilde{n}_e$ profiles in the plasma regions close to the anode (equations of Figure 3 and Figure 4).

B. NUMERICALLY SOLVED CASES

1. Procedure

Numerical solution of the governing differential equation (Figure 3) can be achieved with a fourth-order Runge-Kutta FORTRAN program. First the dependent variable is redefined and the equations are rewritten in accordance with Figure 6.

$$\frac{d}{d\bar{y}}[w] = 2\eta - \eta\left(\frac{E}{E_0} \right) w - \eta\left[\frac{(E/E_0)'}{(\bar{y}+1)^3} \right]$$

$$w(0) = 1$$

$$\text{where} \quad w(\bar{y}) \equiv \frac{\tilde{K}^+(\bar{y})}{E(\bar{y})/E_0}$$

Figure 6   Modified 1-D Cartesian Differential Equation and Boundary Condition for Numerical Solution

8

Application of the Runge-Kutta scheme computes the value of w at each $\bar{y}$.
The data for $\bar{K}^*$ is then recovered with the division of each w datapoint by the
corresponding value for $E(\bar{y})/E_0$. $\left(\bar{K}^*\right)'$ data are extracted with the following steps
for each value of $\bar{y}$:

- compute w' using the defining differential equation (Figure 6)
- perform the operation below (derived from the Quotient Rule)

$$\frac{d}{d\bar{y}}[\bar{K}^*(\bar{y})] = \left\{ w'\left(\frac{E}{E_0}\right)^{\cdot} + \bar{K}^*\left(\frac{E}{E_0}\right)' \right\}\left(\frac{E_\cdot}{E}\right) \tag{7}$$

Finally, the $\bar{n}_e$ profiles are computed as a function of $\bar{y}$ using the available
information and the equations of Figure 4. A single computer routine can be made to
perform all of the required operations (see Appendix A); the resulting data are then
plotted.

Note again that this technique is substantially simpler than alternate methods
that do not presume a specific form of E(y). Ensuing discussions address the
advantages and disadvantages of this approach.

2. Case I: the Nitrogen Problem

The first specific case involves verification of an earlier example [Ref. 2]. A
planar anode in contact with nitrogen plasma was analyzed under the following
conditions (nitrogen is a common discharge gas with well-known properties):

- nitrogen's anode potential drop ($\Delta\phi_a$): 15.51 V (singly ionized)
- the electric field strength in the undisturbed plasma ($E_\cdot$): 12,000. V/m
- the particle density ($n_\cdot$): 10^{19} m^{-3}
- the temperature: 6000°K

The expression used to approximate f(z) (Equation 6a) was truncated after 13 terms, producing an error in the calculation of z which is on the order of $10^{-5}\%$. Using the given data, the following parameters result:

- $z = 1.75626$
- $\eta = 99.12285$
- $a = 1.95421 \times 10^{-4}$ m and $A = 1.17793 \times 10^{-7}$ m^2
- $E_o = 262,265.$ V/m

The computed value for E_o (obtained using Equation 4) relates specifically to all plasmas that are defined by the above values of z and η: this includes nitrogen plasma at the stated conditions. The normalized electric field $E(\bar{y})$ for this case is shown in Figure 7. Note that the field decreases monotonically and abruptly to a constant value in the undisturbed plasma. as is required of the model.

The corresponding $\tilde{K}^*$. $\left(\tilde{K}^*\right)'$, and $\tilde{n}_{e,i}$ profiles are presented in Figure 8 and Figure 9. Note that those Figures also represent all other plasma cases whose gas composition. density. temperature. and electric field intensity are defined by $z=1.75626$ and $\eta=99.12285$. Figure 9 clearly illustrates the distinct sheath and ambipolar regions present for this general case.* The K-term profiles of Figure 8 likewise exhibit expected characteristics. with $\tilde{K}^*$ rising roughly monotonically from $+1$ to $+2$. while $\left(\tilde{K}^*\right)'$ decreases to near-zero at the outer edge of the sheath. The leftmost downturn of $\left(\tilde{K}^*\right)'$. while possibly correct. is quantitatively suspect since the model of ionization by electron impact breaks down at the fringe of the collisionless region (i.e., for $y/a \leq \sim 10^{-2}$).

---

* The sheath is that small region. extending away from the anode. where the electron and ion populations are not equivalent; in the ambipolar region. the ratio of oppositely-charged particles is 1:1. but the populations of both are less than those that exist in the 'undisturbed plasma'
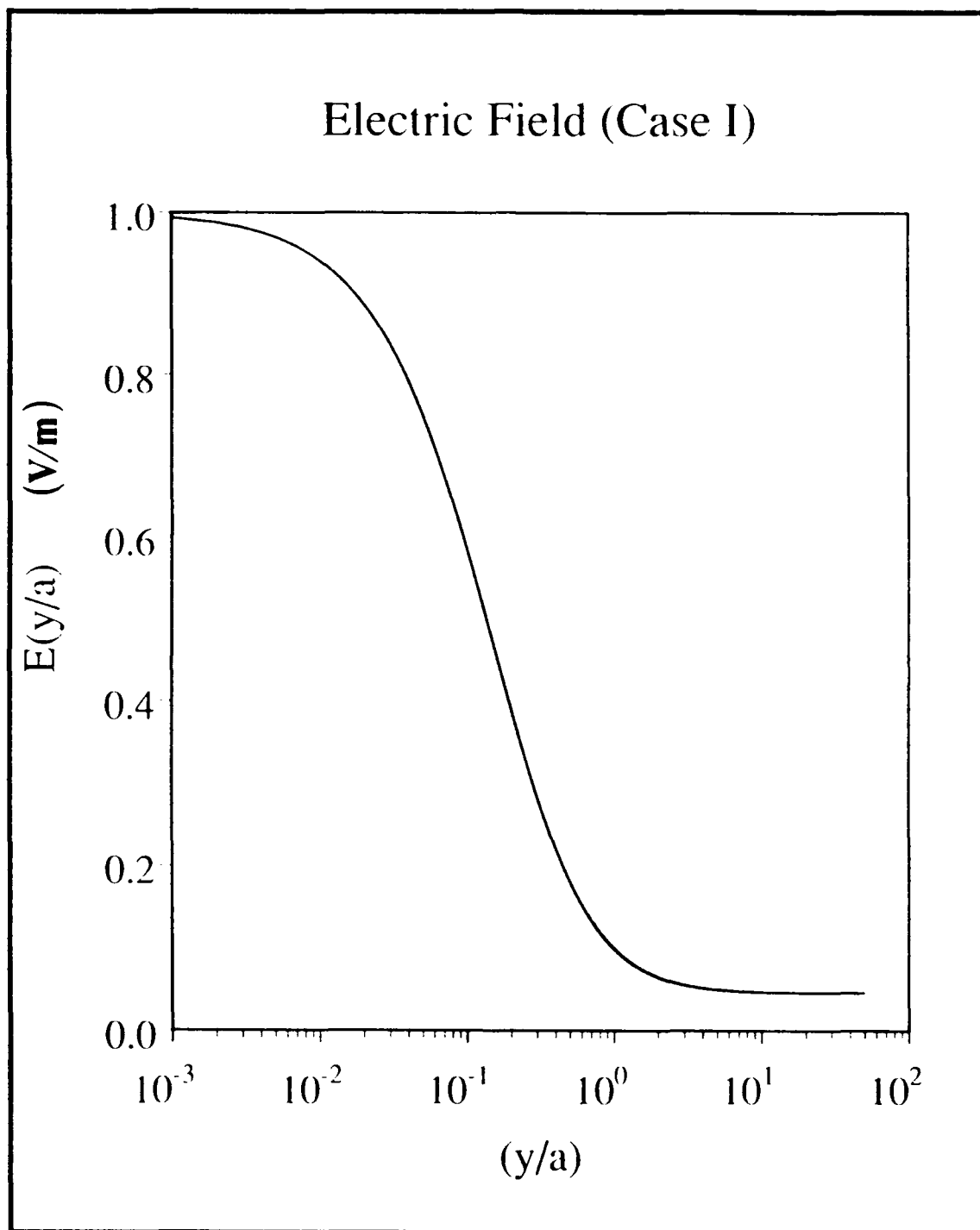
Figure 7 Normalized Electric Field (z=1.75626, η=99.1229)

11

$\tilde{K}$-term Profiles (Case I)

Legend: Kplus (dashed), (Kplus)' (solid)

Axes: $[\tilde{K}^+]'$ (left), $\tilde{K}^+$ (right), (y/a) (horizontal)

Figure 8   K-term profiles (z=1.75626, η=99.1229)

12

Figure 9 $\tilde{n}_{e,i}$ profiles (z=1.75626, η=99.1229)

13

As the parameter 'a' specific to Case I is known, it can be seen that the nitrogen plasma sheath for the particularly defined discharge extends approximately 0.1 mm out from the planar anode. Similarly. the region of undisturbed plasma for such a device begins approximately 6 mm from the anode surface. Both of these results are in accordance with expectations. the generalities of which were obtained after much deliberation [Ref. 4].

These numerically-obtained Case I results confirm the work of Reference 2. Postulation of a suitable ionization/recombination mechanism is left to that discourse. The remaining objectives of this work are as follows:

- investigation of the effects which are produced as the defining parameters are varied over a wide yet practical range

- presentation of an analytical solution to the general Cartesian anode sheath problem

- derivation and examination of the related Cylindrical anode sheath problem

3. Cases II and III: Varying Temperature in the Nitrogen Problem

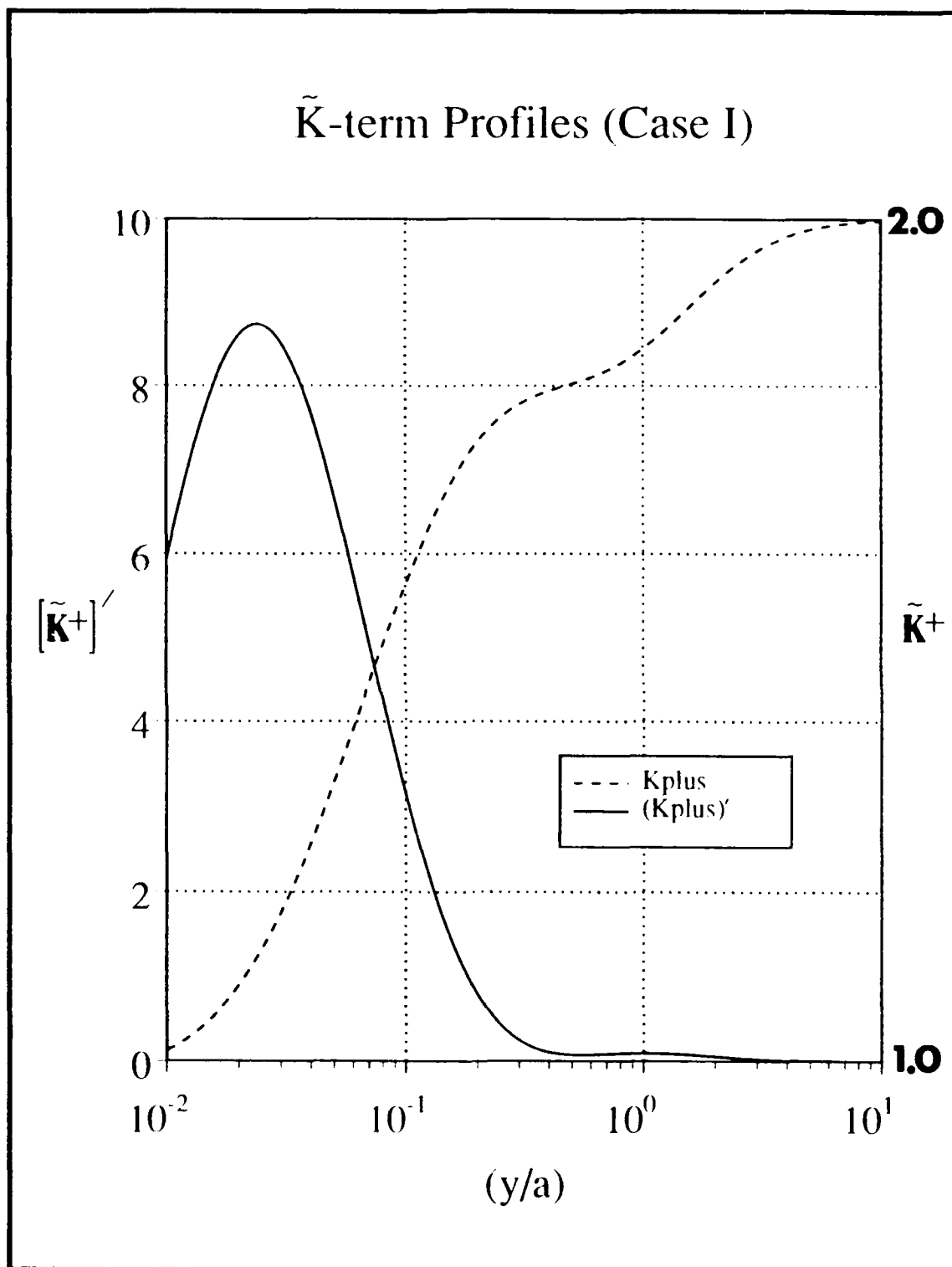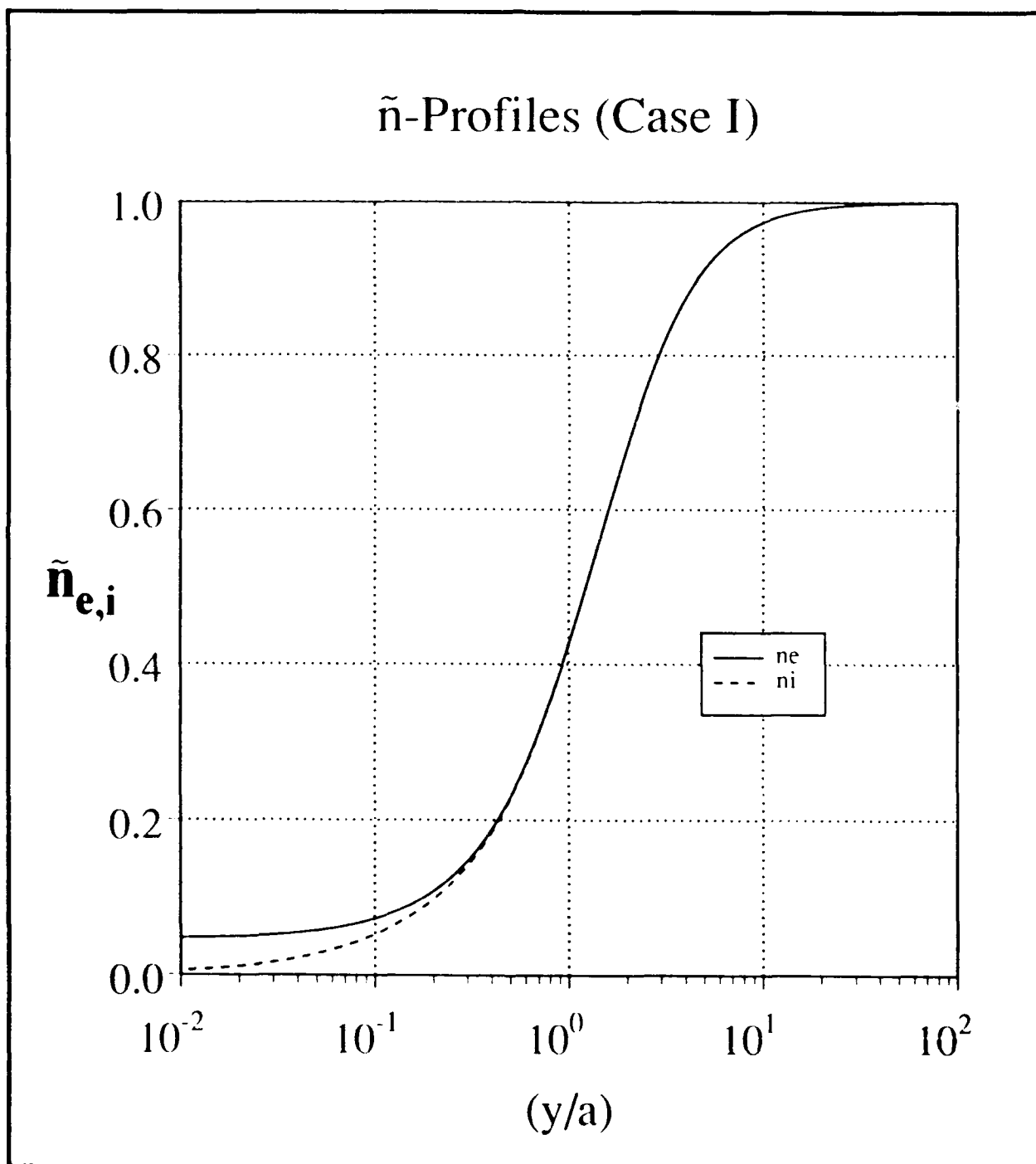Comprehensive investigation of the nitrogen plasma problem requires consideration of temperature's effect on the anode sheath. Thus. while all other Case I conditions are held constant. two somewhat more practical values for the isothermal temperature are considered:

- Case II fixes T_0 at 3000°K

- Case III sets T_0 at 300°K (this is representative of discharges in laser pumping)

Temperature-only variations impact η exclusively: z and the normalized electric field $E(\bar{y})/E_0$ (including the inherent factors A and a) are unaffected. Since η is by definition inversely proportional to T_0 (Figure 2). the decreased temperatures of Cases II and III signify larger values of η. As a result. the first-order derivative term in the governing differential equation (Figure 3) becomes less influential at the lower temperatures. Indeed. for the conditions of Case III. the contribution of the

14

derivative term is negligible (note. however. that this circumstance does not nullify the validity of the formulation; the equation does not become degenerate).

Application of the lower equation in Figure 5 yields η values of 198.246 and 1982.46 for Case II and Case III, respectively. The K-term profiles for these general cases are presented in Figures 10 and 11. Both cases exhibit the same general K-term tendencies that have been recognized previously, with minor variations that illustrate the decreasing importance of the net-ionization term.

The effect of temperature variation (or, equivalently, η variation) on a plasma in the anode region is explored using Figures 12 and 13, which directly compare the $\tilde{K}'$ and $(\tilde{K}')'$ profiles of the three cases. One significant observation, contributed by Biblarz subsequent to Reference 2, hypothesizes that the asymptotic behavior of the K-terms with decreasing temperature reflects the approach to ionization that is generic to the electric field distribution; the overall results are thus independent of the details of ionization and recombination. As an important practical example, measurements of charge density would not reflect relevant details of the ionization/recombination mechanisms.

Conversely, the $\tilde{n}_c$ profiles for this general $z=1.75626$ case are nearly unaffected by the changes in temperature. Figure 14 illustrates charged particle curves that exhibit only a barely perceptible shift of position over the entire range of temperatures tested. This unexpected result has substantial implications; the most significant of these is the acceptability of the isothermal-particle assumption (i.e., the assertion that $T_c = T_i = T_n$). Though such a premise may be unrealistic, its validity appears to be inconsequential to the population profiles. Electric-field effects dominate any temperature effects in the cases examined. In fact, the physical significance of η (stated in Reference 2 as a ratio of electrical to thermal energy) predicts such dominance with its large magnitudes.
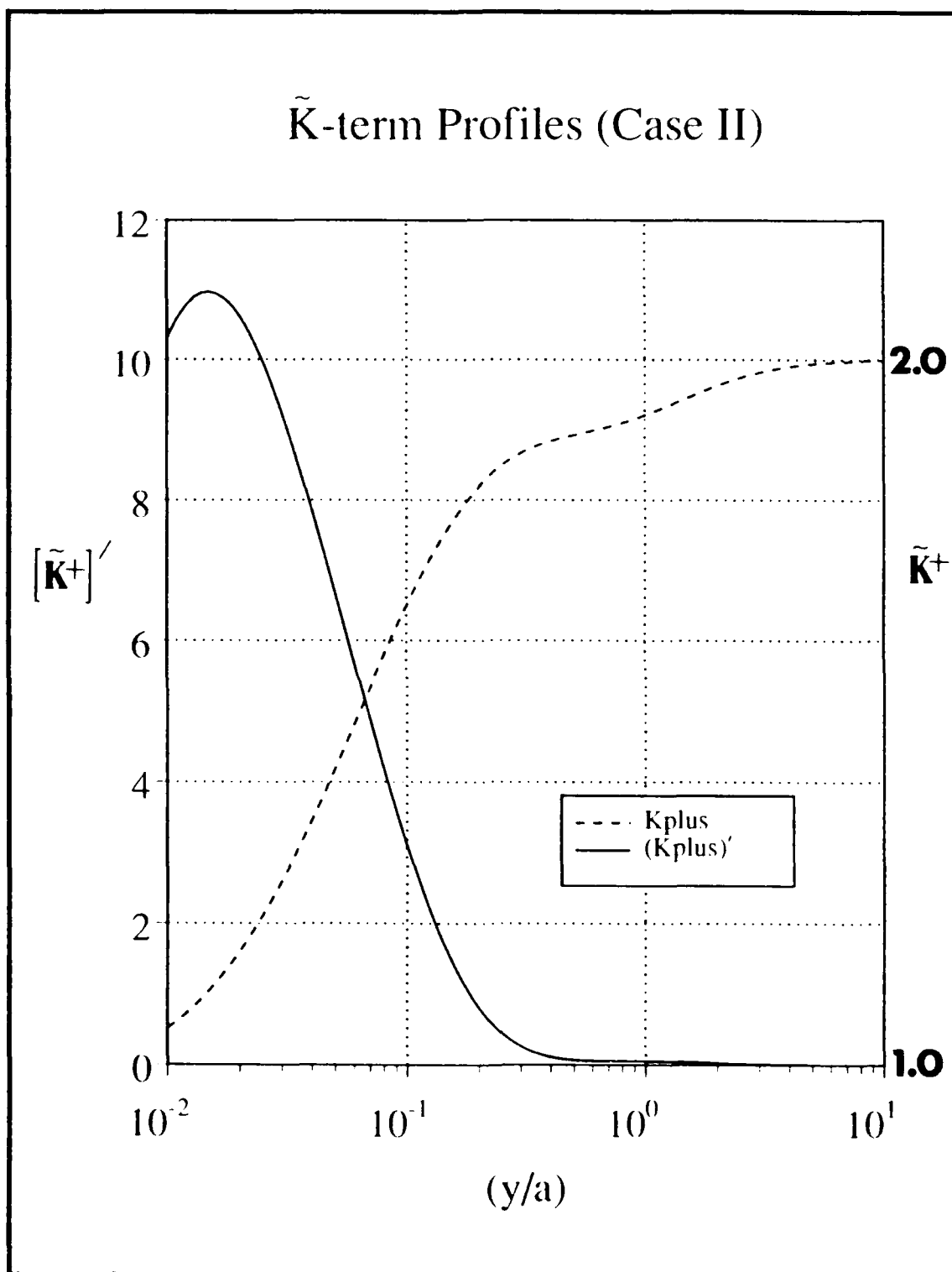
Figure 10 K-term profiles $(z=1.75626, \eta=198.246)$

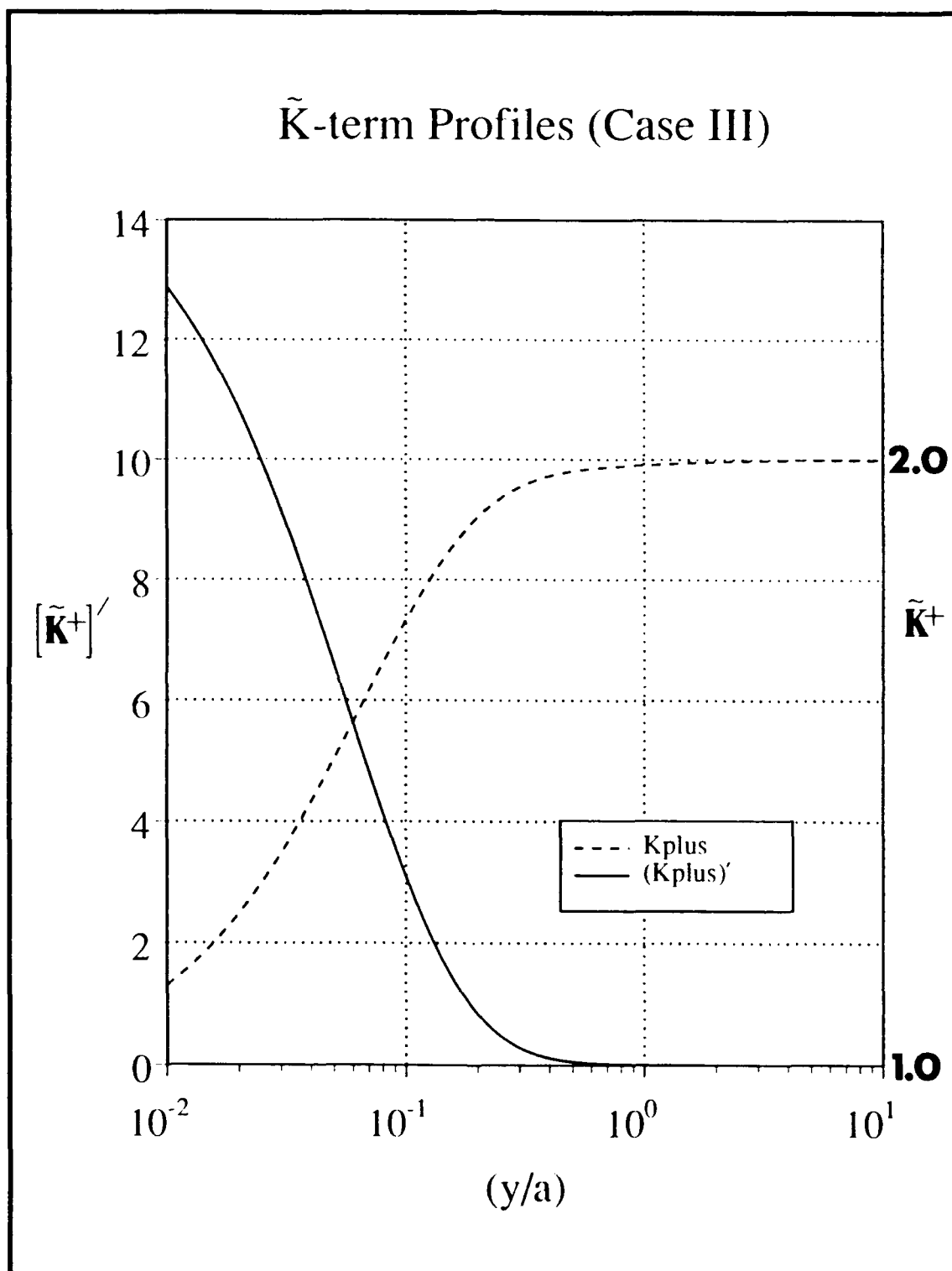**Figure 11   K-term profiles (z=1.75626,   η=1982.46)**
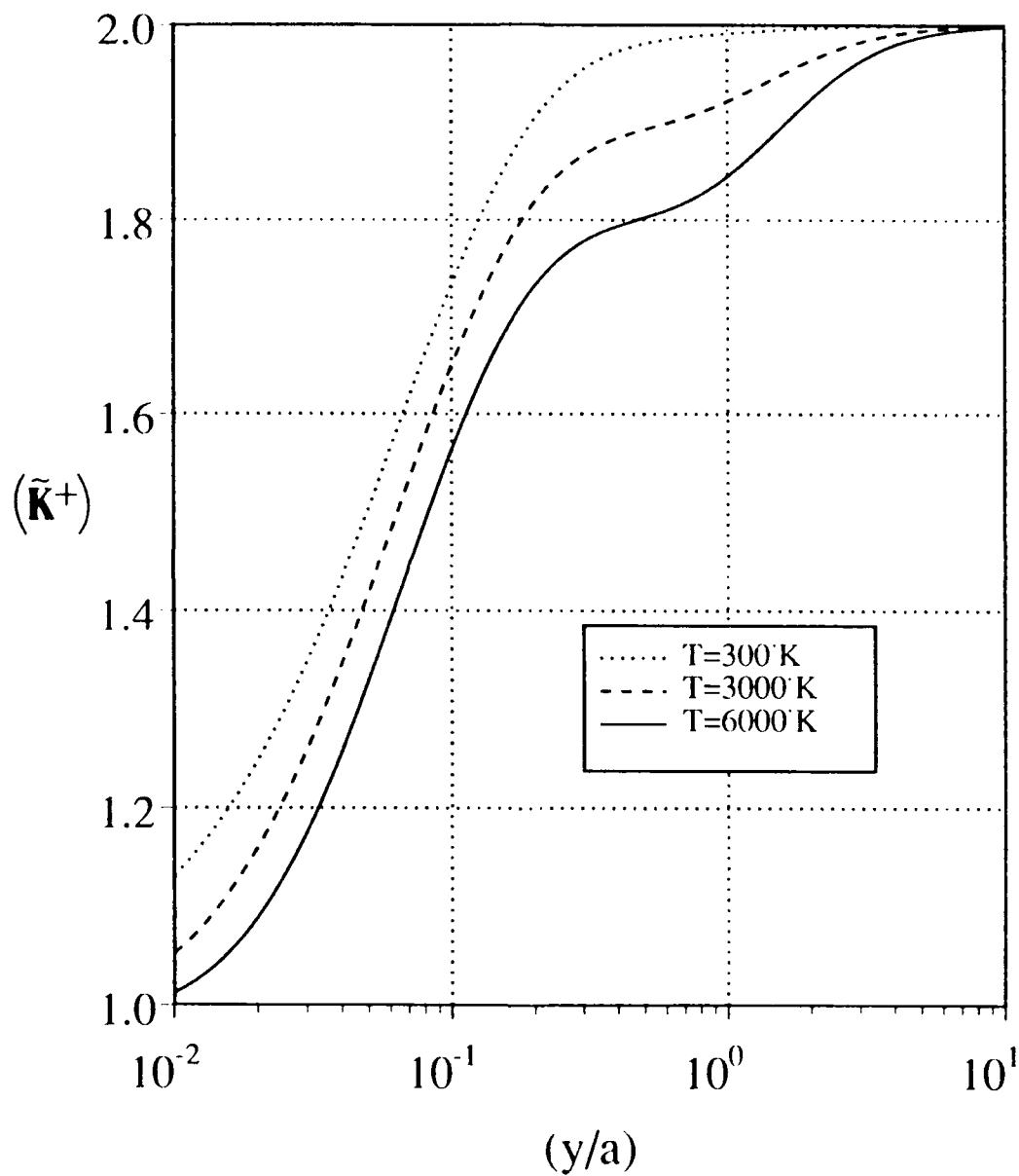
Figure 12 $\tilde{K}^+$ profiles (z=1.75626)
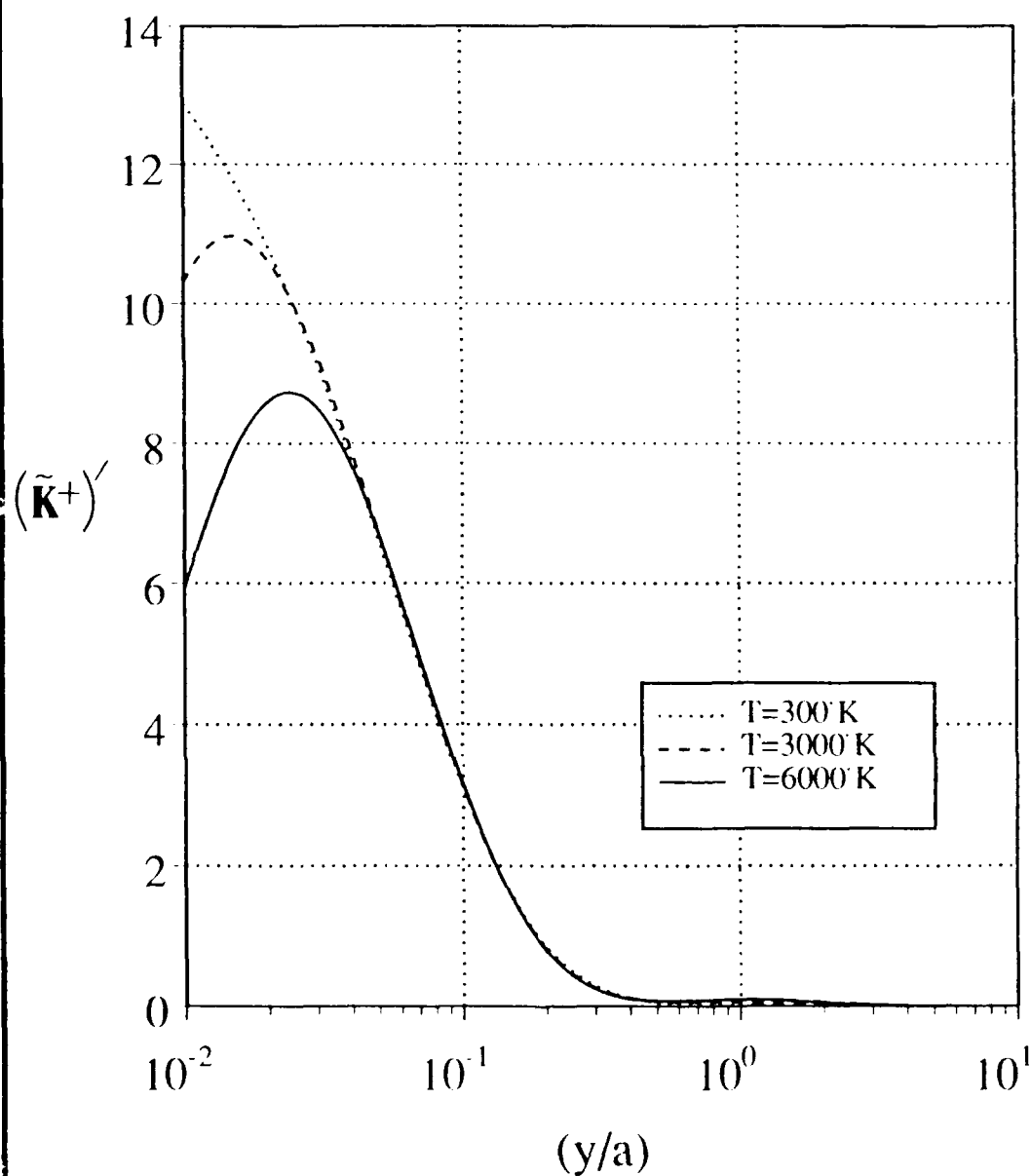
Figure 13 $(\tilde{K}^{+})'$ profiles   (z=1.75626)

19

ñ-Profiles for Varying Temperature
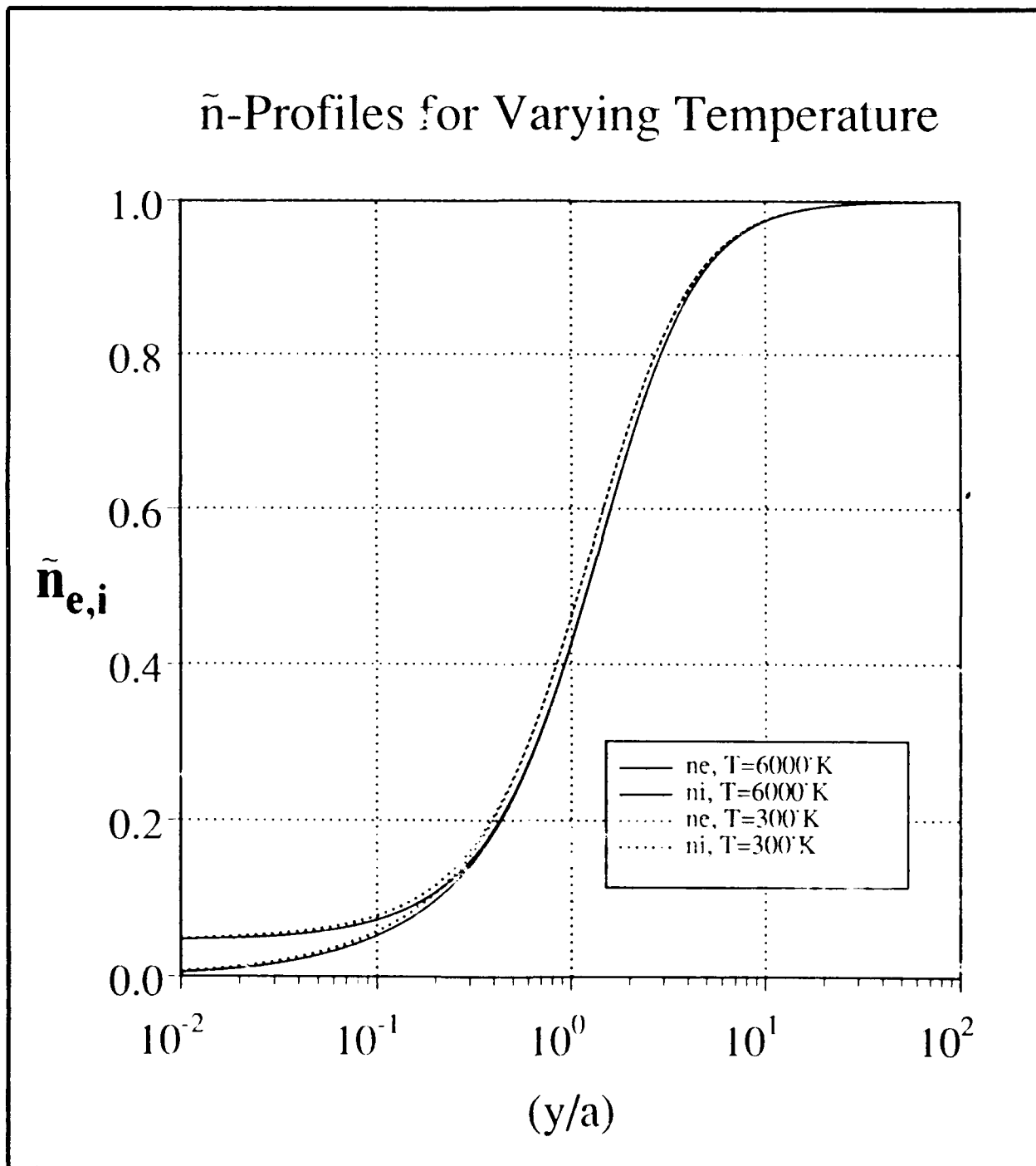
Figure 14 $\tilde{n}_{e,i}$ profiles (z=1.75626)

C. EXPLORING THE ENVELOPE FOR z AND η

The foregoing results include a preliminary investigation into the effect of η-variation on the planar anode sheath. This upcoming section more fully explores how changes in the parameters z and η impact the sheath region.

1. Practical Extremes of z

The parameter z is a dimensionless representation of three basic variables ($\Delta\phi_a$, $E_\cdot$, and $n_\cdot$) that specify the condition of a plasma; several different gases, at differing densities and field strengths, can be related by their equivalent z values. Various diverse plasmas belonging to the same 'z-family', at the same temperature, would theoretically exhibit identical sheath characteristics. Using the technique discussed previously, anode sheaths for plasmas defined by two limiting values of z are examined.

Singly-ionized elements possess anode potential drops ($\Delta\phi_a$) that range from 24.46 Volts (helium) down to 3.87 Volts (cesium), with the low values being preferred. Common densities ($n_\cdot$) for these type collisional plasmas vary approximately from $10^\cdot$ to $10^{\cdot\cdot}$ particles per cubic meter. Finally, reasonable field strengths in the undisturbed plasma ($E_\cdot$) are somewhat arbitrarily set from 5000 to 30,000 Volts per meter. Application of the upper equation in Figure 5 yields the following 'practical' extremes for z:

$$1.1729 \leq z \leq 2.1493 \qquad (8)$$

This relatively small numerical range represents an extremely diverse grouping of plasmas; z is a decidedly sensitive parameter. Small z values represent those plasmas with small potential drops and low densities that are subjected to very high electric fields (e.g., low density cesium at 30,000, V/m). Plasmas with large z values are characterized by gases with large potential drops, at conditions of high

21

density and low field strength (e.g., high pressure helium at 5000. V/m). By way of comparison, the nitrogen plasma considered earlier in this work (median potential drop and density, small field strength) has a slightly-larger-than-median z value of 1.7563.

Values for η are required to completely constrain the problem, which entails the choosing of one or more temperatures. To facilitate direct comparisons, the same arbitrary quantities for T_0 that have been considered for the nitrogen case are designated as the standard values (i.e., $6000°K$, $3000°K$, and $300°K$).

Consequently, numerical sheath solutions are next generated and examined for these forementioned limiting conditions:

- 'Small z' plasmas (z= 1.1729) at the three standard temperatures (η= 16.4135, 32.8269, and 328.269 for T_0 at $6000°K$, $3000°K$, and $300°K$)

- 'Large z' plasmas (z= 2.1493) at the standard temperatures (η= 257.563, 515.125, and 5151.25 as T_0 decreases to $300°K$)

2. Sheath Solutions for 'Small z' Plasmas

K-term profiles for the 'small z' plasmas (at the three standard temperatures) are depicted in Figures 15, 16, and 17. Qualitatively, each of these curves displays the same previously noted characteristics inherent in the nitrogen plasma curves: monotonically increasing and well-behaved $\tilde{K}^*$, and a rate-of-charge-production term $\left(\tilde{K}^*\right)'$ that decreases and vanishes at the outer edge of the sheath. As before, the leftmost downturn of $\left(\tilde{K}^*\right)'$ is quantitatively suspect at the fringe of the collisionless region.

These reassuring results extend to the composite curves of Figures 18 and 19, which depict K-term profile variations as a function of temperature (i.e., η) changes. In particular, the charge production rate curves of Figure 19 again illustrate the striking implication that charge production in the outer sheath is independent of the
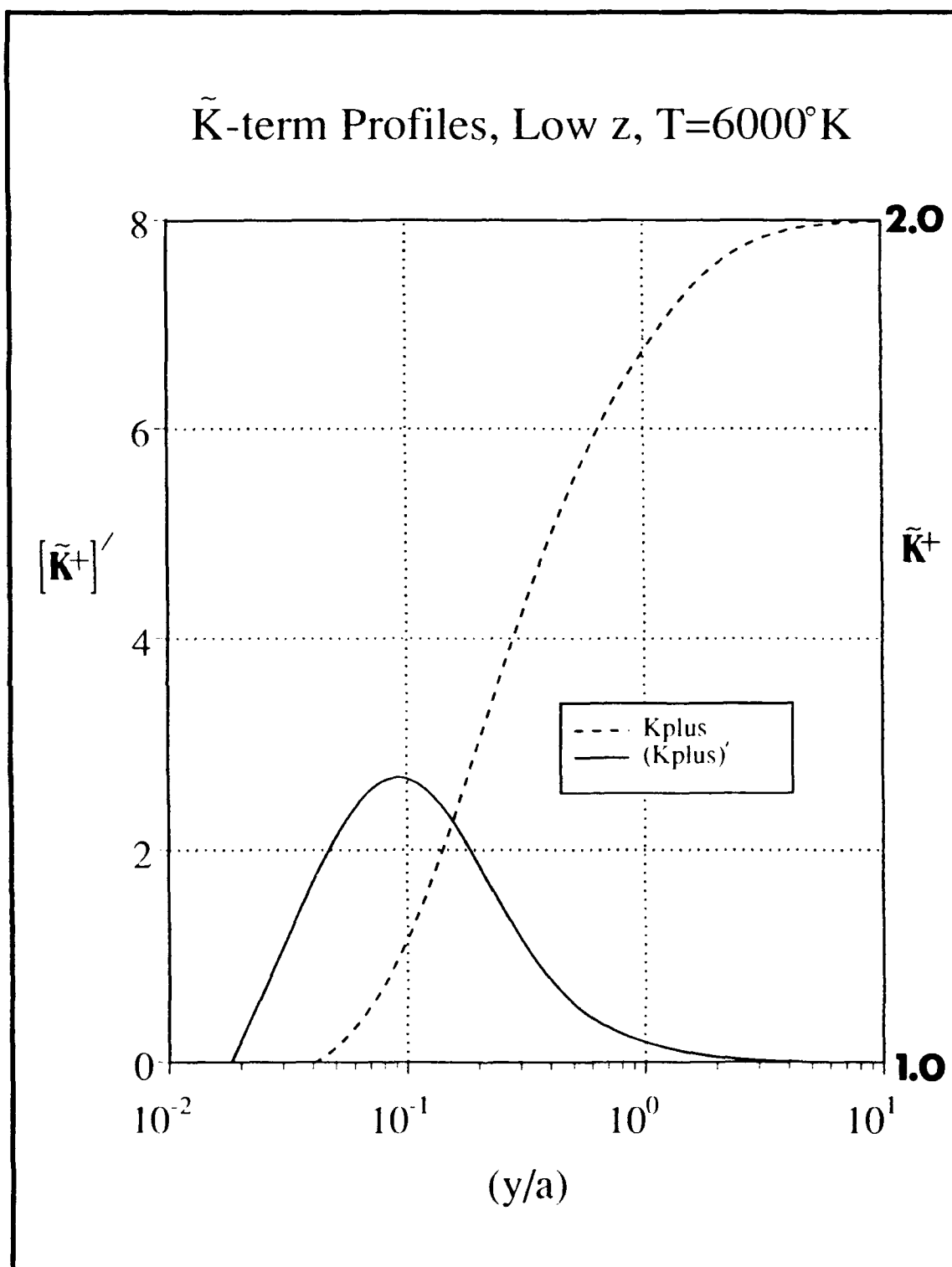
Figure 15   K-term profiles (z=1.1729, η=16.4135)

23
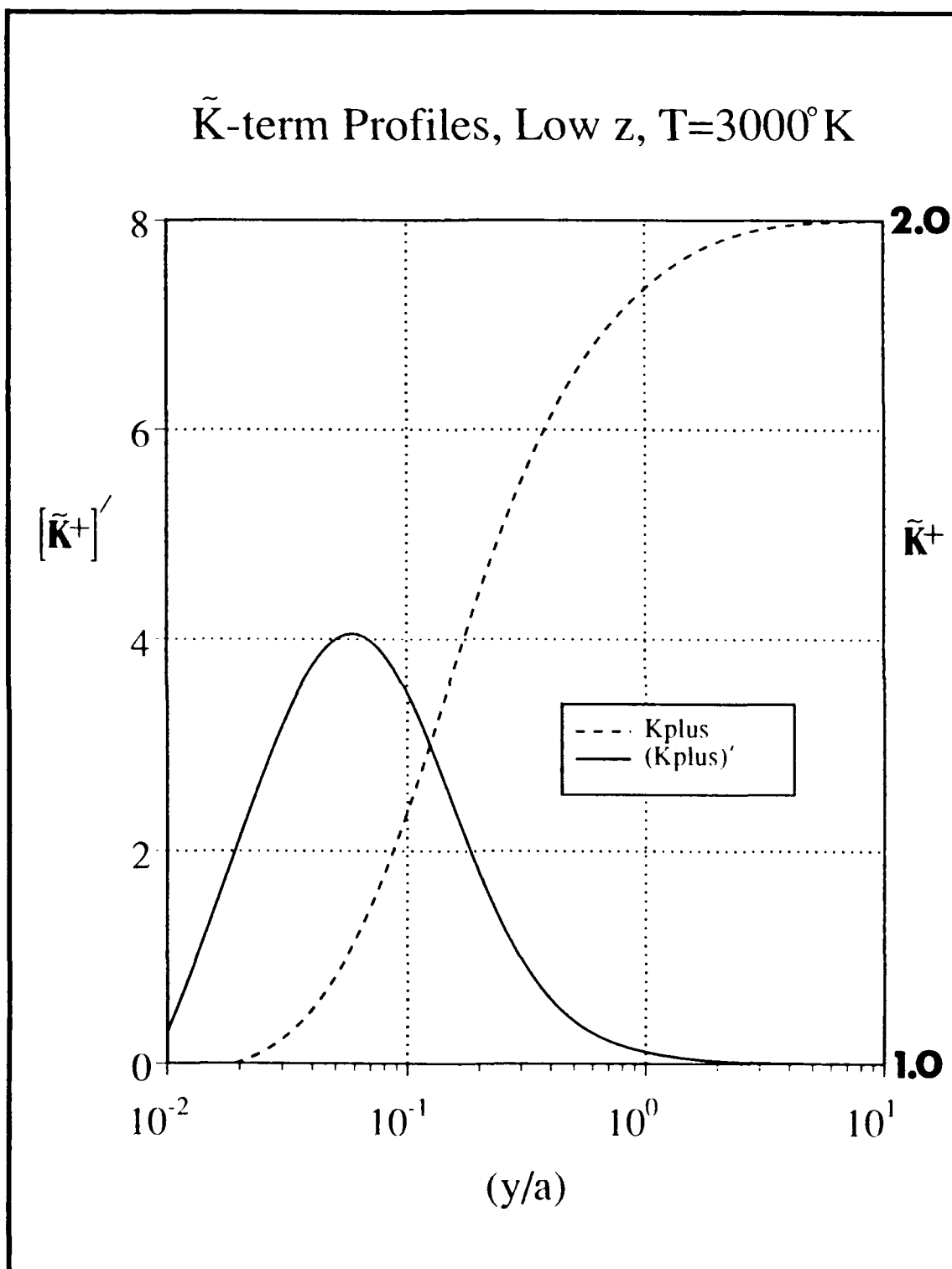
Figure 16   K-term profiles (z=1.1729, η=32.8269)

24
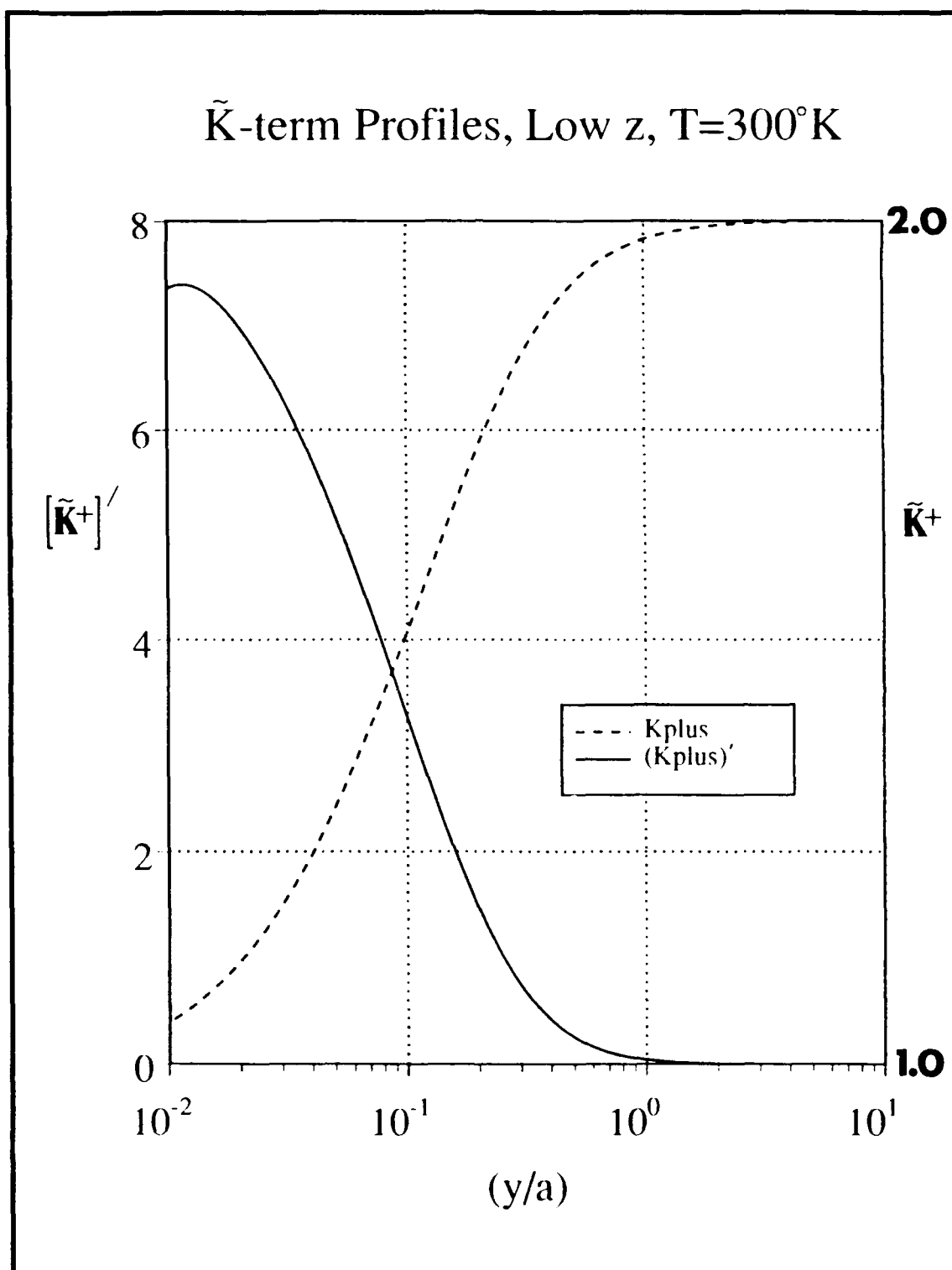
Figure 17 K-term profiles (z=1.1729, η=328.269)

$\tilde{K}$plus Profiles, Low z, Various Temp.
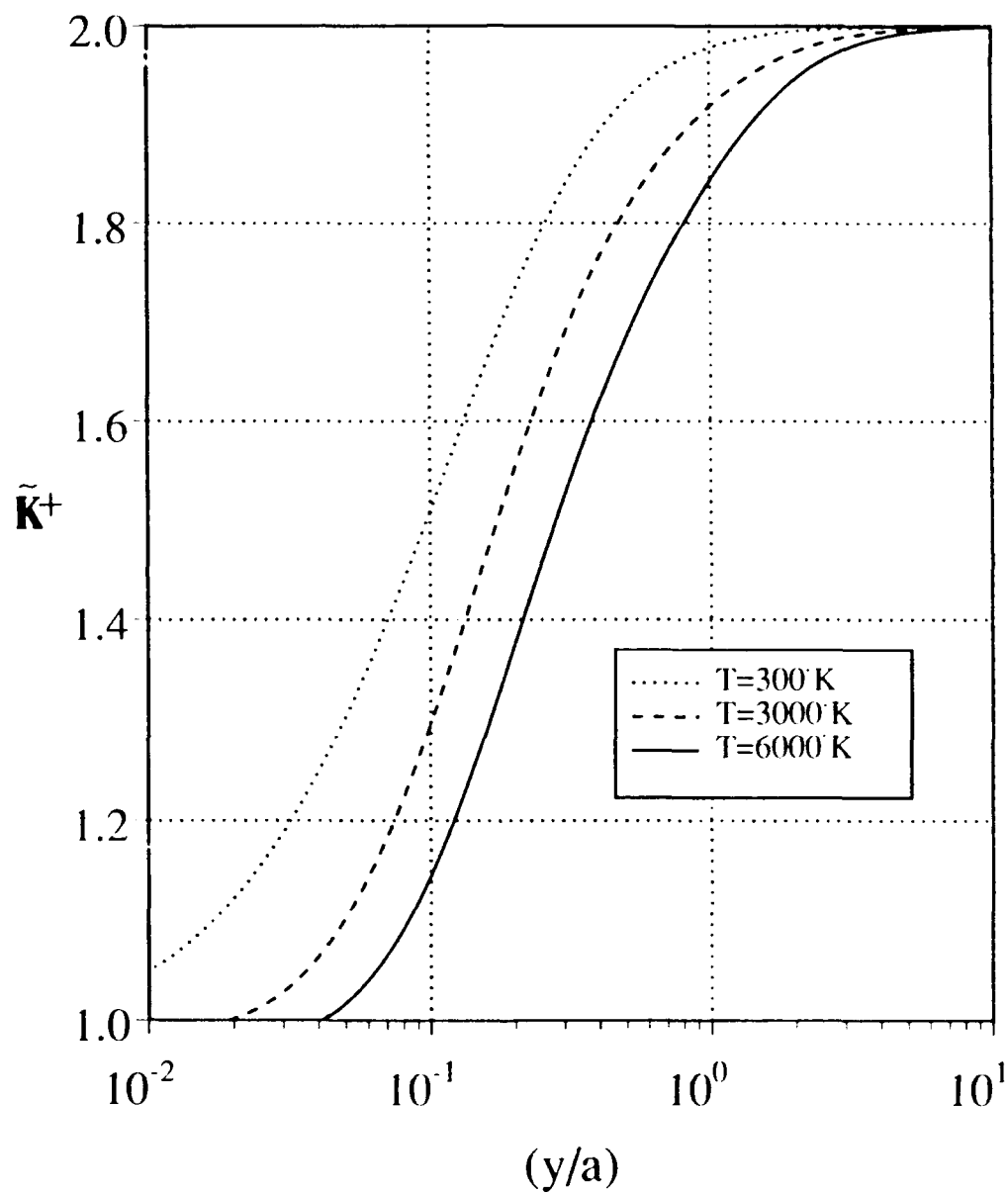
Figure 18 $\tilde{K}^+$ profiles (z=1.1729)

26

(K̃plus)′ Profiles, Low z, Various Temp.
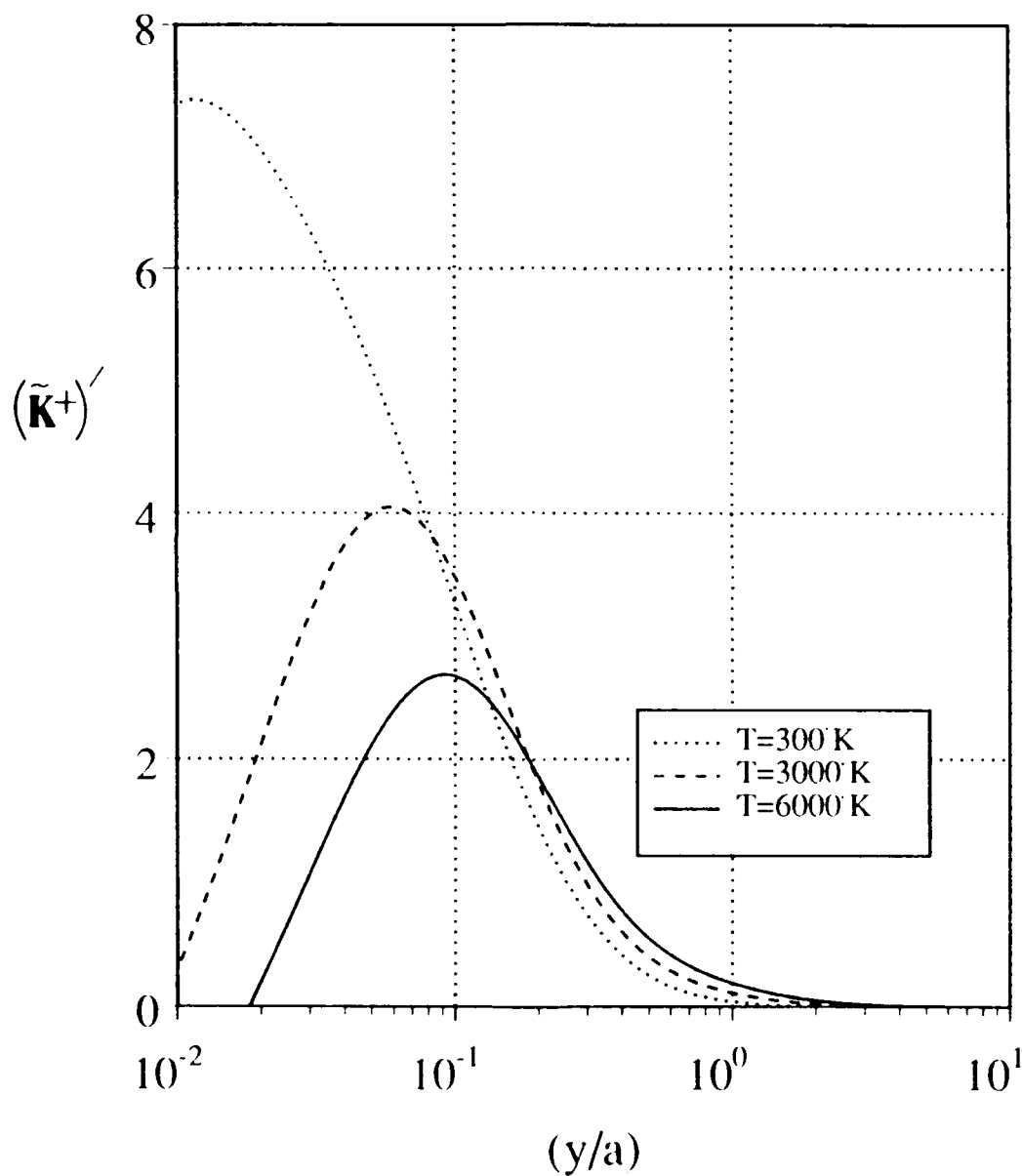
Figure 19 $\left(\tilde{K}^{\cdot}\right)$ profiles   (z=1.1729)

27

temperature. Moreover, the inner sheath once again sees an increase in the net production of charges as the temperature decreases.

Electron and ion population profiles for the 'small z' plasmas are given in Figure 20. As with the nitrogen case (and other plasmas of that z-family), the sheath and ambipolar regions are clearly visible and quite appropriate, while the population curves themselves again appear to be nearly unaffected by large variations in temperature.

Such qualitative observations for the 'small z' plasmas indicate that previous impressions concerning 'median z' plasmas (e.g., nitrogen) are not limited to that one category, but are possibly characteristic of all collisional low-temperature plasmas. The sheath profiles generated for the 'large z' cases of the next section further confirm this hypothesis.

Quantitative deviations in the sheath due to the change of z are addressed in a later section.

3. Sheath Solutions for 'Large z' Plasmas

The high density, small field 'large z' plasmas continue the trends established by the other collisional plasmas, albeit with some minor differences. One such difference is illustrated by the K-term profiles of Figures 21, 22, and 23. The curves display the same general traits of the other plasmas, with the exception that the $\tilde{K}{}^{\cdot}$ curve no longer climbs monotonically. This small anomaly becomes more pronounced at higher temperatures (Figure 21), yet does not appear to significantly impact the charge production rate curves, which still behave as expected.

Similarly, there are no surprises in the composite curves of Figures 24 and 25. In fact, the $\left(\tilde{K}{}^{\cdot}\right)'$ curves of Figure 25 demonstrate even more strikingly the generic, electric-field-dependent nature of ionization and recombination in the sheath.

ñ-Profiles, Low z, Varying Temp.

Legend:
- ne, T=6000 K
- ni, T=6000 K
- ne, T=300 K
- ni, T=300 K

Axis labels: $\tilde{n}_{e,i}$ (vertical), (y/a) (horizontal)
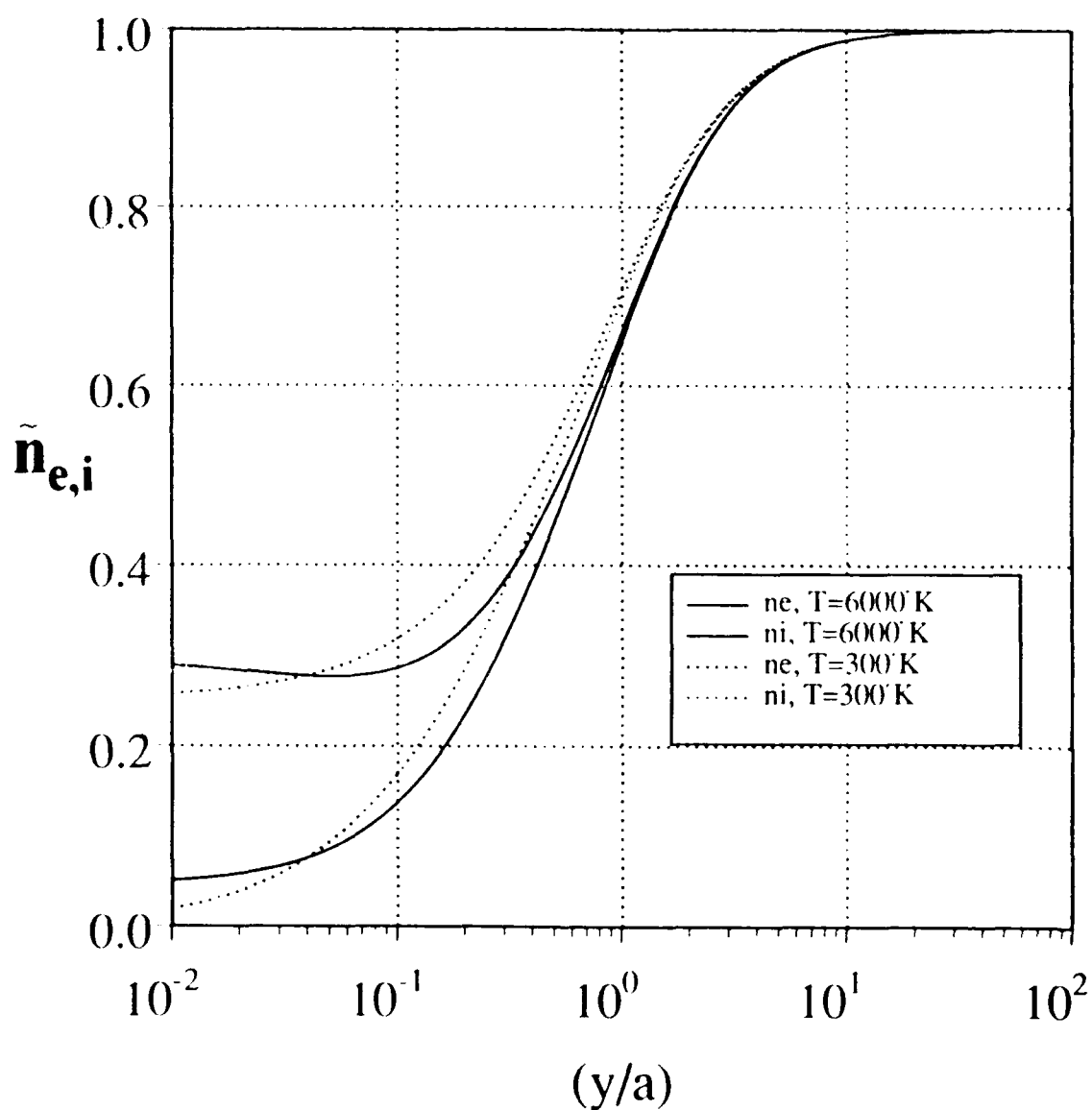
Figure 20 $\tilde{n}_{e,i}$ profiles   (z=1.1729)

29

$\tilde{\text{K}}$-term Profiles, High z, T=6000°K
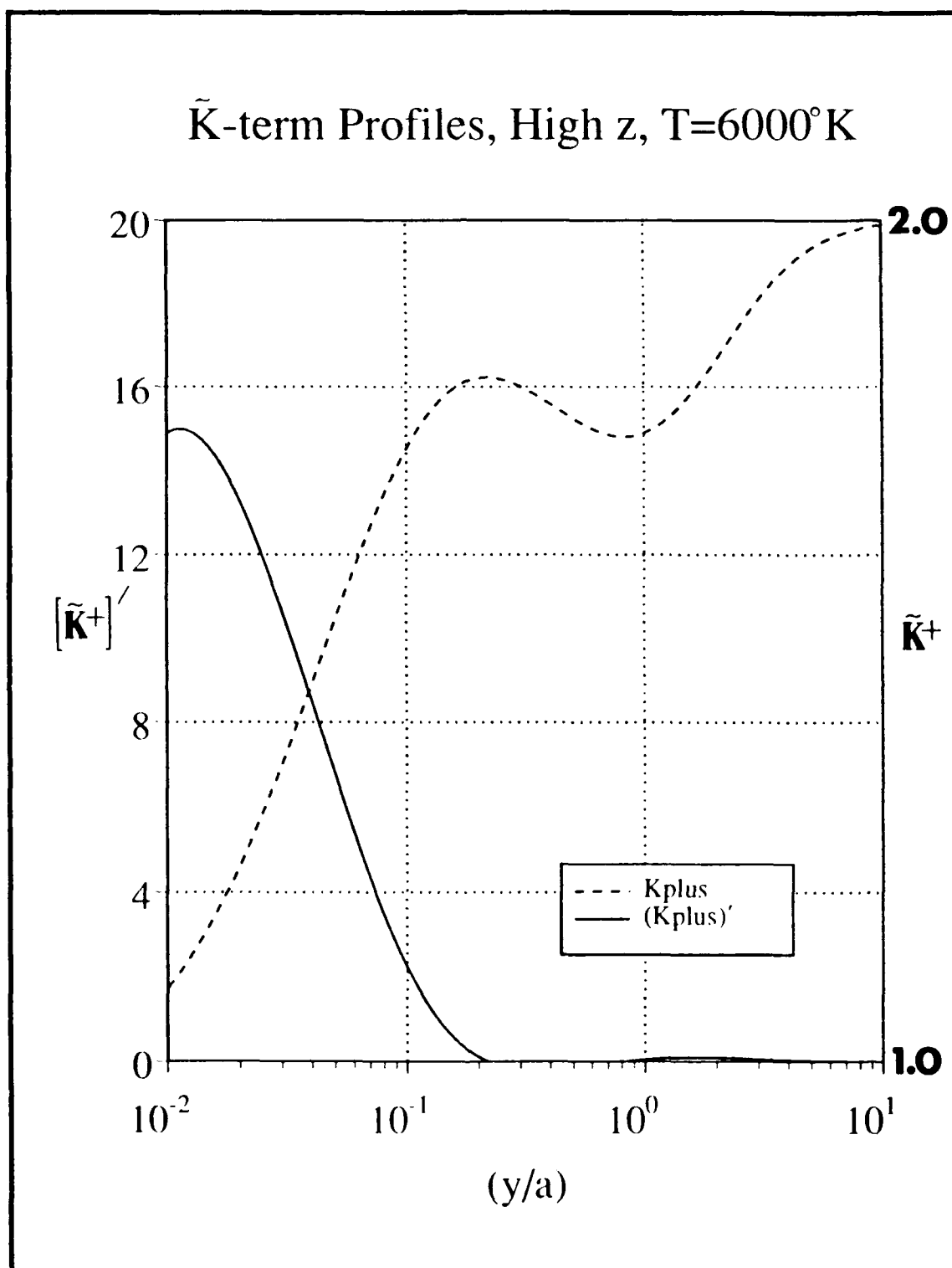
Figure 21 K-term profiles (z=2.1493, η=257.563)

30
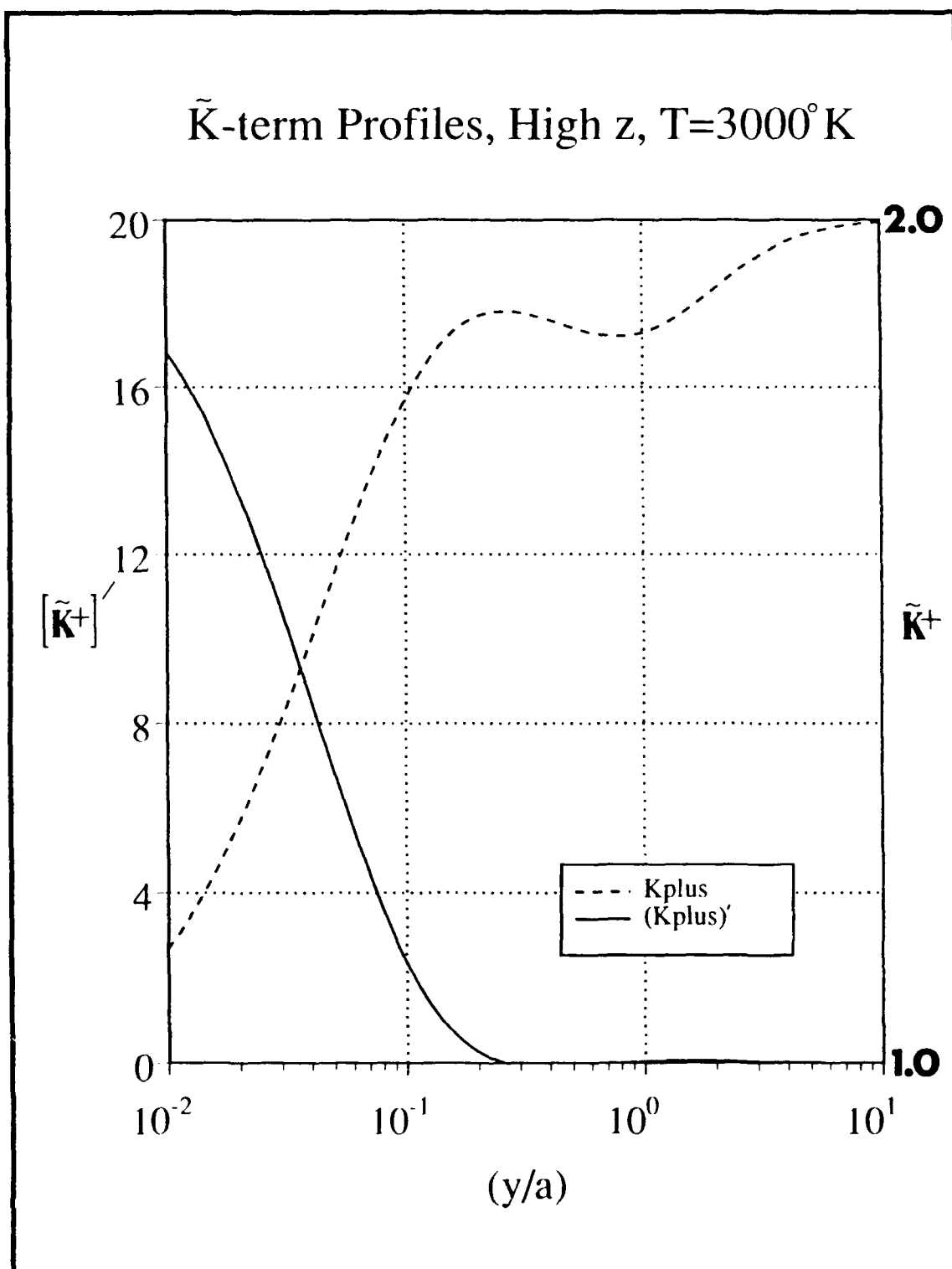
Figure 22   K-term profiles (z=2.1493, η=515.125)

31
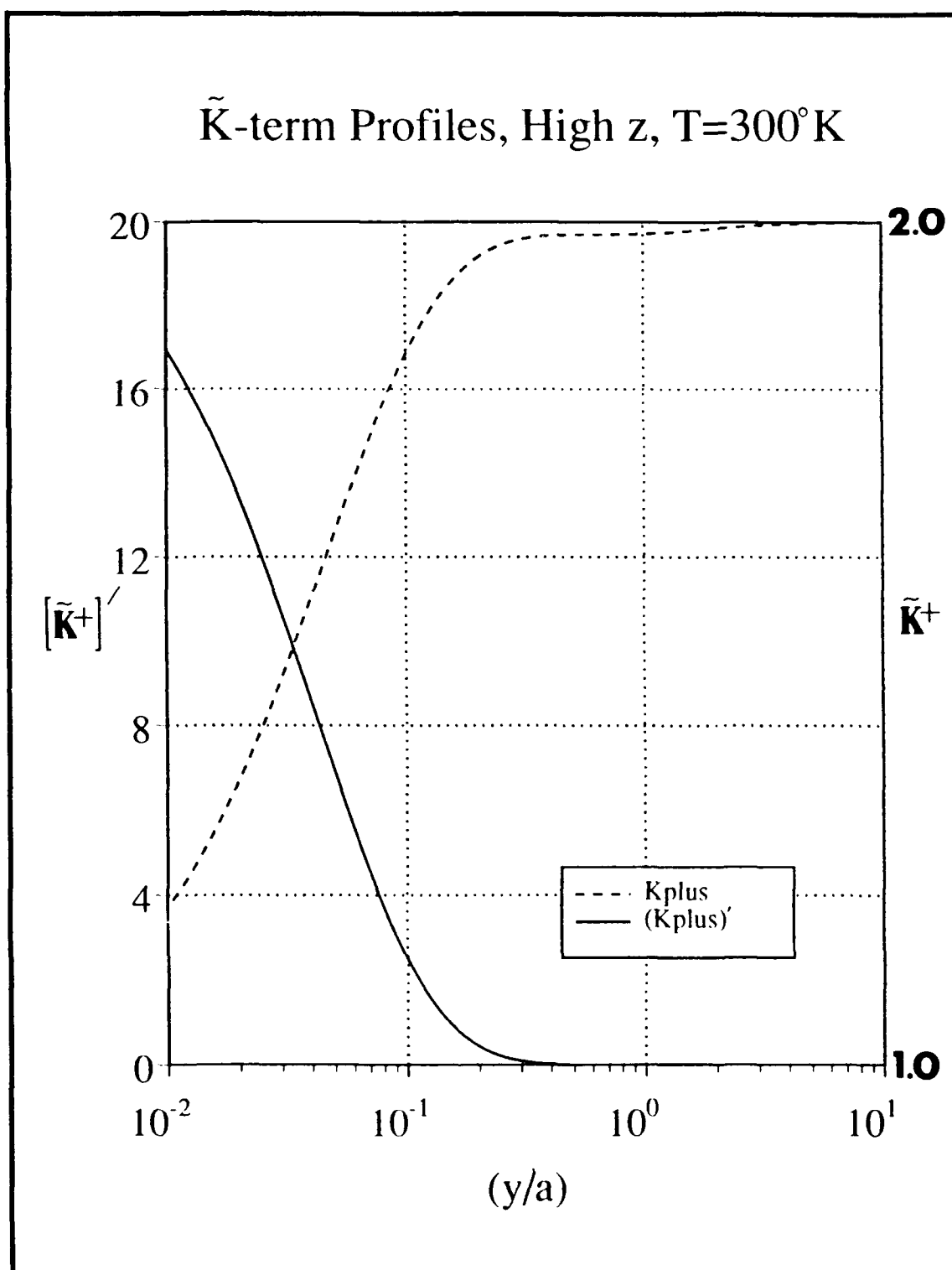
Figure 23   K-term profiles (z=2.1493, η=5151.25)

32

Figure 24 $\tilde{K}^+$ profiles   (z=2.1493)

(K̃plus)′ Profiles, High z, Various Temp.

Legend:
- T=300 K
- T=3000 K
- T=6000 K

Axis labels: $(\tilde{K}^+)'$ (vertical), (y/a) (horizontal)
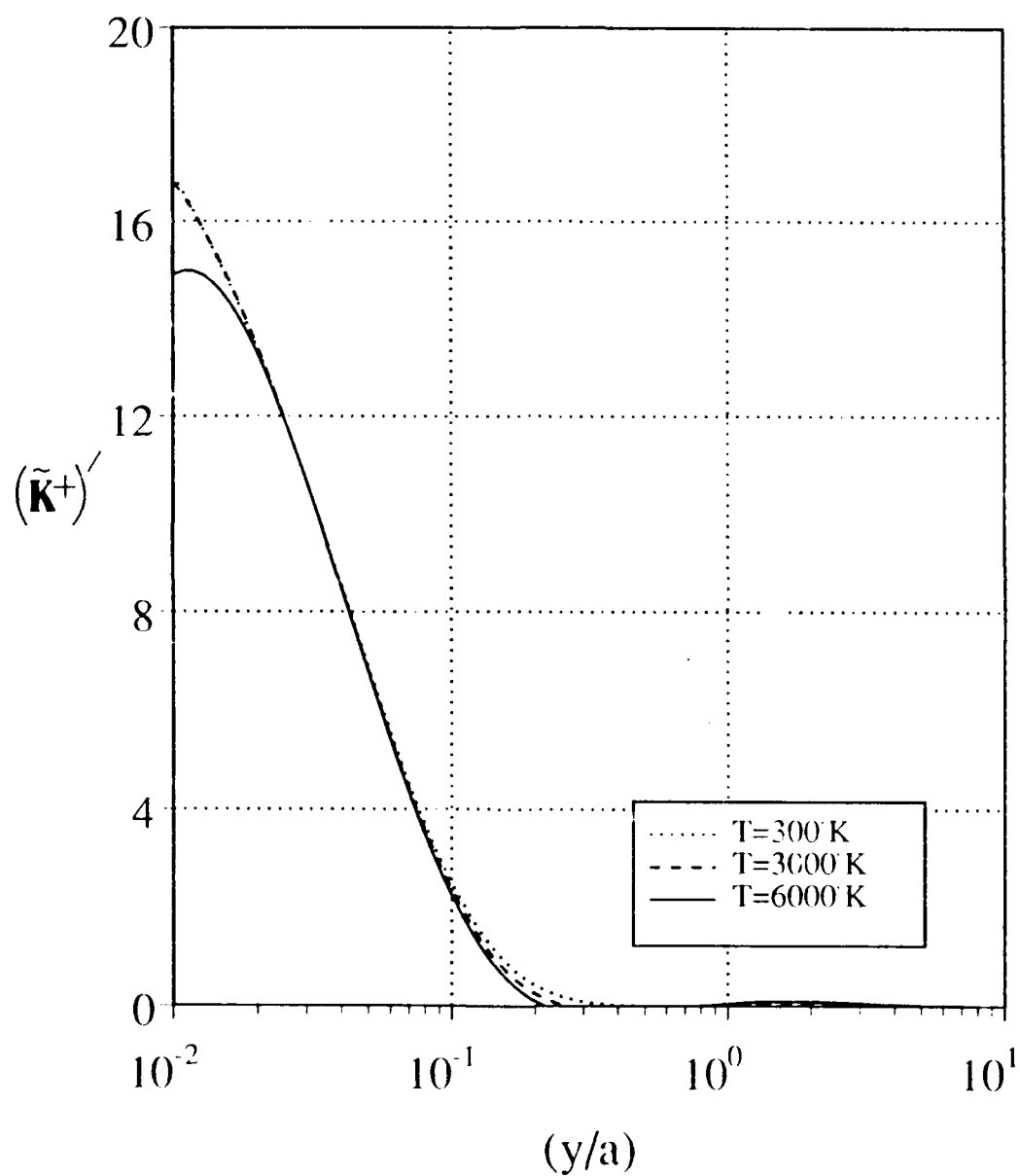
Figure 25 $(\tilde{K})$ profiles (z=2.1493)

34

The n-profiles of this class of plasmas are depicted in Figure 26. While there are some yet-to-be-addressed differences from previous n-profiles, the sheath and ambipolar regions are again evident, as are the profiles' theorized independence from temperature changes.

4. The Effect of z on the Planar Anode Sheath

Results to this point have revealed some important and perhaps non-intuitive concepts concerning the properties of planar anode she..hs, concepts which appear applicable to all low-temperature, collisional plasmas. However, sheath variations attributable solely to changes in the parameter z have yet to be discussed.

Comparison of the n-profiles for each z-family (Figures 14, 20, and 26) illustrates a subtle point: although all n-profiles have been shown to be nearly independent of temperature, they do become slightly more sensitive to temperature variations as the value of z decreases. This is possibly attributable, in part, to the lower densities of 'small z' plasmas: the temperature-dependent kinetic energy changes of the particles may produce a more observable effect on the total ionization/recombination process in a plasma not already saturated with density-driven collisions. Perhaps more contributory is the previously-discussed dominance of electrical energy over thermal effects. The 'small z' plasmas exhibit smaller magnitudes of $E_{()}$ than other plasma families, decreasing such dominance. The involvement of $\Delta\phi_{a}$ in this phenomenon remains unclear. In any event, such n-profile temperature shifts remain nearly negligible for all plasmas considered to this point, which further validates the innocuous nature of the constant temperature assumption.

Figure 27 depicts the $\bar{K}^{*}$ curves of three diverse z-families at the same temperature (6000° K). As noted previously, all are well-behaved and do not differ to

ñ-Profiles, High z, Varying Temp.

Legend:
- ne, T=6000°K
- ni, T=6000°K
- ne, T=300°K
- ni, T=300°K

Y-axis: $\tilde{n}_{e,i}$

X-axis: (y/a)
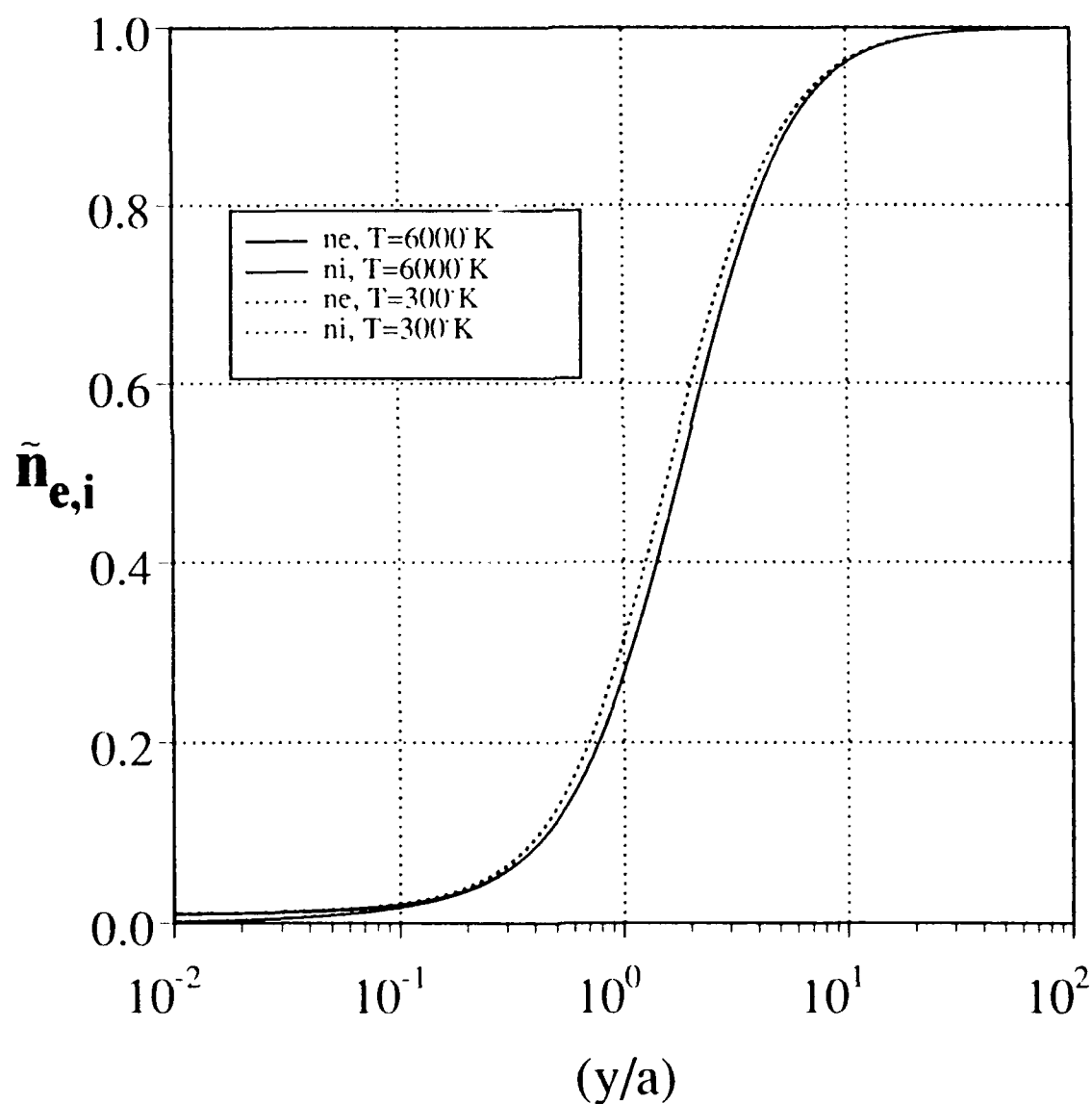
Figure 26 $\tilde{n}_{e,i}$ profiles (z=2.1493)

36
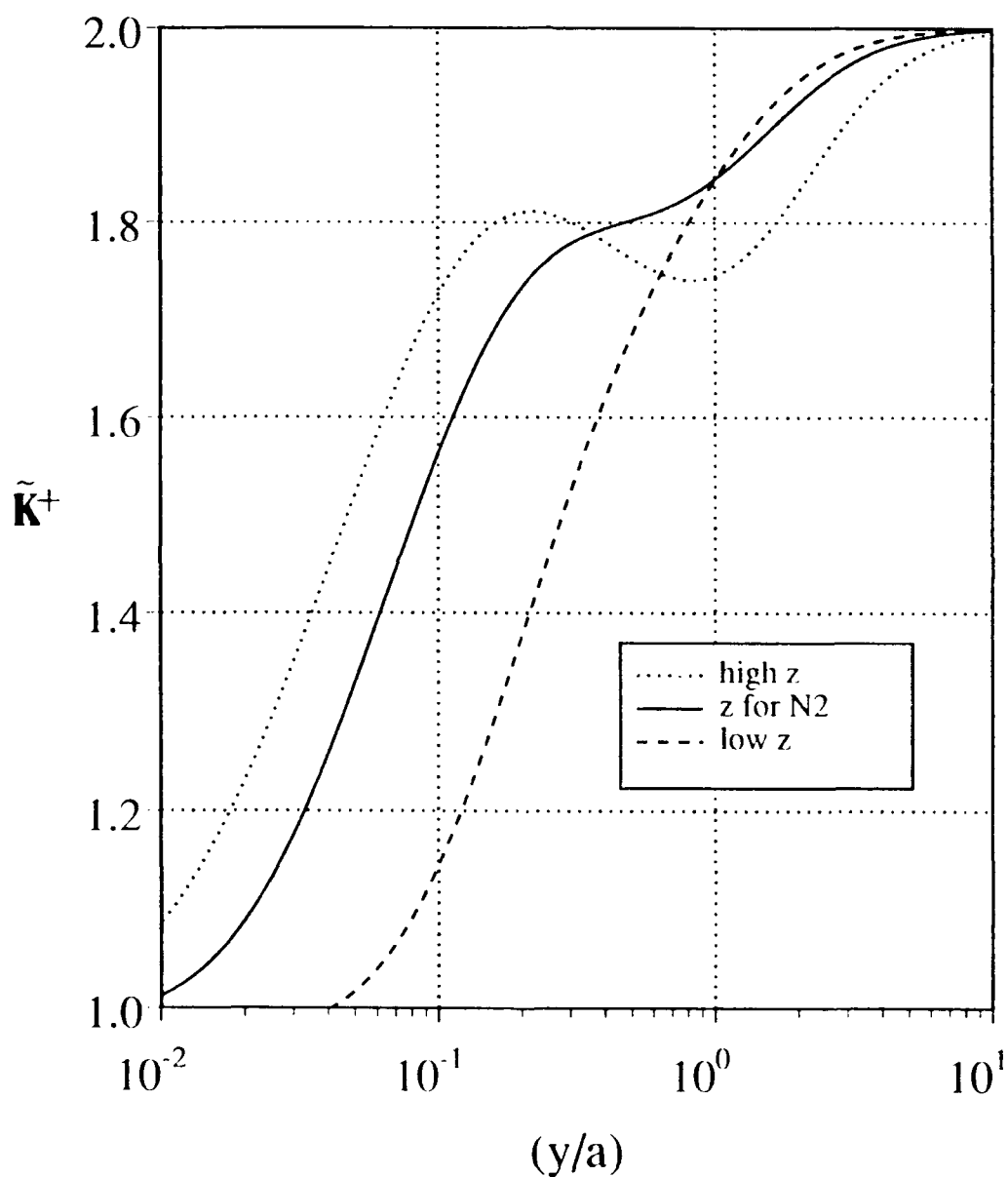
Figure 27 $\tilde{K}^+$ at 6000°K for Different z-Families

37

any significant degree. Contrastingly, the charge production rate curves of these three plasma families (Figure 28) are somewhat disparate and very insightful. 'Large z' plasmas show significant charge production throughout the entire sheath, in contrast to the localized and decreased production rates depicted for the 'small z' plasmas. This may indicate the fact that electric-field effects are more localized for smaller z.

The n-profiles for the three z-families are depicted in Figure 29. Unlike similar profiles for varying temperature (i.e., η), these curves are decidedly affected by changes in z. Most prominently, the magnitude of the charged particles changes dramatically as z varies, especially in the sheath. This is a graphic indication of z-induced changes in both E_0 and current flow for diverse plasmas. Also noteworthy is the fact that the sheath itself extends further from the anode surface as the value of z decreases. In particular, the sheath of the 'small z' plasmas stretches over <u>ten times</u> the distance occupied by the 'large z' sheath.

5. Some Final Thoughts on the Influence of η

The effect of η variations on the anode sheath has already been indirectly addressed via the extensive consideration of temperature's influence on the problem. The bottom equation of Figure 5 inversely relates these two parameters for fixed z and $\Delta\phi_d$. Physical interpretation of η as a ratio of electrical and thermal energy has also been reviewed.

The purely numerical importance of η is apparent with a glance at the governing differential equation (Figure 3); its reciprocal controls the influence of the charge production rate term. Large values of η reduce this term to near zero, the consequences of which can be seen in every low-temperature case (i.e., $300^\circ K$). To fully and completely explore this parameter's effect on the sheath, solutions are presented for the original nitrogen plasma at artificially small values of η (in
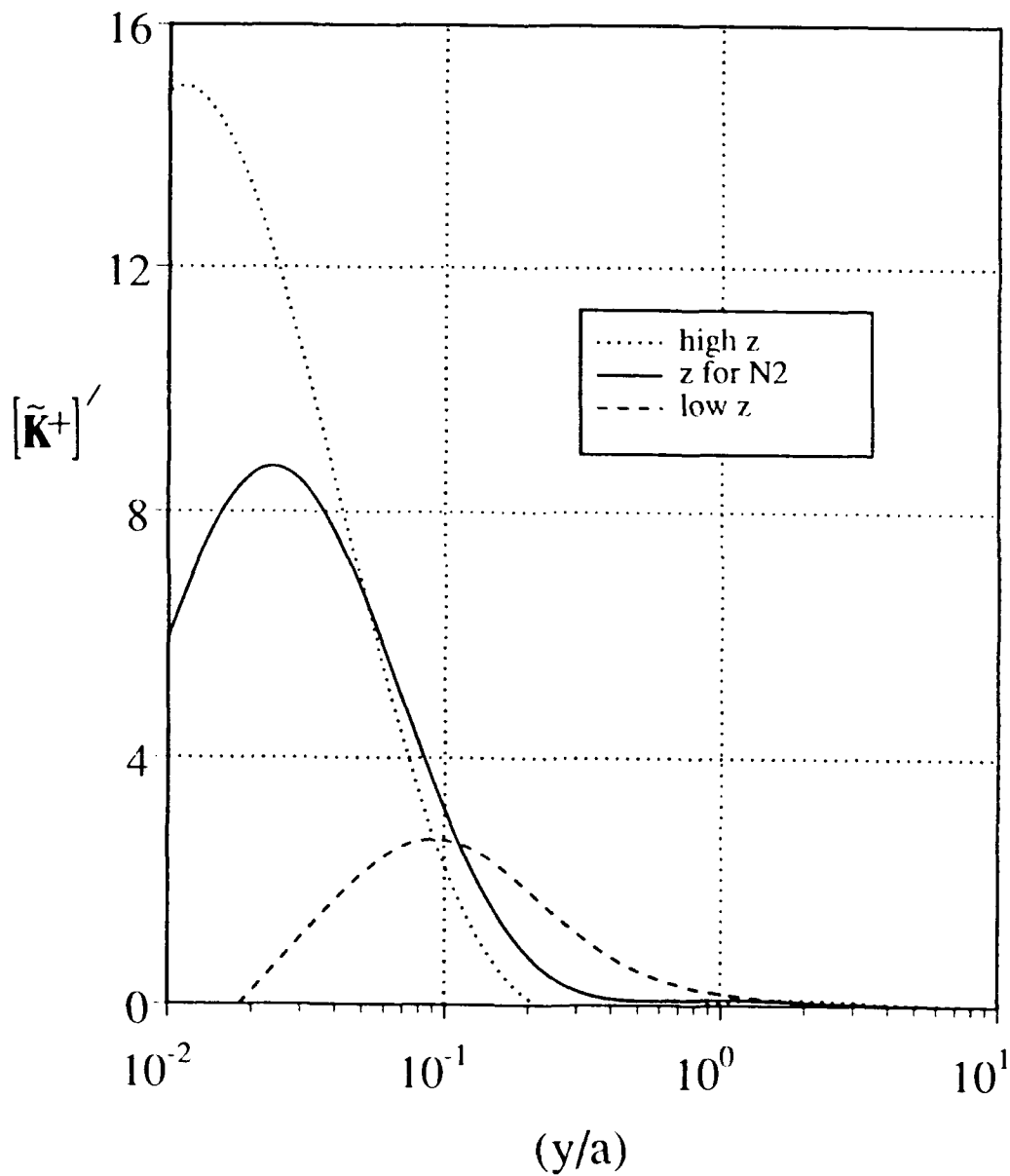
Figure 28 $(\tilde{K}^+)$ at 6000°K for Different z-Families

39
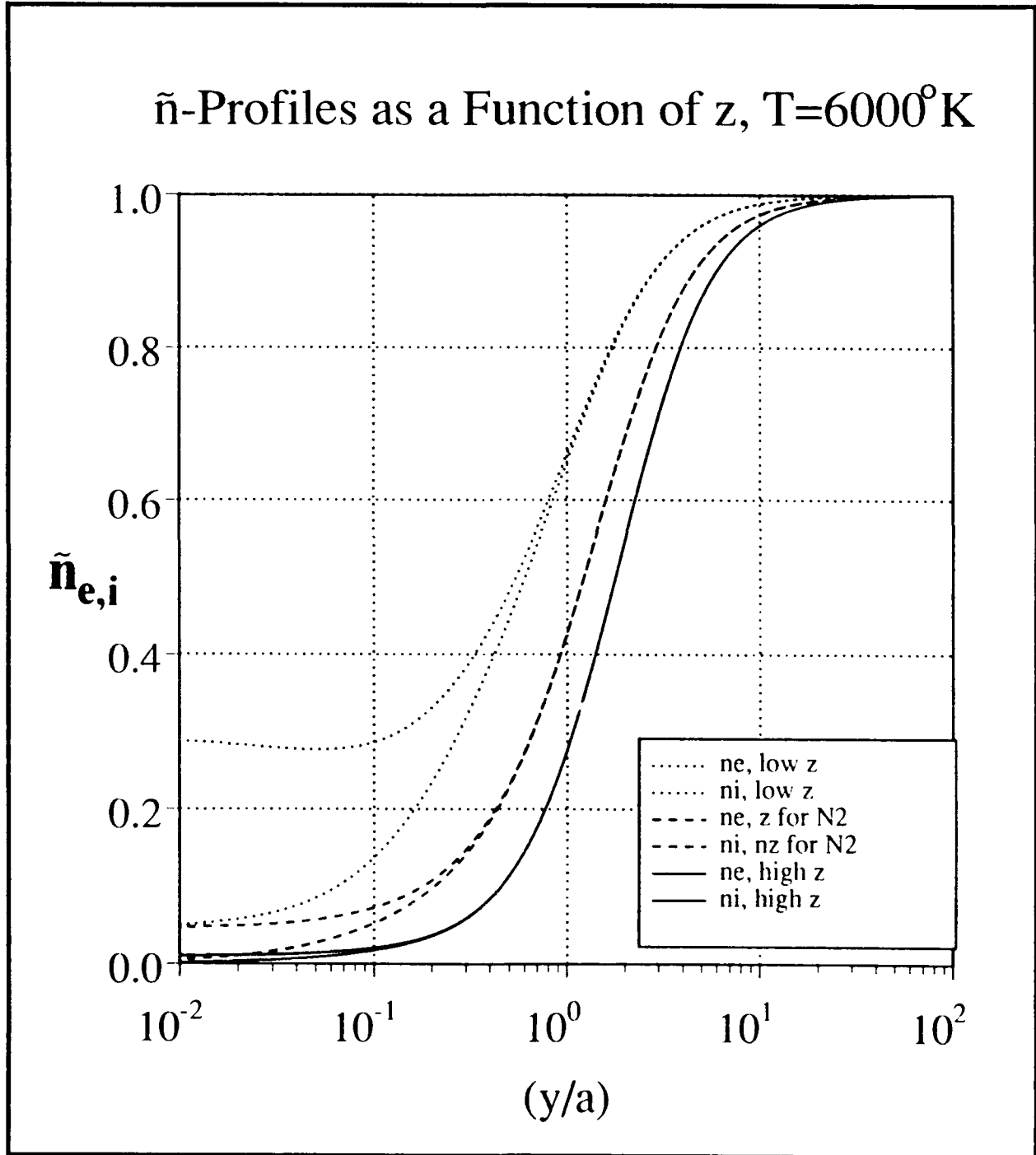
Figure 29 $\tilde{n}_{e,i}$ Profiles at   6000°K   for Different z-Families

particular, η is set equal to 25., 10., and 1.0). Note, however, that the validity of these curves is questionable at best, since such small η values equate to some extraordinarily high temperatures for the nitrogen (up to 595,000°K!), the existence of which contradicts the original assumption of low-temperature plasmas. Nevertheless, the following curves may perhaps reveal some valid trends.

Despite the unusual and probably erroneous $\tilde{K}^*$ plots for the small-η conditions (Figure 30), the $(\tilde{K}^*)'$ curves of Figure 31 hearteningly retain some of the familiar traits concerning charge production rate in the sheath. The corresponding n-profiles are presented in Figure 32; remarkably, only the anomalous '$\eta=1$' profiles exhibit tendencies somewhat contrary to those already observed.

D. ANALYTICAL SOLUTIONS

In order to confirm the validity of the numerically-obtained solutions, an analytical solution to the problem's governing relation (Figure 6) is presented.

1. Procedure for 'The Outer Expansion Method'

Reference 5 offers an approach which is ideally suited to the form of the differential equation in Figure 6. The term $(1/\eta)$ is justly defined as a 'small' parameter, and the equation is already in dimensionless form. A series solution for w is presumed, approximate yet valid for 'non-small' values of $\bar{y}$. Equation (9) depicts the power series expansion for w:

$$w = \sum_{k=0} w_k \left(\frac{1}{\eta}\right)^k = w_0 + \left(\frac{1}{\eta}\right) w_1 + \left(\frac{1}{\eta}\right)^2 w_2 + \left(\frac{1}{\eta}\right)^3 w_3 + \cdots \tag{9}$$

Substitution of Equation (9) into the governing equation allows terms with like powers of $(1/\eta)$ to be equated, which in turn allows each w_k to be solved for analytically. Because the solution for w_0 is purely algebraic in this formulation, the

41

Figure 30 $\tilde{K}^+$ profiles (z=1.75626, Small η^k)

(K̃plus)′ Profiles, z for Nitrogen, Low eta's
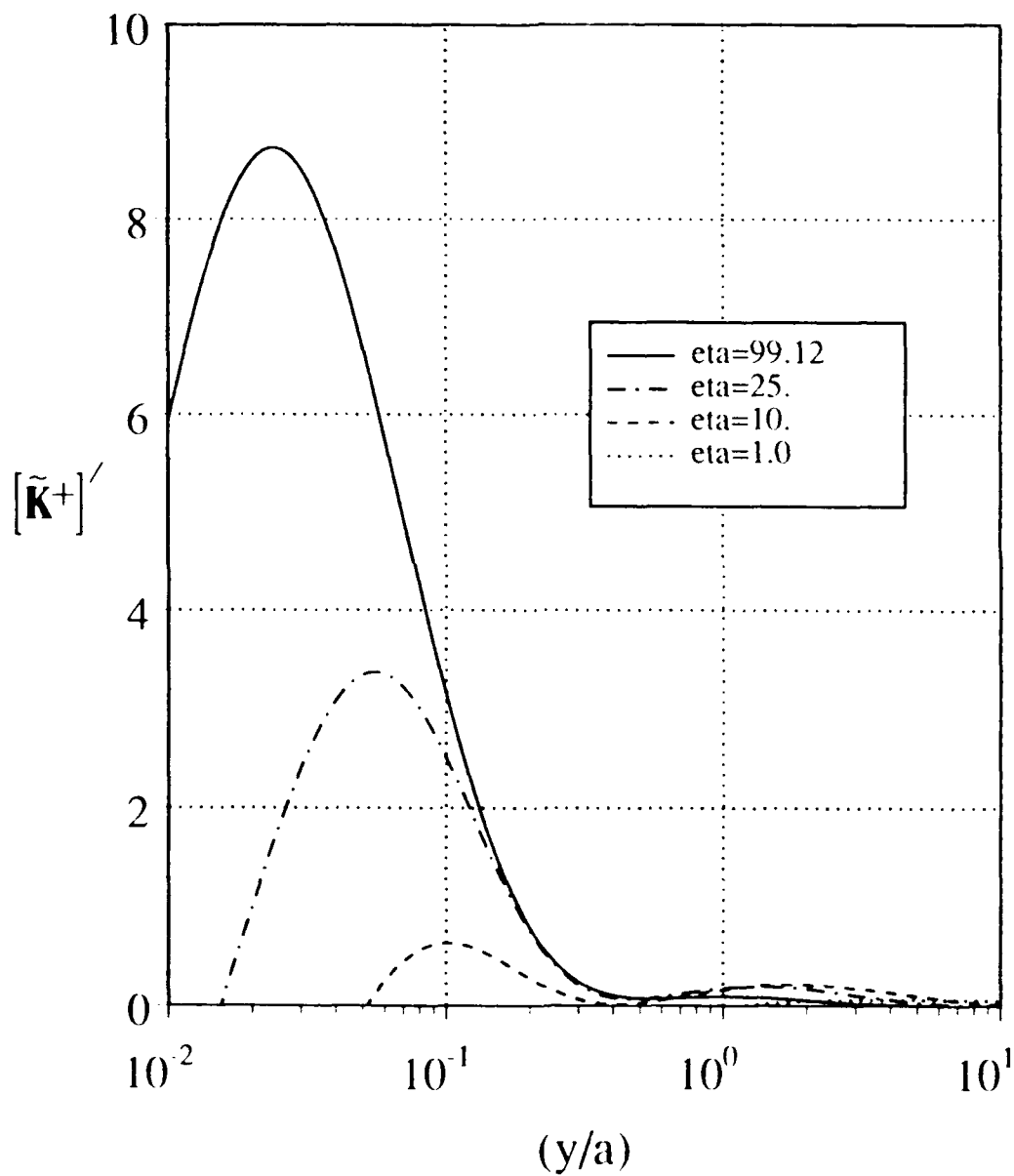
Figure 31   (K̃⁺) profiles (z=1.75626, Small η⁵)

43
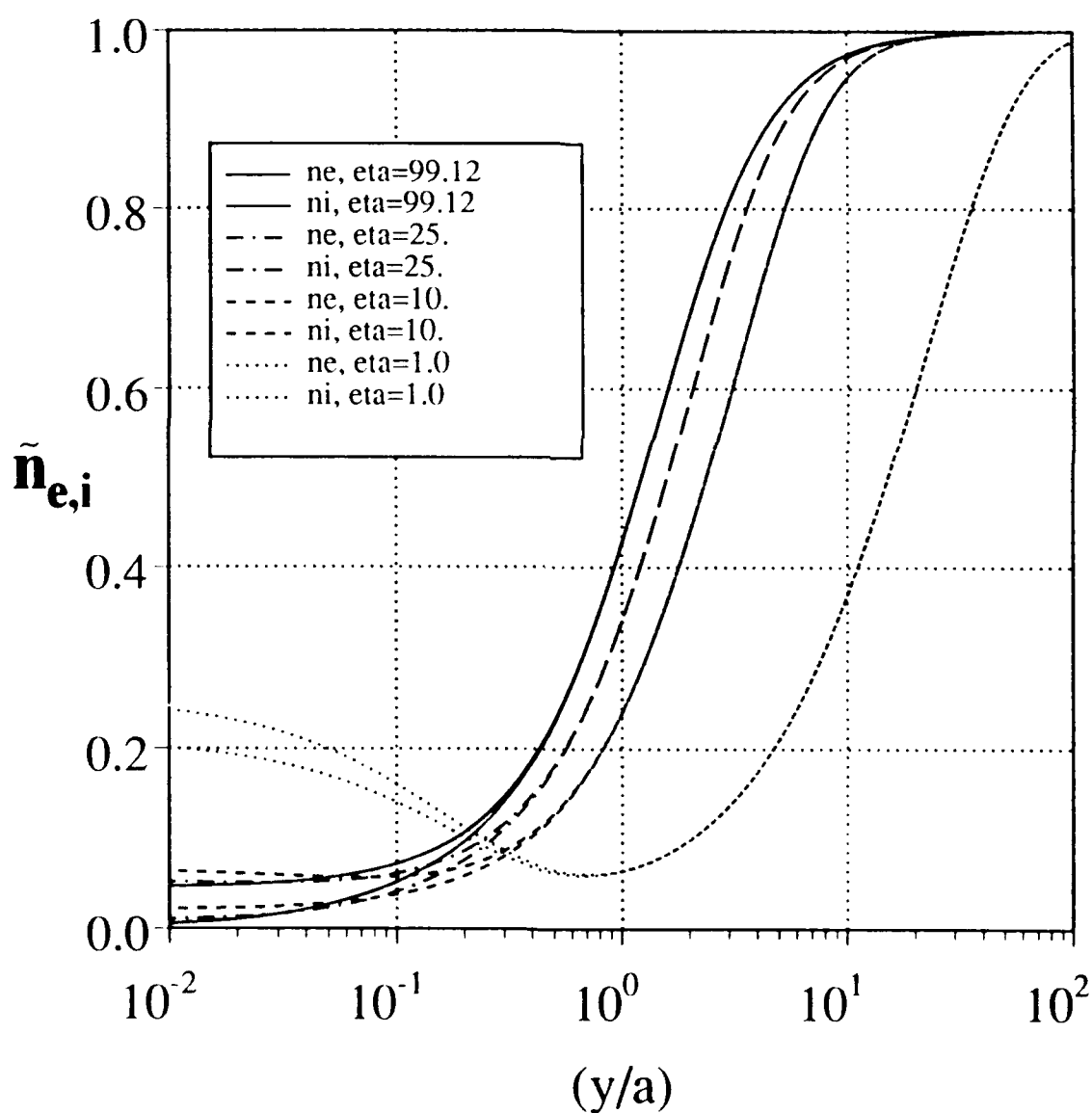
Figure 32 $\tilde{n}_{e,i}$ profiles (z=1.75626, Small η's)

44

first-order derivatives in each of the subsequent w_k expressions can be evaluated exactly (i.e., symbolically). The total solution w is thus an infinite summation of exact expressions. Prevalent magnitudes of η allow highly precise approximations of w with the series truncated to only three terms.

Utilization of this technique produces the following approximate analytical 'outside' solution (w_a) to the governing differential equation of Figure 6:

$$w \cong w_a = w_0 + \left(\frac{1}{\eta}\right)w_1 + \left(\frac{1}{\eta}\right)^2 w_2$$

where:

$$w_0 = \left(\frac{2.0}{E(\bar{y})/E_0}\right) - \left(\frac{E(\bar{y})/E_0}{(\bar{y}+1)^2}\right)$$

$$w_1 = \left[\left(\frac{2.0}{(E(\bar{y})/E_0)^2}\right)\left(\frac{E(\bar{y})}{E_0}\right)\right] + \left[\frac{(E(\bar{y})/E_0)}{(E(\bar{y})/E_0)(\bar{y}+1)^2}\right] - \left[\frac{3.0}{(\bar{y}+1)^2}\right]$$

$$w_2 = \left\{\left[\frac{6.0}{(E(\bar{y})/E_0)^3}\right]\left[\left(\frac{E(\bar{y})}{E_0}\right)\right]^2 - \left[\frac{2.0}{(E(\bar{y})/E_0)^2}\right]\left(\frac{E(\bar{y})}{E_0}\right)\right\} - \left\{\frac{12.0}{(E(\bar{y})/E_0)(\bar{y}+1)^2}\right\} +$$

$$+ \left\{\frac{(E(\bar{y})/E_0)\left[(E(\bar{y})/E_0)(\bar{y}+1) + 3(E(\bar{y})/E_0)\right]}{(E(\bar{y})/E_0)^2(\bar{y}+1)^2} - \left[\frac{(E(\bar{y})/E_0)}{(E(\bar{y})/E_0)(\bar{y}+1)^2}\right]\right\}$$

Figure 33   Three-Term Approximate Analytical Solution (w_a)

The structure of the equations themselves offers insight. Note that each w_k is a function only of z and $\bar{y}$; they are completely independent of η (i.e., temperature). The contribution of η to the total solution manifests itself solely in the series-expanded expression for w_a. Note also that the equation for w_0 is identical to the original governing differential equation for the case when η is allowed to increase to

45

infinity. As a result, the partial solution w_0 is itself a valid approximation for the true solution (w) at large values of η. This fact is also corroborated by the series-expanded expression for w_a: all terms beside w_0 vanish for large η.

As before, plots of $\bar{K}^*$ can be recovered from the data for w (or, in this case, w_a). Using parameter values from the first nitrogen plasma case (z=1.7563 and η=99.1229), $\bar{K}^*$ profiles from both the 'Outer Solution' and the Fourth-Order Runge-Kutta scheme are compared (Figure 34). Although the 'Outer Solution' does indeed appear to diverge for extremely small values of $\bar{y}$, the two curves are nearly identical. Such correlation offers comforting evidence for the validity of the numerical procedures and results presented in this work.

Figure 35 illustrates the soundness of using just w_0 to recover data for large-η cases. The solid curve is from the Runge-Kutta solution for the 300°K nitrogen case (z=1.7563 and η=1982.5); the dotted profile depicts data generated using only the partial solution w_0.

Figure 34   Comparison of Numerical and Analytical Solutions

Kplus (High eta): Numerical vs. Analytical

Legend:
- R-K (η=1982.5)
- 'Outer' ($\eta \to \infty$)

Y-axis: $\tilde{K}^+$

X-axis: (y/a)
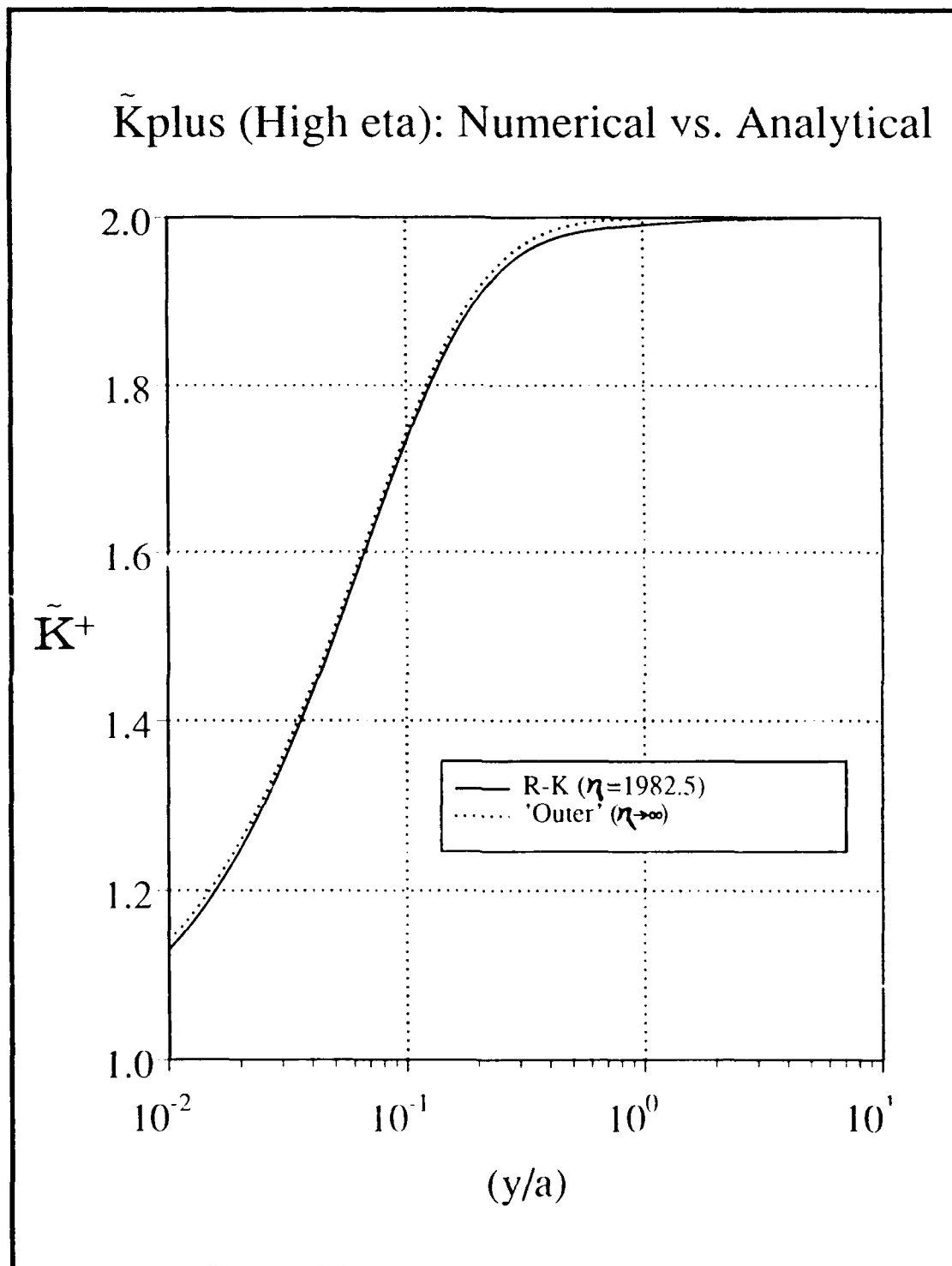
Figure 35 One Term (w_0) Algebraic Approximation for High η's

48

III. THE CYLINDRICAL PROBLEM

The following sections present detailed derivations and analysis for the cylindrical anode sheath problem. As with the planar cases, the focus is limited to steady, low-temperature collisional plasmas. Exploration of the cylindrical sheath is desirable, as several functioning plasma devices contain or employ a cylindrical architecture. In addition, these results can be compared and contrasted to the previously-presented Cartesian results. The geometry of the one-dimensional cylindrical problem is illustrated in Figure 36.
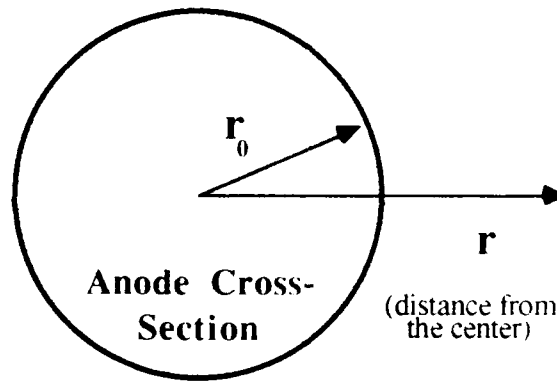
Figure 36   Cylindrical Anode Geometry

A. DERIVATIONS

Attainment of a governing differential equation for the cylindrical case begins with the re-derivation of the applicable relations (Gauss' equation and the two species continuity equations) in cylindrical form. Reference 6 presents the following differential form of Gauss' law:

$$\nabla \cdot \vec{E} = \frac{\rho}{\varepsilon_0} \tag{10}$$

49

∇ is the del operator, $\vec{E}$ is the vector form of the electric field, ρ is the charge density (which can be represented here in accordance with Equation 11), and ε_o is the permittivity of free space. The divergence ($\nabla \cdot \vec{E}$) of the electric field in cylindrical coordinates is given in Equation (12) below:

$$\rho = e(n - n_e)$$ (11)

$$\nabla \cdot \vec{E} = \left(\frac{1}{r}\right)\frac{\partial}{\partial r}(rE_r) + \left(\frac{1}{r}\right)\frac{\partial E_\theta}{\partial \theta} + \frac{\partial E_z}{\partial z}$$ (12)

For a one-dimensional electric field that varies only as a function of radius (r), combination of Equations (10), (11), and (12) yields the following one-dimensional cylindrical form of Gauss' equation:

$$\frac{dE}{dr} + \left(\frac{1}{r}\right)E = \frac{e}{\varepsilon_o}(n - n_e)$$ (13)

Comparison of Equations (13) and (1a) accentuates the appearance of a new term which is the result of the cylindrical derivation.

The species continuity equations are derived from conservation equations [Ref. 7] that can be manipulated into the form given below:

$$-\vec{j}_e = -e\mu_e n_e \vec{E} - eD_e \nabla n_e$$ (14a)

$$\vec{j}_i = e\mu_i n_i \vec{E} - eD_i \nabla n_i$$ (14b)

For a one-dimensional electric field, the previous relations are easily rewritten as shown in Equations (15a) and (15b) on the following page; these are the 1-D cylindrical species continuity equations.

$$j_{\cdot} = e\mu_{\cdot}n_{\cdot}E + eD_{\cdot}\frac{dn_{\cdot}}{dr} \qquad (15a)$$

$$j_{\cdot} = e\mu_{\cdot}n_{\cdot}E - eD_{\cdot}\frac{dn_{\cdot}}{dr} \qquad (15b)$$

Note that these species equations are nearly identical to those for the planar case (Equations 1b and 1c); only the independent variable has been renamed.

The procedure from this point is the same as that of Reference 2:

- Combine these forms of Gauss' equation and the species continuity equations with the Einstein relation
- Incorporate the K-terms as defined by Equation (2)
- Assume isothermal conditions
- Derive a single nonlinear differential equation in $K^{\cdot}$, E, and their derivatives

The desired intermediate differential equation (the cylindrical counterpart to Equation 3) is presented below. Note that all primes here denote derivatives with respect to the variable r.

$$\frac{kT_{0}}{e}\left(\frac{K^{\cdot}}{E}\right) + K^{\cdot} = \frac{2J}{eD_{c}} + \left(\frac{\varepsilon_{0}}{kT_{0}}\right)\left(EE' + \frac{E^{\cdot}}{r}\right)$$

$$-\left(\frac{kT_{0}\varepsilon_{0}}{e^{\cdot}}\right)\left[\left(\frac{E'''}{E}\right) - \left(\frac{E''E'}{E^{\cdot}}\right) + \left(\frac{E''}{rE}\right) - \left(\frac{E'}{r^{\cdot}E}\right) - \left(\frac{(E')^{\cdot}}{rE^{\cdot}}\right) + \left(\frac{2}{r^{\cdot}}\right)\right] \qquad (16)$$

In comparison to Equation (3), several new terms exist that are due solely to the cylindrical nature of the derivation. However, the validity of the above expression is demonstrated by letting r increase towards infinity, which causes the equation to approach the planar case. In that limit, Equation (16) reduces exactly to the corresponding Cartesian expression of Equation (3).

The next step calls for an 'educated guess' of the form for E(r), and substitution of that function into Equation (16). For reasons stated previously, the basic form of

the electric-field function given in Equation (4) will be retained, although in a form modified for use with a cylindrical anode. The plasma electric field begins at the anode surface, which for a cylindrical anode is at $r=r_0$ (as opposed to $r=0$, the anode center). Thus, the presumed electric field function is

$$E(r) = E_0 \exp\left[\frac{B}{\left((r - r_0) + b\right)^2}\right]$$ (17)

where r_0 is the anode radius, B and b are constants that give specific shape to the field, and the range of r is from r_0 to ∞.

Following substitution of $E(r)$ into Equation 16, the resulting lengthy expression is made dimensionless through use of the relations and definitions given in Figure 37.

$$\bar{r} = \left(\frac{r - r_0}{b}\right) \quad , \quad E/E_0 = \left(E_0/E_0\right)\exp\left[\frac{q^2}{(\bar{r}+1)^2}\right] \quad , \quad \tilde{K}^2 = \frac{K^2}{J/eD_e}$$

$$\eta_0 \equiv \left(\frac{eE_0 b}{kT_0}\right) \quad , \quad q \equiv \left(\frac{\sqrt{B}}{b}\right) \quad , \quad \gamma \equiv \left(\frac{\varepsilon_0 E_0^2}{en_0 E}\right)$$

Figure 37   Cylindrical Nondimensionalized Parameters

Note that q is the cylindrical counterpart to z, and that $\bar{r}$ has a more conventional range of zero to infinity. The new parameter γ appears because the simplifications that were previously employed (based on field and current properties at the electrode surface and in the undisturbed plasma) in the Cartesian derivation [Ref. 2] cannot eliminate all of the same constants when applied to the cylindrical case. γ has units of length, and can be thought of as a 'characteristic radius' of the plasma conditions and anode width that define q and η_0.

Further simplification of the differential equation is achieved with the derived expression [Ref. 2]:

$$\left(\frac{J}{eD_e}\right) = \left(\frac{en_iE_o}{kT_o}\right)$$ (18)

Finally, order-of-magnitude analysis reveals that some of the surviving terms cannot be neglected unless the anode radius (r_o) is sufficiently large. As a result, the differential equation can take one of two possible forms; the appropriateness of either is a function mainly of the anode's radial magnitude. Thus, the governing differential equation and boundary condition for 'normal-sized' anodes (e.g., $r_o \approx 10$ mm) are given in Figure 38, while the corresponding equations for a 'wire-thin' anode (e.g., $r_o \approx 0.1$ mm) are given in Figure 39.

$$\left(\frac{1}{\eta_e}\right)\frac{d}{d\tilde{r}}\left[\frac{\tilde{K}^*}{E/E_o}\right] + \tilde{K}^* + \frac{(E/E_r)^*}{(\tilde{r}+1)^*} = 2$$

$$\tilde{K}^*(0) = 1$$

Figure 38   Simplified Nondimensional Differential Equation and Boundary Condition, Governing the 1-D 'Normal Anode' Cylindrical Problem

$$\left(\frac{1}{\eta_e}\right)\frac{d}{d\tilde{r}}\left[\frac{\tilde{K}^*}{E/E_r}\right] + \tilde{K}^* + \left[1+\left(\frac{\gamma}{r_o}\right)\right]\left[\frac{(E/E_{r_o})^*}{(\tilde{r}+1)^*}\right] - \left(\frac{\gamma}{r_o}\right)\left[\frac{(E/E_r)^*}{\tilde{r}(b/r_o)+1}\right] = 2$$

$$\tilde{K}^*(0) = 1$$

Figure 39   Simplified Nondimensional Differential Equation and Boundary Condition, Governing the 1-D 'Wire Anode' Cylindrical Problem

The equations of Figure 39 are actually appropriate for all magnitudes of r_0, but some of the terms become negligible for the larger anodes. In fact, the degree of influence exerted by the extra terms of that differential equation (Figure 39) is directly tied to the ratio γ/r_0 : unless the cylindrical anode's radius is smaller than, or within an order-of-magnitude of, the 'characteristic radius' (γ), then those extra terms are insignificant. For this reason, the simplified differential equation of Figure 38 is also provided.

Note also that this 'normal anode' differential equation is identical in form to the corresponding planar equation (Figure 3), which indicates that in spite of a tortuous derivation, most cylindrical and planar anodes disturb the plasma in nearly the same manner. Finally, as r_0 in the expression of Figure 39 increases toward infinity (approaching the planar case), the extra terms vanish and the planar differential equation is recovered.

The parameters q and η_s have comparable meaning to their planar counterparts, and their specific values are computed using similar techniques. It can be shown through extensive manipulations that the cylindrical equivalents to Equations (5) and (6) are as follows:

$$b = \left[\frac{2\varepsilon_0 E_{\cdot}}{n_{\cdot} e(1 + \gamma/r_0)} \right] q^{\cdot} \exp(2q^{\cdot}) \tag{19}$$

$$\Delta \phi_a = E_{\cdot} \sqrt{B} \; f(q) \tag{20a}$$

$$\text{where} \quad f(q) = q \sum_{k=1} \frac{q^{2k-2}}{(2k-1)k!} \tag{20b}$$

54

Note that the infinite series converges for all values of q, and that the γ/r_a term in the denominator of Equation (19) is only relevant for the 'wire-thin' (and smaller) anodes. The above equations are combined to generate the two important equations of Figure 40, which are used to compute the parameters q and η in accordance with the following familiar procedure:

- the gas composition defines $\Delta\phi_c$
- the particular case or application specifies E and n
- the device in use fixes the anode radius r_a
- q is then computed using the implicit equation at the top of Figure 40
- the plasma temperature T_a then yields η via the bottom equation of Figure 40
- for the extremely thin anodes, γ is computed from its definition and the value of $E(\bar{r} = 0)$; both expressions are found in Figure 37.

$$\left(\frac{en\,\Delta\phi_c}{2\varepsilon_a E}\right) = q'\,f'(q)\exp(2q') - \left(\frac{\Delta\phi_c}{2r_aE}\right)\exp(2q')$$

$$\eta = \left(\frac{e\,\Delta\phi_c}{kT_a}\right)\exp(q')\Big/q\,f(q)$$

Figure 40   Equations That Yield q and η_c

As with the planar cases, specific values of q and η allow computation of the electric field parameters B and b (Equations 19 and 20), which in turn yield the fitted form of the E distribution (Equation 17), and ultimately permit the creation of $\tilde{K}$, $(\tilde{K}')$, and $\tilde{n}_{c.i}$ profiles in the plasma regions close to the anode. All that remains to be derived are the cylindrical forms of the equations that compute those n-profiles, which are produced through manipulation of Equations (2), (13), and (15). The resulting elaborate expressions are presented in Figures 41 and 42.

$$\bar{n} = \frac{n}{n_-} = \left(\frac{1}{2}\right)\left\{\left[\left(\frac{\check{K}^+}{E/E_i}\right)\left(\frac{E_-}{E_i}\right) + \left(\frac{kT_0\varepsilon_0}{e\,n_-b^2}\right)\left[\frac{6q^-}{(\bar{r}+1)^4} + \frac{4q^+}{(\bar{r}+1)^3} + \right.\right.\right.$$

$$\left.\left.\left. + \left(\frac{1}{\bar{r}+r_0/b}\right)\left(\frac{-2q^-}{(\bar{r}+1)^3}\right) - \left(\frac{1}{(\bar{r}+r_0/b)^2}\right)\right]\right] + \left(\frac{\gamma E_-}{E_i b}\right)\left(\frac{E}{E_i}\right)\left[\frac{-2q^-}{(\bar{r}+1)^3} + \left(\frac{1}{\bar{r}+r_0/b}\right)\right]\right\}$$

Figure 41   Ion Population Equation

$$\bar{n}_e = \frac{n_e}{n_-} = \left(\frac{n_-}{n_-}\right) - \left(\frac{\gamma E_-}{E_i b}\right)\left(\frac{E}{E_i}\right)\left[\frac{-2q^-}{(\bar{r}+1)^3} + \frac{1}{(\bar{r}+r_0/b)}\right]$$

Figure 42   Electron Population Equation

Gratifyingly, these n-profile equations produce their planar counterparts as r_0 approaches infinity. Note also that the expressions for $\bar{n}$ and $\bar{n}_e$ are valid for all cylindrical anodes. Unfortunately, only one term in Figure 41 could be neglected for larger, 'normal-sized' anodes, which stifles the notion of a separate 'simplified' equation for such cases.

B. NUMERICALLY SOLVED CASES

1. Procedure

The previous derivations allow detailed numerical analysis of cylindrical anode sheaths in certain plasma conditions, using a procedure similar to that performed on the planar problem. As before, the governing equation is rewritten in terms of w, as defined in Equation (21). The resulting differential equations and boundary conditions for both the 'normal-sized' anode (~5 mm radius and larger; this form also applies when $(\gamma/r_0) << 1$) and the 'wire-thin' anode (~0.5 mm radius and smaller, or when $(\gamma/r_0) \approx 1$) cases are presented in Figures 43 and 44. Note that the

form of the equations for the 'normal-sized' anode is identical to that of the corresponding planar equations (Figure 6).

$$w(\tilde{r}) = \frac{\tilde{K}(\tilde{r})}{E(\tilde{r})/E_i} \qquad (21)$$

$$\frac{d}{d\tilde{r}}[w] = 2\eta_c - \eta_i\left(\frac{E}{E_r}\right)w - \eta_i\left[\frac{(E/E_i)}{(\tilde{r}+1)}\right]$$

$$w(0) = 1$$

**Figure 43   Modified 1-D Cylindrical Equations
for Numerical Solution ('Normal-Sized' Anode)**

$$\frac{d}{d\tilde{r}}[w] = 2\eta_c - \eta_i\left(\frac{E}{E_i}\right)w - \eta_i\left(1 + \frac{\gamma}{r_o}\right)\left[\frac{(E/E_i)}{(\tilde{r}+1)}\right] + \eta_i\left(\frac{\gamma}{r_o}\right)\left[\frac{(E/E_i)}{\tilde{r}(b/r_o)+1}\right]$$

$$w(0) = 1$$

**Figure 44   Modified 1-D Cylindrical Equations
for Numerical Solution ('Wire-Thin' Anode)**

As before, application of a FORTRAN Runge-Kutta algorithm (see Appendix A), combined with the previously-outlined data manipulations, yield the numerical profiles for $\tilde{K}^*$, $(\tilde{K}^*)'$, and $\tilde{n}_{c,i}$ for any desired plasma and anode width.

2.   The Nitrogen Problem with a Cylindrical Anode

The nitrogen plasma conditions designated previously as 'Case I' for the planar anode are now analyzed for both the 'normal-sized' and 'wire-thin' cylindrical anodes. The Case I conditions are repeated on the next page:

- nitrogen's anode potential drop ($\Delta\phi_a$): 15.51 V (singly ionized)

- the electric field strength in the undisturbed plasma (E_∞): 12,000. V/m

- the particle density (n_∞): 10^{17} m^{-3}

- the temperature (T_0): 6000°K

- the anode radii under consideration (r_a): 10.0 mm and 0.1 mm

These specifications and the newly-derived equations produce the following parameter values for their respective anodes:

TABLE 1   CYLINDRICAL PARAMETERS FOR CASE 1 CONDITIONS

	$r_a = 10.$ mm	$r_a = 0.1.$ mm
q →	1.75656	1.78774
η →	99.1571	102.818
γ →	N/A	3.9597×10^{-5} m
b →	1.953×10^{-4} m	1.813×10^{-5} m
E_r →	262,543. V/m	293,216. V/m

A comparison reveals that the parameter values for the 'normal-sized' (10. mm) anode differ negligibly (only 0.1% and less) from their corresponding planar values. This is not an unexpected result, in light of the cylindrical equations' similarity to their planar counterparts for the bigger anodes. More surprising are the values computed for the 'wire-thin' (0.1 mm) anode; while their differences from the planar values are not insignificant, only E_{r_a} differs by more than 8%. The extreme sensitivity of the parameter q, however, implies that percentage comparisons may be misleading.

Direct comparison of the planar and cylindrical profiles best illustrates the near-negligible differences in their respective sheath and ambipolar regions. Figures 45 and 46 present the Case I K-term profiles produced by the three anode types (plane, 'normal' (10. mm) cylinder, and 'wire' (0.1 mm) cylinder), while Figure 47 depicts the n-profiles for each of those anodes. As can be seen, profiles for the 'normal' cylindrical anode are visually indistinguishable from the planar anode profiles. Amazingly, even the 'wire' anode profiles are nearly identical to those of the planar anode. This is a welcome result; despite many differences in the derivation and appearance of the governing equations for each type of anode, it seems that for this 'small γ' family of plasmas those cylindrical anodes whose radius is greater than that of a human hair can be treated to behave as planar. For such plasmas, only those cylindrical anodes whose radii are on the order of the sheath thickness itself would exhibit significant non-planar characteristics.

To further validate this hypothesis, the three anodes are also compared under the lower-temperature 'Case III' circumstances, which represent the same conditions as Case I except that $T_0 = 300°K$. Consequently, the only parameter listed in Table 1 that changes is η: its Case III values are 1983.14 for the 'normal-sized' cylinder, and 2056.36 for the 'wire' anode. Figures 48, 49, and 50 show the $\bar{K}$, $(\bar{K}')$, and $\bar{n}_e$ profiles (respectively) for Case III conditions. Once again, the planar and 10-mm-radius anodes disturb the plasma in identical fashion, while the 0.1-mm-radius anode exhibits nearly negligible variations.

It is worth noting that the ratio (γ/r_0) can theoretically become a meaningful factor even for the 'normal-sized' anodes; extremely low-density plasmas could possibly generate values of γ in the millimeter range. Thus, the notion of sheath characteristics being strictly a function of anode radius is valid only for the conditions being considered in this work.

59
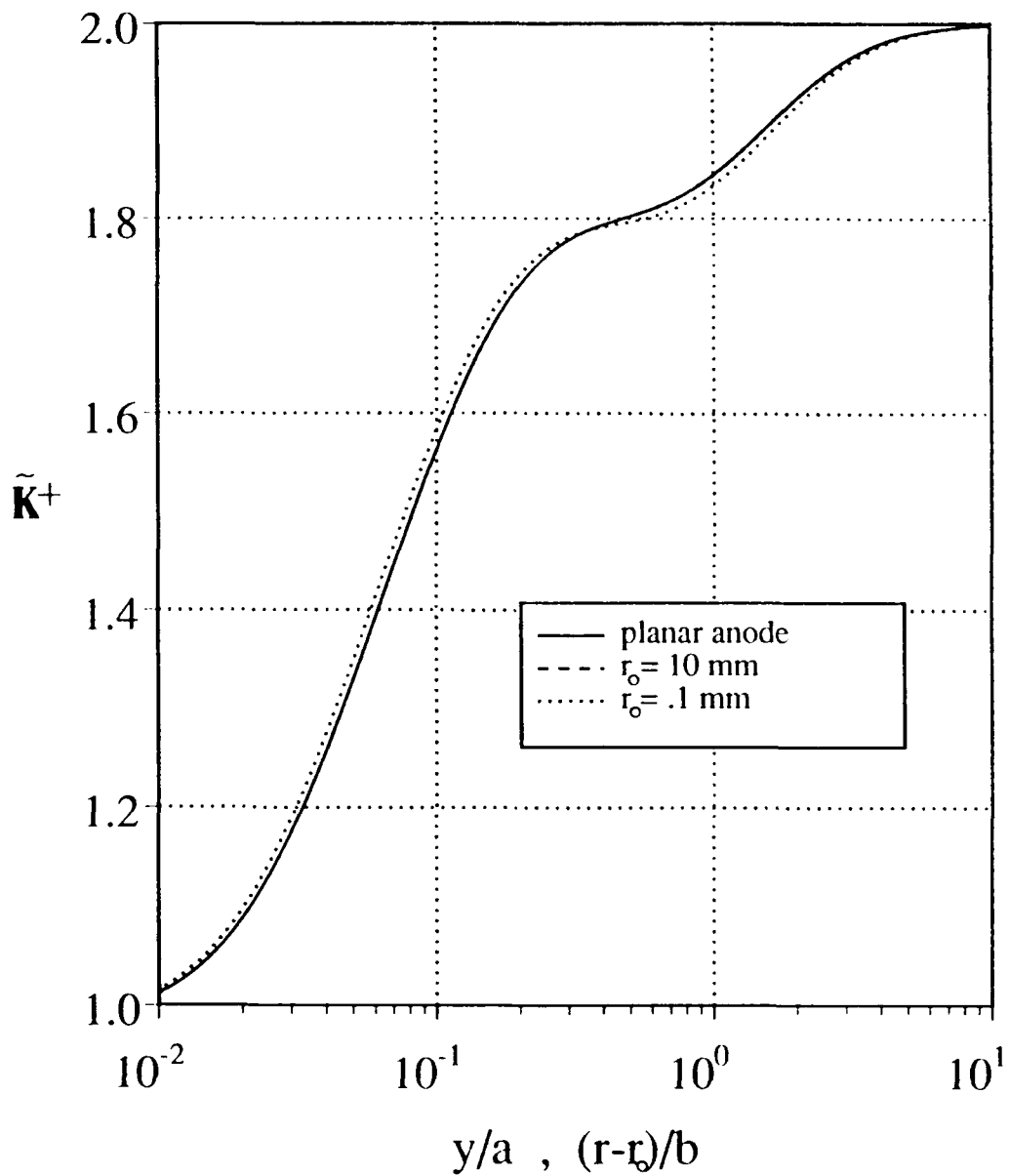
Figure 45 $\tilde{K}^+$ **Profiles, a Three-Anode Comparison**

60
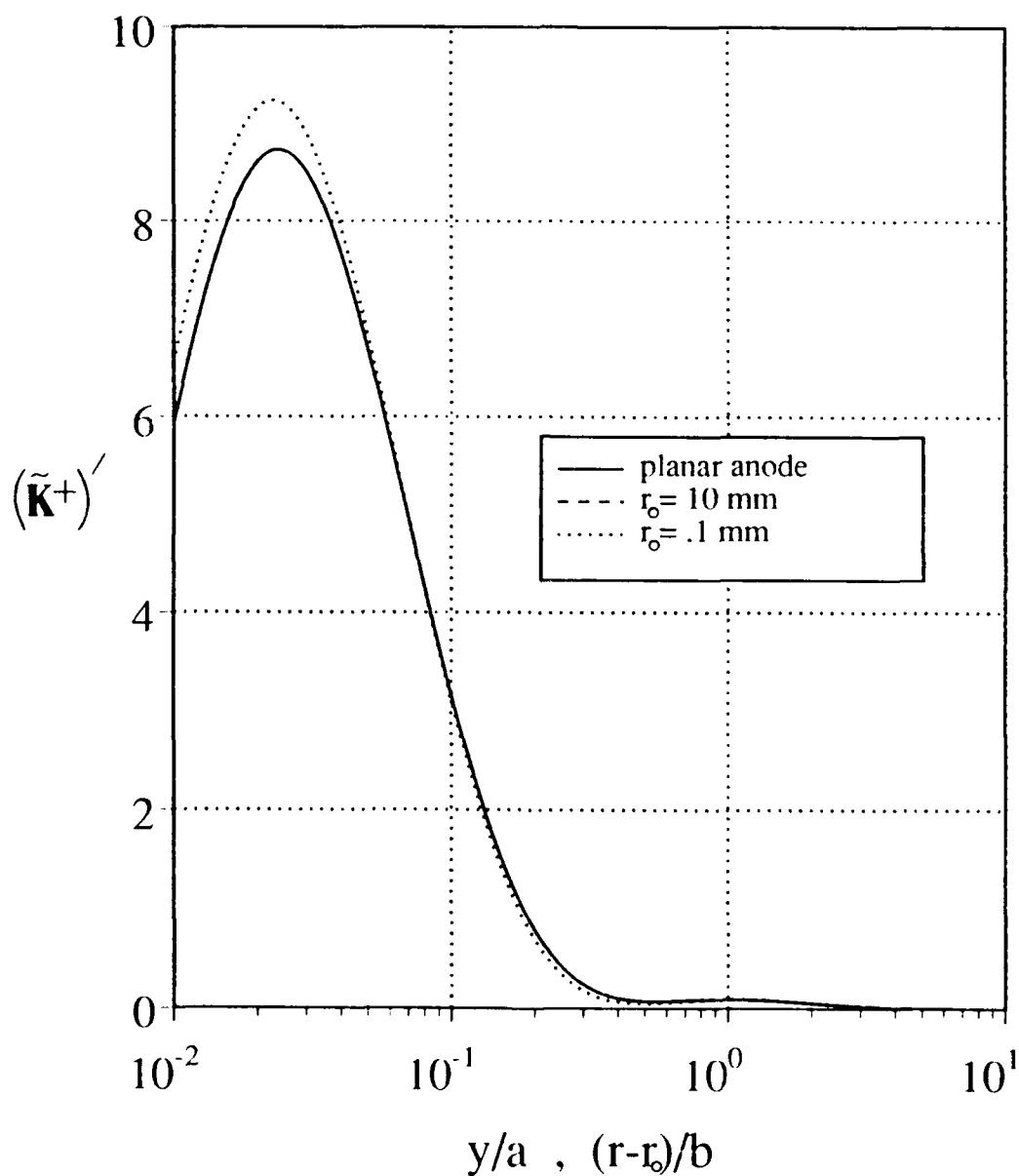
Figure 46 $\left(\tilde{K}^{+}\right)^{\prime}$ **Profiles, a Three-Anode Comparison**

61

ñ-Profiles, Cyl. Anode Comparison, Case I

Legend:
- ne, planar anode
- ni, planar anode
- ne, r_o= 10 mm
- ni, r_o= 10 mm
- ne, r_o= .1 mm
- ni, r_o= .1 mm

x-axis: y/a , $(r-r_o)/b$

y-axis: $\tilde{n}_{e,i}$
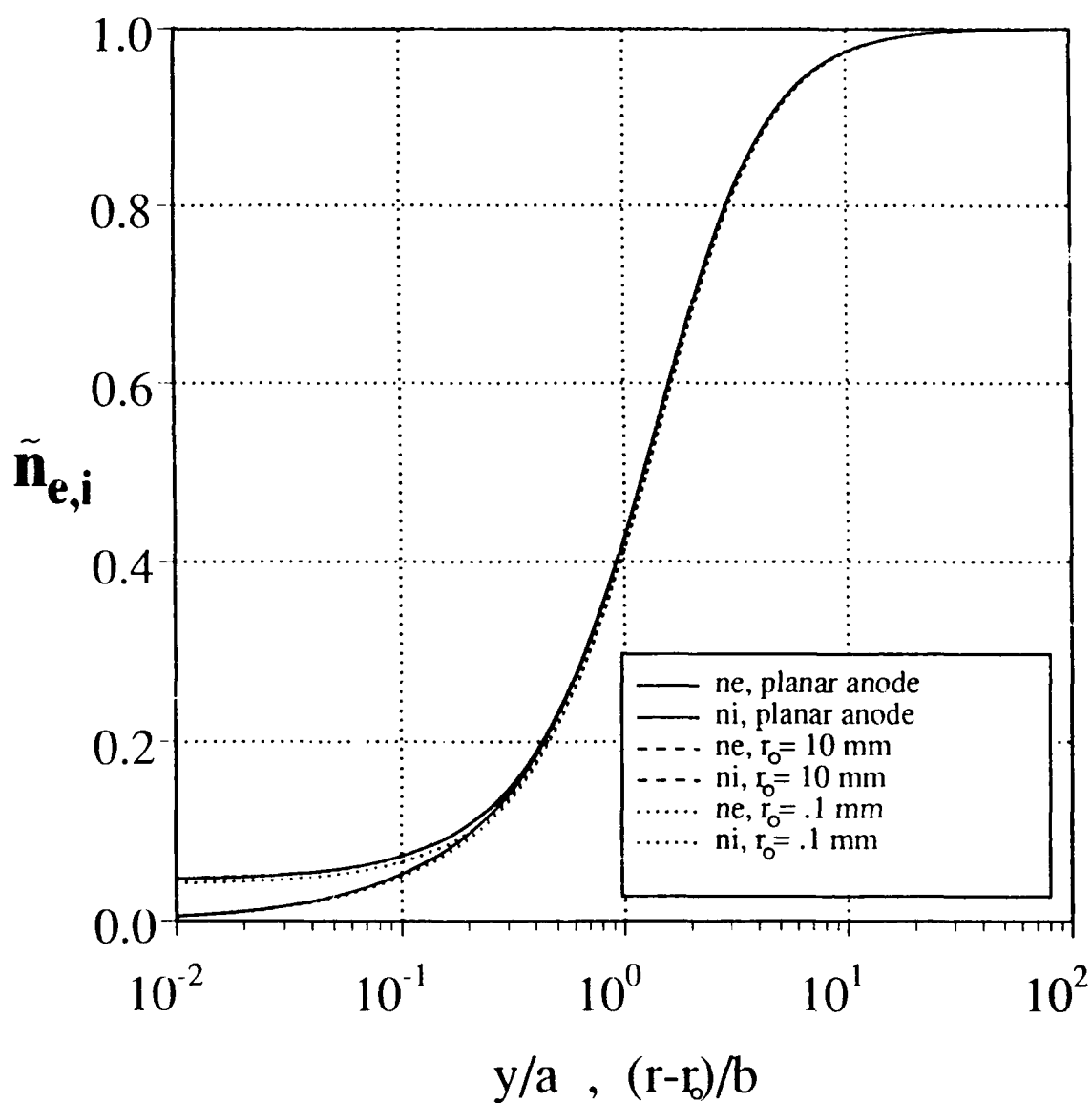
Figure 47 $\tilde{n}_{e,i}$ **Profiles, a Three-Anode Comparison**

Figure 48 $\tilde{K}^+$ **Profiles, a Three-Anode Comparison**

$(\tilde{K}plus)'$, Cyl. Anode Comparison, Case III

Legend:
— planar anode
- - - $r_o = 10$ mm
...... $r_o = .1$ mm

Axes:
- y-axis: $(\tilde{K}^+)'$
- x-axis: y/a , $(r-r_o)/b$
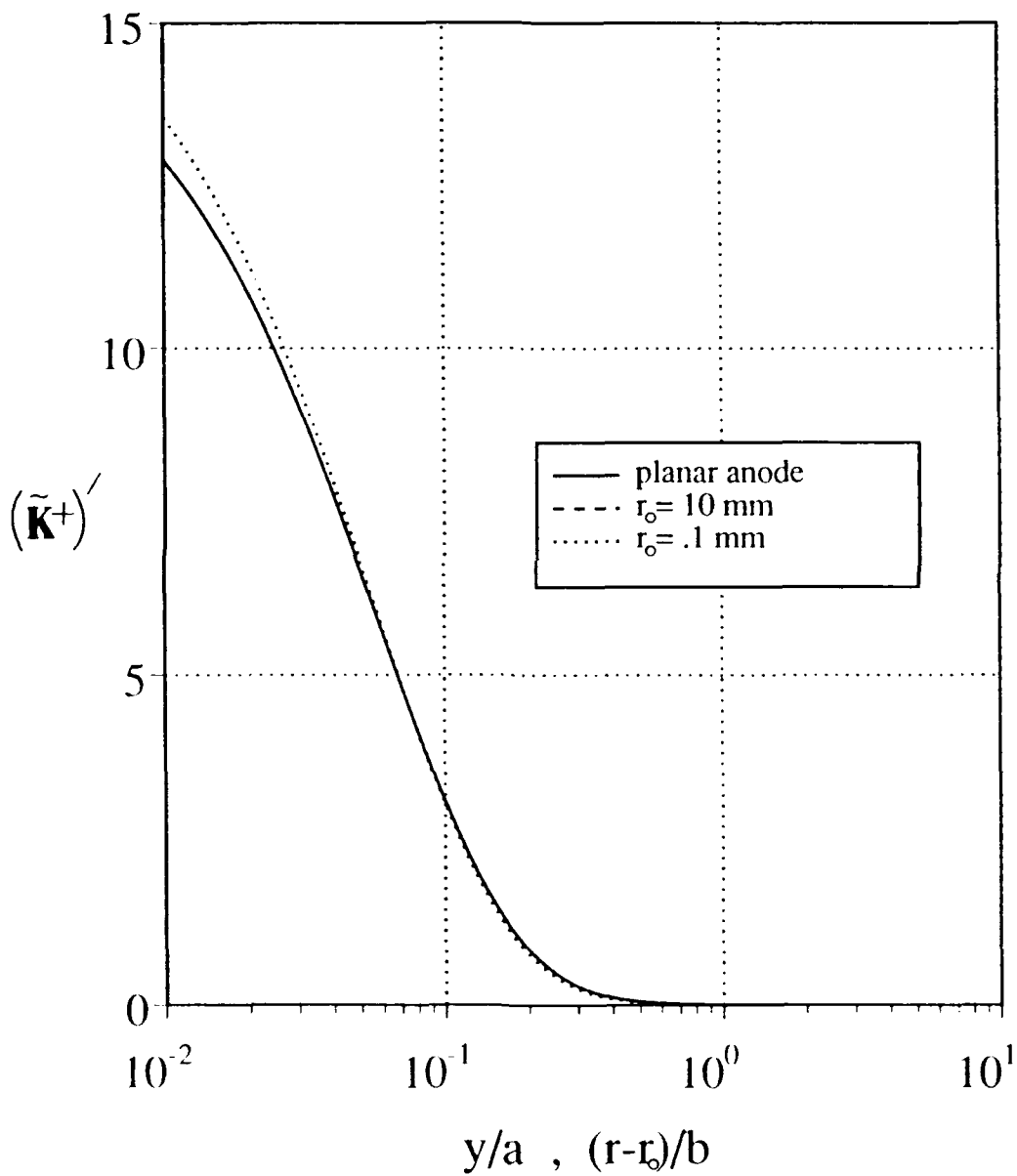
Figure 49 $(\tilde{K}^{\cdot})'$ Profiles, a Three-Anode Comparison

64

ñ Profiles, Cyl. Anode Comparison, Case III

Legend:
- ne, planar anode
- ni, planar anode
- ne, r_o= 10 mm
- ni, r_o= 10 mm
- ne, r_o= .1 mm
- ni, r_o= .1 mm

y-axis: $\tilde{n}_{e,i}$

x-axis: y/a , (r-r_o)/b
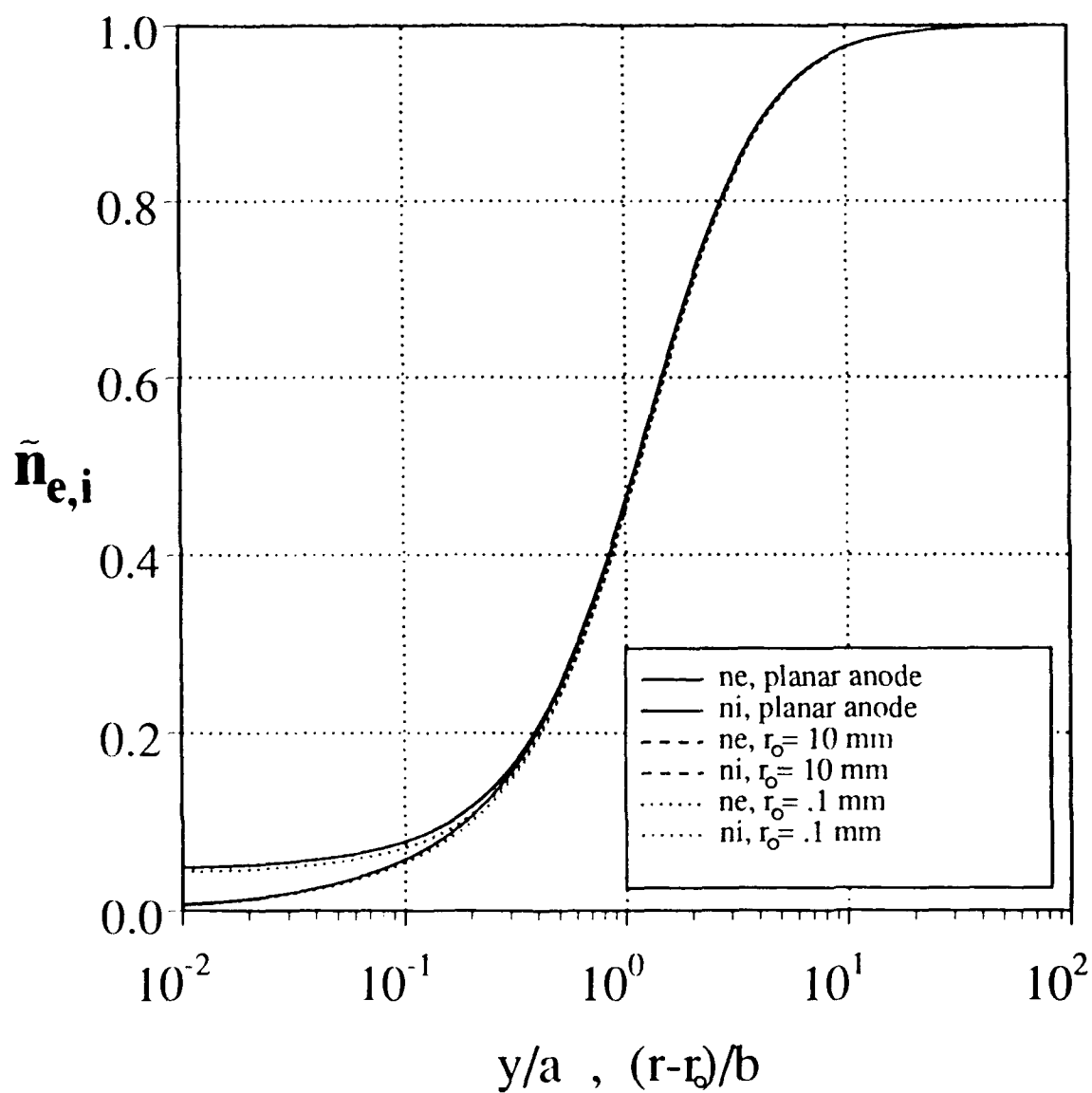
Figure 50 $\tilde{n}_{e,i}$ Profiles, a Three-Anode Comparison

65

IV. CONCLUSIONS

The manner in which one-dimensional planar and cylindrical anodes disturb collisional, isothermal plasmas has been explored in detail. Appropriate sheath and ambipolar regions have been shown to develop, for a given specific and reasonable electric field distribution, across a wide range of plasma types and conditions. Numerical solutions of the nondimensional governing equations have allowed specific and important observations to be made concerning:

- the effect of temperature variation on plasmas in the anode region
- traits that are characteristic of various plasma 'families', and traits that appear to be common to all collisional, low-temperature plasmas
- the effect that differing anode radii have on the sheath for cylindrical anodes
- the degree of difference between sheaths of planar and cylindrical anodes

In addition, an analytical method has been presented that offers a simplified yet accurate algebraic solution for the lower-temperature plasmas.

The following briefly summarizes the specifics for each of these results.

Appropriate Sheath Existence: In each case considered, the $(\check{K}^*)'$ curves showed that the net rate-of-charge-production decreases and vanishes toward the outer edge of the sheath. Moreover, each of the n-profiles clearly depicted sheath and ambipolar regions which were reasonably located with respect to the anode surface.

Overall-Temperature Variation Effects: Results of this work indicate that at lower temperatures, charge production in the outer sheath is generic to the electric field distribution, and is thus independent of the details of ionization and recombination. Additionally, the $\tilde{n}_{e,i}$ profiles, and thus the sheaths themselves, have been shown to be nearly unaffected by substantial changes in temperature. This somewhat unexpected result, which held for every plasma case considered, reduces any consequences caused by the isothermal-particle assumption (i.e., the assertion that

$T_e = T = T_i$). It is interesting to note that the large magnitudes and physical meaning of η (the ratio of electrical energy to thermal energy in the sheath) actually predict such independence from temperature variations.

Plasma 'Family' Characteristics: All low-temperature, collisional plasmas can be partitioned into broad groupings based on their specific nondimensional 'z' or 'q' value (z denoting a planar anode problem, and q signifying cylindrical anodes). Each plasma 'family' thus exhibits its own characteristic electric field and sheath properties, even though its members may be widely diverse in composition and condition.

Plasmas with large z (or q) values show significant charge production throughout the entire sheath, in contrast to the localized and decreased production rates depicted for the 'small z/q' plasmas. This may indicate the fact that electric-field effects are more modest and thus localized in those plasmas with smaller values of z or q. In addition, the magnitude of the charged particles near the anode changes dramatically as 'z/q' varies, especially in the sheath. The sheaths of 'large z/q' plasmas exhibit charged-particle densities up to one order-of-magnitude smaller than those of the 'small z/q' sheaths. More importantly, the sheath itself extends further from the anode surface as the value of 'z/q' decreases. In particular, the sheath of the 'small z/q' plasmas stretches over ten times the distance occupied by the 'large z/q' sheath.

Cylindrical Anode Radius Effects: The sheath and the charge production rates have been shown to vary as the anode radius varies; however, the differences are almost negligible for all practical anodes and conditions. It appears that only extremely low-density plasmas, or cylindrical anodes whose radii are on the order of the sheath thickness itself, would exhibit significantly different characteristics.

<u>Planar and Cylindrical Anode Differences</u>: In an extension of the previous paragraph, the results of this work indicate that for the range of conditions explored. all practical cylindrical anodes can be treated to behave as planar anodes.

<u>Simple Analytical Approximations (Low Temperatures Only)</u>: Using the 'Outer Solution' technique, an algebraic solution can be used to generate highly accurate approximations to low-temperature anode problems. In addition. as long as derivatives of the presumed electric field distribution exist. the sheath profiles for all cases can be produced analytically to any desired accuracy.

One suggestion for further work involves researching the ef.·cts that other electric field distributions would have on the anode problem. Such distributions may be derived from empirical data or from other 'guesstimates'. and may have three or more adjustable parameters. The most prominent reason for this suggestion is the need to corroborate the generic charge production rate observed at lower temperatures.

Another area requiring further study is the exploration of two-temperature plasmas and their anode sheaths. Results for such conditions could confirm the assertion of sheath insensitivity to temperature changes.

REFERENCES

1. Marshall, J., 'Performance of a Hydromagnetic Plasma Gun', The Physics of Fluids, v. 3, pp.134-135, January-February 1960.

2. Biblarz, O., 'Approximate Sheath Solutions for a Planar Plasma Anode', Naval Postgraduate School, Monterey, California, 1990 (to be published in IEEE Transactions on Plasma Science, December 1991).

3. Air Force Wright Aeronautical Laboratories Report AFWAL-TR-80-2088, Electrode Boundary Layers in Dense, Diffuse Plasmas, by O. Biblarz, R.E. Ball, and S.T. Van Brocklin, p. 63, October 1980.

4. Brown, S.C., Introduction to Electrical Discharges in Gases, John Wiley and Sons, 1966.

5. Ashley, H., and Landahl, M., Aerodynamics of Wings and Bodies, pp. 62-65, Addison-Wesley Publishing Co.,1965.

6. Cheng, D.K., Field and Wave Electromagnetics, 2d ed., pp. 75-77, Addison-Wesley Publishing Co., 1990.

7. Mitchner, M., and Kruger, C.H., Partially Ionized Gases, pp. 146-155, John Wiley and Sons, 1973.

APPENDIX A

Applicable FORTRAN Programs

```
C       THIS PROGRAM IS BUILT AROUND A GRAFkit 3.1 RUNGE-KUTTA
C       ALGORITHM PRODUCED BY SCO, INC.


        DOUBLE PRECISION YA(0:10),YN(0:10),EK(0:4,0:10),Y(0:10),XA
        DOUBLE PRECISION XP,XB,XM,H,HH,E,W,KPLUS,WPRM,KPLSPRM
        REAL PI,XL,XCHK,EINF,E0,Z,ETA
        INTEGER NS,P1
        PRINT *
        PRINT *,'               FOURTH ORDER RUNGE-KUTTA SCHEME '
        PRINT *,'              FOR THE CARTESIAN COMPUTATION '
        PRINT *,'               OF W, KPLUS, & KPLSPRM'

        PRINT *,'INPUT VALUES FOR EINF, E0, Z, AND ETA'
        READ *,EINF,E0,Z,ETA

1       IM=1            ! Number of equations
        Y(1) = 1.00     ! Initial condition for y~1 at x=XP.
C       Y(2) = 0      ! Initial condition for y~2 at x=XP (if nec)

        PRINT *
        PRINT *,'INTERVAL OF X FOR PRINTING ?'
        READ *,PI

        PRINT *,'INPUT THE STEP SIZE (delta-x)'
        READ *,H

        NS = NINT(PI/H)

        PRINT *,'MAXIMUM X TO STOP CALCULATION ?'
        READ *,XL

        PRINT *,' H= ',H

        P1=0
        XP=0
        HH=H/2
        KPLUS=1.0


        print *,' HH= ',HH
        print *,' NS= ', NS
        PRINT *


        LI = 0                  ! Line no. initialization
        PRINT*,'LINE    y/a            KPLUS'
        WRITE (*,98) LI,XP, KPLUS

28      LI=LI+1
        DO N=1,NS
           XB=XP                ! Old time
           XP=XP+H              ! New time
           XM=XB+HH             ! Midpoint time

           J=1                  ! This part computes k~1.
           DO I=1,IM
              YA(I)=Y(I)
           END DO
           XA=XB
```
71

```fortran
      CALL   FUNCT(EK,J,YA,H,XA,EINF,E0,Z,ETA)

      J=2                    ! This part computes k~2.
      DO I=1,IM
         YA(I)=Y(I)+EK(1,I)/2
      END DO
      XA=XM
      CALL   FUNCT(EK,J,YA,H,XA,EINF,E0,Z,ETA)

      J=3                    ! This part computes k~3.
      DO I=1,IM
         YA(I)=Y(I)+EK(2,I)/2
      END DO
      XA=XM
        CALL   FUNCT(EK,J,YA,H,XA,EINF,E0,Z,ETA)

      J=4                    ! This part computes k~4.
      DO I=1,IM
         YA(I)=Y(I)+EK(3,I)
      END DO
      XA=XP
      CALL   FUNCT(EK,J,YA,H,XA,EINF,E0,Z,ETA)

        DO I=1,IM          ! 4-th order Runge-Kutta scheme
          Y(I)=Y(I)+(EK(1,I)+EK(2,I)*2+EK(3,I)*2+EK(4,I))/6
        END DO


      W=Y(1)
c     You now have W( y/a ) --  to get K+( y/a ) you must
c     multiply by      { E( y/a ) / E(0) }

      E=(EINF/E0)*DEXP((Z**2.)/((XP+1.)**2.))
      KPLUS=W*E

c     To get the derivative of W [ W'( y/a ) ], just plug the
c     computed values of W back in the original 1st-order ODE

      J=5
      YA(1)=W
      XA=XP
      CALL FUNCT(EK,J,YA,H,XA,EINF,E0,Z,ETA)
      WPRM=EK(5,1)/H

C     NOW, to get  d/dy [K+] from  d/dy [ K+/(E/E0) ] , must
C     perform the following operation:
      KPLSPRM=(WPRM*(E**2.)+KPLUS*E*(-2.*(Z**2.)/((XP+1.)**3.)))/E

C     To keep from generating unplottable 50,000 point data files,
c      the following will edit out data points depending on
c      'where' they occur

      XCHK=(XP/H)
      IF (XCHK .GT. 100000) GOTO 72
      IF (XCHK .GT. 10000) GOTO 73
      IF (XCHK .GT. 1000) GOTO 74
      IF (XCHK .GT. 100) GOTO 75
      GOTO 44

72    P1=P1+1
```

```
      IF (P1 .NE. 10000) GOTO 88
      P1=0
      GOTO 44
73    P1=P1+1
      IF (P1 .NE. 1000) GOTO 88
      P1=0
      GOTO 44
74    P1=P1+1
      IF (P1 .NE. 100) GOTO 88
      P1=0
      GOTO 44
75    P1=P1+1
      IF (P1 .NE. 10) GOTO 88
      P1=0


44       WRITE (13,*) XP,   KPLSPRM
         WRITE (12,*) XP,   KPLUS
C         WRITE (10,*) XP,   W

88     CONTINUE


       END DO
       WRITE (*,98) LI,XP, KPLUS
98     FORMAT(1X, I2, F10.6, 2X, 1P4E16.8)

       IF (XP .LT. XL) GOTO 28

200    PRINT*
       PRINT*,'TYPE 1 TO CONTINUE, OR 0 TO STOP.'
       READ *,K
       IF(K.EQ.1) GOTO 1
       PRINT*
       END

C********************************************

       SUBROUTINE FUNCT(EK,J,YA,H,XA,EINF,E0,Z,ETA) ! DEFINES SET OF EQS
       DOUBLE PRECISION EK(0:4,0:10),YA(0:10),H,XA,PART1(0:4,0:10)
       DOUBLE PRECISION PART2(0:4,0:10)
       PART1(J,1)=DEXP((2.*Z**2.)/((XA+1.)**2.))/((XA+1.)**3.)
       PART2(J,1)=(DEXP((Z**2.)/((XA+1.)**2.)))*(ETA*EINF/E0)
       EK(J,1)=(2.*ETA-PART2(J,1)*YA(1)-(ETA*(EINF/E0)**2.)*PART1(J,1))*H
C      EK(J,2)=  the second ode, if nec.
       RETURN
       END
```

73

```
C          THIS PROGRAM IS BUILT AROUND A GRAFkit 3.1 RUNGE-KUTTA
C          ALGORITHM PRODUCED BY SCO, INC.


           DOUBLE PRECISION YA(0:10),YN(0:10),EK(0:4,0:10),Y(0:10),XA
           DOUBLE PRECISION XP,XB,XM,H,HH,E,W,KPLUS,WPRM,KPLSPRM
           DOUBLE PRECISION NI,NE,NI1,NI2,NI3,NI2A,NI3A,NE1
           REAL PI,XL,XCHK,EINF,E0,Z,ETA
           REAL EPS0,CHRG,K,TEMP,NINF,A
           INTEGER NS,P1

           EPS0=8.853742E-12
           CHRG=1.602E-19
           K=1.38054E-23

           PRINT *
           PRINT *,'              FOURTH ORDER RUNGE-KUTTA SCHEME '
           PRINT *,'              FOR THE CARTESIAN COMPUTATION '
           PRINT *,'                      OF NI AND NE'

           PRINT *,'INPUT VALUES FOR EINF, E0, Z, AND ETA'
           READ *,EINF,E0,Z,ETA
           PRINT *,'INPUT VALUES FOR TEMP. AND NINF'
           READ *,TEMP,NINF
           PRINT *,'INPUT VALUE FOR a'
           READ *,A

1          IM=1              ! Number of equations
           Y(1) = 1.00       ! Initial condition for y~1 at x=XP.
C          Y(2) = 0          ! Initial condition for y~2 at x=XP (if nec)

           PRINT *
           PRINT *,'INTERVAL OF X FOR PRINTING ?'
           READ *,PI

           PRINT *,'INPUT THE STEP SIZE (delta-x)'
           READ *,H

           NS = NINT(PI/H)

           PRINT *,'MAXIMUM X TO STOP CALCULATION ?'
           READ *,XL

           PRINT *,' H= ',H

           P1=0
           XP=0
           HH=H/2
           KPLUS=1.0


           print *,' HH= ',HH
           print *,' NS= ', NS
           PRINT *


           LI = 0                    ! Line no. initialization
           PRINT*,'LINE    y/a           KPLUS'
           WRITE (*,98) LI,XP, KPLUS
```

```
28      LI=LI+1
        DO N=1,NS
            XB=XP                   ! Old time
            XP=XP+H                 ! New time
            XM=XB+HH                ! Midpoint time

            J=1                     ! This part computes k~1.
            DO I=1,IM
                YA(I)=Y(I)
            END DO
            XA=XB
            CALL   FUNCT(EK,J,YA,H,XA,EINF,E0,Z,ETA)

            J=2                     ! This part computes k~2.
            DO I=1,IM
                YA(I)=Y(I)+EK(1,I)/2
            END DO
            XA=XM
            CALL   FUNCT(EK,J,YA,H,XA,EINF,E0,Z,ETA)

            J=3                     ! This part computes k~3.
            DO I=1,IM
                YA(I)=Y(I)+EK(2,I)/2
            END DO
            XA=XM
              CALL   FUNCT(EK,J,YA,H,XA,EINF,E0,Z,ETA)

            J=4                     ! This part computes k~4.
            DO I=1,IM
                YA(I)=Y(I)+EK(3,I)
            END DO
            XA=XP
            CALL   FUNCT(EK,J,YA,H,XA,EINF,E0,Z,ETA)

              DO I=1,IM        ! 4-th order Runge-Kutta scheme
                Y(I)=Y(I)+(EK(1,I)+EK(2,I)*2+EK(3,I)*2+EK(4,I))/6
              END DO


        W=Y(1)
c       You now have W( y/a ) --  to get K+( y/a ) you must
c       multiply by      { E( y/a ) / E(0) }

        E=(EINF/E0)*DEXP((Z**2.)/((XP+1.)**2.))
        KPLUS=W*E

c       To get the derivative of W [ W'( y/a ) ], just plug the
c       computed values of W back in the original 1st-order ODE

        J=5
        YA(1)=W
        XA=XP
        CALL FUNCT(EK,J,YA,H,XA,EINF,E0,Z,ETA)
        WPRM=EK(5,1)/H

C       NOW, to get  d/dy [K+] from  d/dy [ K+/(E/E0) ] , must
C       perform the following operation:
        KPLSPRM=(WPRM*(E**2.)+KPLUS*E*(-2.*(Z**2.)/((XP+1.)**3.)))/E
```

75

```fortran
C       AND NOW, to generate the non-dimensionalized n-curves
C               ne( y/a )    and     ni( y/a )
C       just compute these equations:

        NI1=(KPLUS/E)*(EINF/E0)
         NI2A=(EPS0*K*TEMP)/((CHRG**2.)*NINF*(A**2.))
        NI2=NI2A*((6.*(Z**2.)/((XP+1.)**4.))+(4.*(Z**4.)/((XP+1.)**6.)))
         NI3A=((EPS0*E0)/(CHRG*NINF*A))*E
        NI3=NI3A*(-2.*(Z**2.)/((XP+1.)**3.))
        NI=.5*(NI1+NI2+NI3)
         NE1=((E0*EPS0*(Z**2.))/(CHRG*NINF*A))*E*(2./((XP+1.)**3.))
        NE=NI+NE1


C       To prevent every data point from being written to the file
C        (resulting in unplottable 50,000 pt. data files), the following
C        edits out a percentage of the data depending on 'where' it
C        was generated.

        XCHK=(XP/H)
        IF (XCHK .GT. 100000) GOTO 72
        IF (XCHK .GT. 10000) GOTO 73
        IF (XCHK .GT. 1000) GOTO 74
        IF (XCHK .GT. 100) GOTO 75
        GOTO 44
72      P1=P1+1
        IF (P1 .NE. 10000) GOTO 88
        P1=0
        GOTO 44
73      P1=P1+1
        IF (P1 .NE. 1000) GOTO 88
        P1=0
        GOTO 44
74      P1=P1+1
        IF (P1 .NE. 100) GOTO 88
        P1=0
        GOTO 44
75      P1=P1+1
        IF (P1 .NE. 10) GOTO 88
        P1=0


44         WRITE (10,*) XP,  NI
           WRITE (11,*) XP,  NE

88      CONTINUE


        END DO
        WRITE (*,98) LI,XP, KPLUS
98      FORMAT(1X, I2, F10.6, 2X, 1P4E16.8)

        IF (XP .LT. XL) GOTO 28

200     PRINT*
        PRINT*,'TYPE 1 TO CONTINUE, OR 0 TO STOP.'
        READ *,K1
        IF(K1.EQ.1) GOTO 1
        PRINT*
```

```fortran
      END

C******************************************

      SUBROUTINE FUNCT(EK,J,YA,H,XA,EINF,E0,Z,ETA) ! DEFINES SET OF EQS
      DOUBLE PRECISION EK(0:4,0:10),YA(0:10),H,XA,PART1(0:4,0:10)
      DOUBLE PRECISION PART2(0:4,0:10)
      PART1(J,1)=DEXP((2.*Z**2.)/((XA+1.)**2.))/((XA+1.)**3.)
      PART2(J,1)=(DEXP((Z**2.)/((XA+1.)**2.)))*(ETA*EINF/E0)
      EK(J,1)=(2.*ETA-PART2(J,1)*YA(1)-(ETA*(EINF/E0)**2.)*PART1(J,1))*H
C     EK(J,2)=  the second ode, if nec.
      RETURN
      END
```

```fortran
C          THIS PROGRAM IS BUILT AROUND A GRAFkit 3.1 RUNGE-KUTTA
C          ALGORITHM PRODUCED BY SCO, INC.


           DOUBLE PRECISION YA(0:10),YN(0:10),EK(0:4,0:10),Y(0:10),XA
           DOUBLE PRECISION XP,XB,XM,H,HH,E,W,KPLUS,WPRM,KPLSPRM
           REAL PI,XL,XCHK,EINF,ER0,Q,ETA
           INTEGER NS,P1
           PRINT *
           PRINT *,'                FOURTH ORDER RUNGE-KUTTA SCHEME '
           PRINT *,'                FOR THE CYLINDRICAL COMPUTATION '
           PRINT *,'                   OF W, KPLUS, & KPLSPRM'
           PRINT *,'                ( NORMAL-SIZED ANODE:   r0 = 1 cm )'

           PRINT *,'INPUT VALUES FOR EINF, Er0, Q, AND ETA'
           READ *,EINF,ER0,Q,ETA

1          IM=1              ! Number of equations
           Y(1) = 1.00      ! Initial condition for w1 at r~=XP.
C          Y(2) = 0      ! Initial condition for w2 at r~=XP (if nec)

           PRINT *
           PRINT *,'INTERVAL OF r~ FOR PRINTING ?'
           READ *,PI

           PRINT *,'INPUT THE STEP SIZE (delta-r~)'
           READ *,H

           NS = NINT(PI/H)

           PRINT *,'MAXIMUM r~ TO STOP CALCULATION ?'
           READ *,XL

           PRINT *,' dr~ = ',H

           P1=0
           XP=0
           HH=H/2.
           KPLUS=1.0


           print *,' NS= ', NS
           PRINT *


           LI = 0                 ! Line no. initialization
           PRINT*,'LINE      r~              KPLUS'
           WRITE (*,98) LI,XP, KPLUS


28         LI=LI+1
           DO N=1,NS
               XB=XP              ! Old time
               XP=XP+H            ! New time
               XM=XB+HH           ! Midpoint time

C          ----------Runge-Kutta Scheme------------------

               J=1                ! This is part 1.
               DO I=1,IM
```
78

```fortran
         YA(I)=Y(I)
      END DO
      XA=XB
      CALL  FUNCT(EK,J,YA,H,XA,EINF,ER0,Q,ETA)

      J=2                 ! This is part 2.
      DO I=1,IM
         YA(I)=Y(I)+EK(1,I)/2
      END DO
      XA=XM
      CALL  FUNCT(EK,J,YA,H,XA,EINF,ER0,Q,ETA)

      J=3                 ! This is part 3.
      DO I=1,IM
         YA(I)=Y(I)+EK(2,I)/2
      END DO
      XA=XM
        CALL  FUNCT(EK,J,YA,H,XA,EINF,ER0,Q,ETA)

      J=4                 ! This is part 4.
      DO I=1,IM
         YA(I)=Y(I)+EK(3,I)
      END DO
      XA=XP
      CALL  FUNCT(EK,J,YA,H,XA,EINF,ER0,Q,ETA)

        DO I=1,IM         ! 4-th order Runge-Kutta scheme
          Y(I)=Y(I)+(EK(1,I)+EK(2,I)*2+EK(3,I)*2+EK(4,I))/6
        END DO
```

```fortran
C  ------------------------------------------------------------


      W=Y(1)
C     You now have W( r~ ) --  to get K+( r~ ) you must
C     multiply by       { E( r~ ) / E(0) }

      E=(EINF/ER0)*DEXP((Q**2.)/((XP+1.)**2.))
      KPLUS=W*E

C     To get the derivative of W  [ W'( r~ ) ], just plug the
C     computed values of W back in the original 1st-order ODE

      J=5
      YA(1)=W
      XA=XP
      CALL FUNCT(EK,J,YA,H,XA,EINF,ER0,Q,ETA)
      WPRM=EK(5,1)/H

C     NOW, to get  d/dr~ [K+] from  d/dr~ [ K+/(E/Er0) ] , must
C     perform the following operation:
      KPLSPRM=(WPRM*(E**2.)+KPLUS*E*(-2.*(Q**2.)/((XP+1.)**3.)))/E

C     To keep from generating unplottable 50,000 point data files,
C     the following edits out some of the data points depending
C     on 'where' they occur

      XCHK=(XP/H)
      IF (XCHK .GT. 100000) GOTO 72
      IF (XCHK .GT. 10000) GOTO 73
```

```fortran
          IF (XCHK .GT. 1000) GOTO 74
          IF (XCHK .GT. 100) GOTO 75
          GOTO 44

72        P1=P1+1
          IF (P1 .NE. 10000) GOTO 88
          P1=0
          GOTO 44
73        P1=P1+1
          IF (P1 .NE. 1000) GOTO 88
          P1=0
          GOTO 44
74        P1=P1+1
          IF (P1 .NE. 100) GOTO 88
          P1=0
          GOTO 44
75        P1=P1+1
          IF (P1 .NE. 10) GOTO 88
          P1=0

44         WRITE (13,*) XP,  KPLSPRM
           WRITE (12,*) XP,  KPLUS
           WRITE (14,*) XP,  W

88         CONTINUE


           END DO

           WRITE (*,98) LI,XP, KPLUS
98         FORMAT(1X, I2, F10.6, 2X, 1P4E16.8)

           IF (XP .LT. XL) GOTO 28

200        PRINT*
           PRINT*,'TYPE 1 TO CONTINUE, OR 0 TO STOP.'
           READ *,K1
           IF(K1.EQ.1) GOTO 1
           PRINT*
           END

C**********************************************

           SUBROUTINE FUNCT(EK,J,YA,H,XA,EINF,ER0,Q,ETA) ! DEFINES SET OF EQS
           DOUBLE PRECISION EK(0:4,0:10),YA(0:10),H,XA,PART1(0:4,0:10)
           DOUBLE PRECISION PART2(0:4,0:10)
           PART1(J,1)=ETA*(DEXP((2.*Q**2.)/((XA+1.)**2.))/((XA+1.)**3.))
           PART2(J,1)=(DEXP((Q**2.)/((XA+1.)**2.)))*(ETA*EINF/ER0)
           EK(J,1)=(2.*ETA-PART2(J,1)*YA(1)-((EINF/ER0)**2.)*PART1(J,1))*H
C          EK(J,2)=  the second ode, if nec.
           RETURN
           END
```

```
THIS PROGRAM IS BUILT AROUND A GRAFkit 3.1 RUNGE-KUTTA
ALGORITHM PRODUCED BY SCO, INC.


      DOUBLE PRECISION YA(0:10),YN(0:10),EK(0:4,0:10),Y(0:10),XA
      DOUBLE PRECISION XP,XB,XM,H,HH,E,W,KPLUS,WPRM,KPLSPRM
      DOUBLE PRECISION NI,NE,NI1,NI2,NI3,NE1
      REAL CC1,CC2,CC3,S2,S3,S2A,S2B,S2C
      REAL PI,XL,XCHK,EINF,ER0,Q,ETA
      REAL EPS0,CHRG,K,TEMP,NINF,B,R0
      INTEGER NS,P1

      EPS0=8.853742E-12
      CHRG=1.602E-19
      K=1.38054E-23
      R0=.01

      PRINT *
      PRINT *,'            FOURTH ORDER RUNGE-KUTTA SCHEME '
      PRINT *,'            FOR THE CYLINDRICAL COMPUTATION '
      PRINT *,'                 OF NE AND NI'
      PRINT *,'            ( NORMAL-SIZED ANODE:   r0 = 1 cm )'

      PRINT *,'INPUT VALUES FOR EINF, Er0, Q, AND ETA'
      READ *,EINF,ER0,Q,ETA
      PRINT *,'INPUT VALUES FOR TEMP. AND NINF'
      READ *,TEMP,NINF
      PRINT *,'INPUT VALUE FOR b'
      READ *,B

      IM=1           ! Number of equations
      Y(1) = 1.00    ! Initial condition for w1 at r~=XP.
      Y(2) = 0       ! Initial condition for w2 at r~=XP (if nec)

      PRINT *
      PRINT *,'INTERVAL OF r~ FOR PRINTING ?'
      READ *,PI

      PRINT *,'INPUT THE STEP SIZE (delta-r~)'
      READ *,H

      NS = NINT(PI/H)

      PRINT *,'MAXIMUM r~ TO STOP CALCULATION ?'
      READ *,XL

      PRINT *,' dr~ = ',H

      P1=0
      XP=0
      HH=H/2.
      KPLUS=1.

      print *,' NS= ', NS
      PRINT *


      LI = 0              ! Line no. initialization
      PRINT*,'LINE    r~              KPLUS'
      WRITE (*,98) LI,XP, KPLUS
```

```
28      LI=LI+1
        DO N=1,NS
            XB=XP                ! Old time
            XP=XP+H              ! New time
            XM=XB+HH             ! Midpoint time

C       ----------Runge-Kutta Scheme-------------------

            J=1                  ! This is part 1.
            DO I=1,IM
                YA(I)=Y(I)
            END DO
            XA=XB
            CALL  FUNCT(EK,J,YA,H,XA,EINF,ER0,Q,ETA)

            J=2                  ! This is part 2.
            DO I=1,IM
                YA(I)=Y(I)+EK(1,I)/2
            END DO
            XA=XM
            CALL  FUNCT(EK,J,YA,H,XA,EINF,ER0,Q,ETA)

            J=3                  ! This is part 3.
            DO I=1,IM
                YA(I)=Y(I)+EK(2,I)/2
            END DO
            XA=XM
              CALL  FUNCT(EK,J,YA,H,XA,EINF,ER0,Q,ETA)

            J=4                  ! This is part 4.
            DO I=1,IM
                YA(I)=Y(I)+EK(3,I)
            END DO
            XA=XP
            CALL  FUNCT(EK,J,YA,H,XA,EINF,ER0,Q,ETA)

              DO I=1,IM          ! 4-th order Runge-Kutta scheme
                Y(I)=Y(I)+(EK(1,I)+EK(2,I)*2+EK(3,I)*2+EK(4,I))/6
              END DO

C       -------------------------------------------------------


        W=Y(1)
c       You now have W( r~ ) --  to get K+( r~ ) you must
c       multiply by      { E( r~ ) / E(0) }

        E=(EINF/ER0)*DEXP((Q**2.)/((XP+1.)**2.))
        KPLUS=W*E

c       To get the derivative of W  [ W'( r~ ) ], just plug the
c       computed values of W back in the original 1st-order ODE

        J=5
        YA(1)=W
        XA=XP
        CALL FUNCT(EK,J,YA,H,XA,EINF,ER0,Q,ETA)
        WPRM=EK(5,1)/H                        82
```

```fortran
C       NOW, to get  d/dr~ [K+] from  d/dr~ [ K+/(E/Er0) ] , must
C       perform the following operation:
        KPLSPRM=(WPRM*(E**2.)+KPLUS*E*(-2.*(Q**2.)/((XP+1.)**3.)))/E


C       AND NOW, to generate the nondimensionalized n-curves
C                   ne( r~ )  and  ni( r~ )
.C      compute the following equations

        NI1=(KPLUS/E)*(EINF/ER0)
         CC2=(K*TEMP*EPS0)/((CHRG**2.)*NINF*(B**2.))
          S2A=(6.*(Q**2.))/((XP+1.)**4.)
          S2B=(4.*(Q**4.))/((XP+1.)**6.)
          S2C=(1/(XP+(R0/B)))*((-2.*(Q**2.))/((XP+1.)**3.))
         S2=S2A+S2B+S2C
        NI2=CC2*S2
         CC3=(EPS0*ER0)/(CHRG*NINF*B)
         S3=((-2.*(Q**2.))/((XP+1.)**3.))+(1./(XP+(R0/B)))
        NI3=CC3*E*S3

       NI=.5*(NI1+NI2+NI3)

        CC1=(EPS0*ER0)/(CHRG*NINF*B)
        NE1=CC1*E*((-2.*(Q**2.))/((XP+1.)**3.)+(1./(XP+(R0/B))))

       NE=NI-NE1


C       To keep from generating unplottable 50,000 point data files,
C       the following edits out some of the data points depending
.C      on 'where' they occur

        XCHK=(XP/H)
        IF (XCHK .GT. 100000) GOTO 72
        IF (XCHK .GT. 10000) GOTO 73
        IF (XCHK .GT. 1000) GOTO 74
        IF (XCHK .GT. 100) GOTO 75
        GOTO 44

72      P1=P1+1
        IF (P1 .NE. 10000) GOTO 88
        P1=0
        GOTO 44
73      P1=P1+1
        IF (P1 .NE. 1000) GOTO 88
        P1=0
        GOTO 44
74      P1=P1+1
        IF (P1 .NE. 100) GOTO 88
        P1=0
        GOTO 44
75      P1=P1+1
        IF (P1 .NE. 10) GOTO 88
        P1=0

44       WRITE (10,*) XP, NI
         WRITE (11,*) XP, NE

88       CONTINUE
```

```fortran
      END DO

      WRITE (*,98) LI,XP, KPLUS
98    FORMAT(1X, I2, F10.6, 2X, 1P4E16.8)

      IF (XP .LT. XL) GOTO 28

200   PRINT*
      PRINT*,'TYPE 1 TO CONTINUE, OR 0 TO STOP.'
      READ *,K1
      IF(K1.EQ.1) GOTO 1
      PRINT*
      END

C*******************************************

      SUBROUTINE FUNCT(EK,J,YA,H,XA,EINF,ER0,Q,ETA) ! DEFINES SET OF EQS
      DOUBLE PRECISION EK(0:4,0:10),YA(0:10),H,XA,PART1(0:4,0:10)
      DOUBLE PRECISION PART2(0:4,0:10)
      PART1(J,1)=ETA*(DEXP((2.*Q**2.)/((XA+1.)**2.))/((XA+1.)**3.))
      PART2(J,1)=(DEXP((Q**2.)/((XA+1.)**2.)))*(ETA*EINF/ER0)
      EK(J,1)=(2.*ETA-PART2(J,1)*YA(1)-((EINF/ER0)**2.)*PART1(J,1))*H
C     EK(J,2)=  the second ode, if nec.
      RETURN
      END
```

```
C          THIS PROGRAM IS BUILT AROUND A GRAFkit 3.1 RUNGE-KUTTA
C          ALGORITHM PRODUCED BY SCO, INC.


           DOUBLE PRECISION YA(0:10),YN(0:10),EK(0:4,0:10),Y(0:10),XA
           DOUBLE PRECISION XP,XB,XM,H,HH,E,W,KPLUS,WPRM,KPLSPRM
           REAL PI,XL,XCHK,EINF,ER0,Q,ETA,R0,G,B,EPS0,CHRG
           INTEGER NS,P1
           PRINT *
           PRINT *,'               FOURTH ORDER RUNGE-KUTTA SCHEME '
           PRINT *,'               FOR THE CYLINDRICAL COMPUTATION '
           PRINT *,'                   OF W, KPLUS, & KPLSPRM'
           PRINT *,'               ( WIRE-THIN ANODE:   r0 = 0.1 mm )'


           PRINT *,'INPUT VALUES FOR EINF, Er0, Q, AND ETA'
           READ *,EINF,ER0,Q,ETA
           PRINT *,'INPUT VALUES FOR GAMMA AND B'
           READ *,G,B

           R0=.0001
           EPS0=8.853742E-12
           CHRG=1.602E-19

1          IM=1              ! Number of equations
           Y(1) = 1.00       ! Initial condition for w1 at r~=XP.
C          Y(2) = 0          ! Initial condition for w2 at r~=XP (if nec)

           PRINT *
           PRINT *,'INTERVAL OF r~ FOR PRINTING ?'
           READ *,PI

           PRINT *,'INPUT THE STEP SIZE (delta-r~)'
           READ *,H

           NS = NINT(PI/H)

           PRINT *,'MAXIMUM r~ TO STOP CALCULATION ?'
           READ *,XL

           PRINT *,' dr~ = ',H

           P1=0
           XP=0
           HH=H/2.
           KPLUS=1.

           print *,' NS= ', NS
           PRINT *


           LI = 0                    ! Line no. initialization
           PRINT*,'LINE      r~            KPLUS'
           WRITE (*,98) LI,XP, KPLUS


28         LI=LI+1
           DO N=1,NS
              XB=XP              ! Old time
              XP=XP+H            ! New time
```
85

```
      XM=XB+HH              ! Midpoint time

C        ----------Runge-Kutta Scheme------------------

      J=1                   ! This is part 1.
      DO I=1,IM
         YA(I)=Y(I)
      END DO
      XA=XB
      CALL  FUNCT(EK,J,YA,H,XA,EINF,ER0,Q,ETA,G,B)

      J=2                   ! This is part 2.
      DO I=1,IM
         YA(I)=Y(I)+EK(1,I)/2
      END DO
      XA=XM
      CALL  FUNCT(EK,J,YA,H,XA,EINF,ER0,Q,ETA,G,B)

      J=3                   ! This is part 3.
      DO I=1,IM
         YA(I)=Y(I)+EK(2,I)/2
      END DO
      XA=XM
        CALL  FUNCT(EK,J,YA,H,XA,EINF,ER0,Q,ETA,G,B)

      J=4                   ! This is part 4.
      DO I=1,IM
         YA(I)=Y(I)+EK(3,I)
      END DO
      XA=XP
      CALL  FUNCT(EK,J,YA,H,XA,EINF,ER0,Q,ETA,G,B)

         DO I=1,IM          ! 4-th order Runge-Kutta scheme
           Y(I)=Y(I)+(EK(1,I)+EK(2,I)*2+EK(3,I)*2+EK(4,I))/6
         END DO

C      ----------------------------------------------------------


     W=Y(1)
c     You now have W( r~ ) --  to get K+( r~ ) you must
c     multiply by      { E( r~ ) / E(0) }

     E=(EINF/ER0)*DEXP((Q**2.)/((XP+1.)**2.))
     KPLUS=W*E

c     To get the derivative of W  [ W'( r~ ) ], just plug the
c     computed values of W back in the original 1st-order ODE

     J=5
     YA(1)=W
     XA=XP
     CALL FUNCT(EK,J,YA,H,XA,EINF,ER0,Q,ETA,G,B)
     WPRM=EK(5,1)/H

C     NOW, to get  d/dr~ [K+] from  d/dr~ [ K+/(E/Er0) ] , must
C     perform the following operation:
     KPLSPRM=(WPRM*(E**2.)+KPLUS*E*(-2.*(Q**2.)/((XP+1.)**3.)))/E

C     To keep from generating unplottable 50,000 point data files,
```

```fortran
C       the following edits out some of the data points depending
C       on 'where' they occur

        XCHK=(XP/H)
        IF (XCHK .GT. 100000) GOTO 72
        IF (XCHK .GT. 10000) GOTO 73
        IF (XCHK .GT. 1000) GOTO 74
        IF (XCHK .GT. 100) GOTO 75
        GOTO 44

72      P1=P1+1
        IF (P1 .NE. 10000) GOTO 88
        P1=0
        GOTO 44
73      P1=P1+1
        IF (P1 .NE. 1000) GOTO 88
        P1=0
        GOTO 44
74      P1=P1+1
        IF (P1 .NE. 100) GOTO 88
        P1=0
        GOTO 44
75      P1=P1+1
        IF (P1 .NE. 10) GOTO 88
        P1=0

44       WRITE (13,*) XP,   KPLSPRM
         WRITE (12,*) XP,   KPLUS
         WRITE (14,*) XP,   W

88      CONTINUE


        END DO

        WRITE (*,98) LI,XP, KPLUS
98      FORMAT(1X, I2, F10.6, 2X, 1P4E16.8)

        IF (XP .LT. XL) GOTO 28

200     PRINT*
        PRINT*,'TYPE 1 TO CONTINUE, OR 0 TO STOP.'
        READ *,K1
        IF(K1.EQ.1) GOTO 1
        PRINT*
        END

C*******************************************

        SUBROUTINE FUNCT(EK,J,YA,H,XA,EINF,ER0,Q,ETA,G,B) ! DEFINES ODEs
        DOUBLE PRECISION EK(0:4,0:10),YA(0:10),PART2(0:4,0:10)
        DOUBLE PRECISION PART3(0:4,0:10),PART4(0:4,0:10),H,XA,C1
        REAL R0
        R0=.0001
        C2=ETA*G*((EINF/ER0)**2.)
        PART4(J,1)=C2*(DEXP((2.*(Q**2.))/((XA+1.)**2.)))/(XA*B+R0)
        C1=ETA*((G/R0)+1.)*((EINF/ER0)**2.)
        PART3(J,1)=C1*(DEXP((2.*Q**2.)/((XA+1.)**2.))/((XA+1.)**3.))
        PART2(J,1)=(DEXP((Q**2.)/((XA+1.)**2.)))*(ETA*EINF/ER0)
        EK(J,1)=(2.*ETA-PART2(J,1)*YA(1)-PART3(J,1)+PART4(J,1))*H
```

```
C      EK(J,2)=  the second ode, if nec.
       RETURN
       END
```

```
C        THIS PROGRAM IS BUILT AROUND A GRAFkit 3.1 RUNGE-KUTTA
C        ALGORITHM PRODUCED BY SCO, INC.


         DOUBLE PRECISION YA(0:10),YN(0:10),EK(0:4,0:10),V(0:10),XA
         DOUBLE PRECISION XP,XB,XM,H,HH,E,W,KPLUS,WPRM,KPLSPRM
         DOUBLE PRECISION NI,NE,NI1,NI2,NI3,NE1
         REAL CC1,CC2,CC3,S2,S3,S2A,S2B,S2C,S2D
         REAL PI,XL,XCHK,EINF,ER0,Q,ETA
         REAL EPS0,CHRG,K,TEMP,NINF,B,G,R0
         INTEGER NS,P1

         EPS0=8.853742E-12
         CHRG=1.602E-19
         K=1.38054E-23
         R0=.0001

         PRINT *
         PRINT *,'            FOURTH ORDER RUNGE-KUTTA SCHEME '
         PRINT *,'            FOR THE CYLINDRICAL COMPUTATION '
         PRINT *,'                   OF NE AND NI'
         PRINT *,'            ( WIRE-THIN ANODE:   r0 = 0.1 mm )'

         PRINT *,'INPUT VALUES FOR EINF, Er0, Q, AND ETA'
         READ *,EINF,ER0,Q,ETA
         PRINT *,'INPUT VALUES FOR TEMP. AND NINF'
         READ *,TEMP,NINF
         PRINT *,'INPUT VALUES FOR GAMMA AND b'
         READ *,G,B

1        IM=1           ! Number of equations
         Y(1) = 1.00    ! Initial condition for w1 at r~=XP.
C        Y(2) = 0       ! Initial condition for w2 at r~=XP (if nec)

         PRINT *
         PRINT *,'INTERVAL OF r~ FOR PRINTING ?'
         READ *,PI

         PRINT *,'INPUT THE STEP SIZE (delta-r~)'
         READ *,H

         NS = NINT(PI/H)

         PRINT *,'MAXIMUM r~ TO STOP CALCULATION ?'
         READ *,XL

         PRINT *,' dr~ = ',H

         P1=0
         XP=0
         HH=H/2.
         KPLUS=1.

         print *,' NS= ', NS
         PRINT *


         LI = 0                  ! Line no. initialization
         PRINT*,'LINE      r~             KPLUS'
         WRITE (*,98) LI,XP, KPLUS
```

```
28      LI=LI+1
        DO N=1,NS
            XB=XP               ! Old time
            XP=XP+H             ! New time
            XM=XB+HH            ! Midpoint time

C       ----------Runge-Kutta Scheme------------------

            J=1                 ! This is part 1.
            DO I=1,IM
                YA(I)=Y(I)
            END DO
            XA=XB
            CALL    FUNCT(EK,J,YA,H,XA,EINF,ER0,Q,ETA,G,B)

            J=2                 ! This is part 2.
            DO I=1,IM
                YA(I)=Y(I)+EK(1,I)/2
            END DO
            XA=XM
            CALL    FUNCT(EK,J,YA,H,XA,EINF,ER0,Q,ETA,G,B)

            J=3                 ! This is part 3.
            DO I=1,IM
                YA(I)=Y(I)+EK(2,I)/2
            END DO
            XA=XM
             CALL   FUNCT(EK,J,YA,H,XA,EINF,ER0,Q,ETA,G,B)

            J=4                 ! This is part 4.
            DO I=1,IM
                YA(I)=Y(I)+EK(3,I)
            END DO
            XA=XP
            CALL    FUNCT(EK,J,YA,H,XA,EINF,ER0,Q,ETA,G,B)

              DO I=1,IM         ! 4-th order Runge-Kutta scheme
                Y(I)=Y(I)+(EK(1,I)+EK(2,I)*2+EK(3,I)*2+EK(4,I))/6
              END DO

C       ------------------------------------------------------------


        W=Y(1)
c       You now have W( r~ ) --  to get K+( r~ ) you must
c       multiply by       { E( r~ ) / E(0) }

        E=(EINF/ER0)*DEXP((Q**2.)/((XP+1.)**2.))
        KPLUS=W*E

c       To get the derivative of W  [ W'( r~ ) ], just plug the
c       computed values of W back in the original 1st-order ODE

        J=5
        YA(1)=W
        XA=XP
        CALL FUNCT(EK,J,YA,H,XA,EINF,ER0,Q,ETA,G,B)
        WPRM=EK(5,1)/H
                                90
```

```
C       NOW, to get  d/dr~ [K+] from  d/dr~ [ K+/(E/Er0) ] , must
C       perform the following operation:
        KPLSPRM=(WPRM*(E**2.)+KPLUS*E*(-2.*(Q**2.)/((XP+1.)**3.)))/E


C       AND NOW, to generate the nondimensionalized n-curves
c                     ne( r~ )   and   ni( r~ )
c       compute the following equations

        NI1=(KPLUS/E)*(EINF/ER0)
         CC2=(K*TEMP*EPS0)/((CHRG**2.)*NINF*(B**2.))
          S2A=(6.*(Q**2.))/((XP+1.)**4.)
          S2B=(4.*(Q**4.))/((XP+1.)**6.)
          S2C=(1./(XP+(R0/B)))*((-2.*(Q**2.))/((XP+1.)**3.))
          S2D=(1./((XP+(R0/B))**2.))
         S2=S2A+S2B+S2C-S2D
        NI2=CC2*S2
         CC3=(EPS0*ER0)/(CHRG*NINF*B)
         S3=((-2.*(Q**2.))/((XP+1.)**3.))+(1./(XP+(R0/B)))
        NI3=CC3*E*S3

        NI=.5*(NI1+NI2+NI3)

        CC1=(EPS0*ER0)/(CHRG*NINF*B)
        NE1=CC1*E*((-2.*(Q**2.))/((XP+1.)**3.)+(1./(XP+(R0/B))))

         =NI-NE1


C       To keep from generating unplottable 50,000 point data files,
C       the following edits out some of the data points depending
C       on 'where' they occur

        XCHK=(XP/H)
        IF (XCHK .GT. 100000) GOTO 72
        IF (XCHK .GT. 10000) GOTO 73
        IF (XCHK .GT. 1000) GOTO 74
        IF (XCHK .GT. 100) GOTO 75
        GOTO 44

72      P1=P1+1
        IF (P1 .NE. 10000) GOTO 88
        P1=0
        GOTO 44
73      P1=P1+1
        IF (P1 .NE. 1000) GOTO 88
        P1=0
        GOTO 44
74      P1=P1+1
        IF (P1 .NE. 100) GOTO 88
        P1=0
        GOTO 44
75      P1=P1+1
        IF (P1 .NE. 10) GOTO 88
        P1=0

44       WRITE (10,*) XP, NI
         WRITE (11,*) XP, NE
```

```fortran
88      CONTINUE

        END DO

        WRITE (*,98) LI,XP, KPLUS
98      FORMAT(1X, I2, F10.6, 2X, 1P4E16.8)

        IF (XP .LT. XL) GOTO 28

200     PRINT*
        PRINT*,'TYPE 1 TO CONTINUE, OR 0 TO STOP.'
        READ *,K1
        IF(K1.EQ.1) GOTO 1
        PRINT*
        END

C*******************************************

        SUBROUTINE FUNCT(EK,J,YA,H,XA,EINF,ER0,Q,ETA,G,B) ! DEFINES ODEs
        DOUBLE PRECISION EK(0:4,0:10),YA(0:10),H,XA,PART2(0:4,0:10)
        DOUBLE PRECISION PART3(0:4,0:10),PART4(0:4,0:10)
        REAL R0,KK4,KK3
        R0=.0001
        KK4=ETA*G*((EINF/ER0)**2.)
        PART4(J,1)=KK4*(DEXP((2.*(Q**2.))/((XA+1.)**2.)))/(XA*B+R0)
        KK3=ETA*((G/R0)+1.)*((EINF/ER0)**2.)
        PART3(J,1)=KK3*(DEXP((2.*Q**2.)/((XA+1.)**2.))/((XA+1.)**3.))
        PART2(J,1)=(DEXP((Q**2.)/((XA+1.)**2.)))*(ETA*EINF/ER0)
        EK(J,1)=(2.*ETA-PART2(J,1)*YA(1)-PART3(J,1)+PART4(J,1))*H
C       EK(J,2)=   the second ode, if nec.
        RETURN
        END
```

INITIAL DISTRIBUTION LIST

	No. Copies
1. Defense Technical Information Center Cameron Station Alexandria, Virginia 22304-6145	2
2. Library, Code 52 Naval Postgraduate School Monterey, California 93943-5002	2
3. Chairman Department of Aeronautics, Code AA Naval Postgraduate School Monterey, California 93943-5000	1
4. Commander, Naval Air Systems Command Code 05T Washington, D.C. 20361-5000	1
5. Professor Oscar Biblarz Department of Aeronautics and Astronautics, Code AA/Bi Naval Postgraduate School Monterey, California 93943-5000	5
6. LCDR Scott Brown c/o Savage 292 Nichols St. Norwood, Massachusetts 02062	3